Hybrid Sorbent-Ultrafiltration Systems for the Removal of Hormones and Fluoride from Water

İme Akanyeti

A thesis submitted for the degree of Doctor of Philosophy

University of Edinburgh

School of Engineering

November 2013

Declaration

I declare that the thesis has been composed by myself and the work contained in it is my own, except where stated otherwise. Further, this work has not been submitted for any other degree or professional qualification except as specified.

İme Akanyeti

November 2013

Thesis Supervisor

Dr Maria-Chiara Ferrari, University of Edinburgh, School of Engineering, Edinburgh, United Kingdom

Thesis Internal Examiner

Professor Stefano Brandani, University of Edinburgh, School of Engineering, Edinburgh, United Kingdom

Thesis External Examiner

Professor Andrew G. Livingston, Imperial College of Science, Technology and Medicine, Faculty of Engineering, London, United Kingdom

Abstract

The presence of trace contaminants in drinking water resources has been related to adverse health effects in living organisms and humans. Current technologies do not adequately remove these contaminants from water and/or require high energy supply. Exploring low cost, low energy processes in order to eliminate trace contaminants is essential considering that access to clean drinking water and energy is becoming more challenging in many parts of the world. Hormones and fluoride are the two contaminants studied in this research and hybrid systems which combine sorption with low pressure ultrafiltration are proposed for their removal. Sorption is a promising removal mechanism if efficient sorbents and operational conditions are selected, however, the introduction of sorbent materials can cause fouling in ultrafiltration. Fouling reduces the membrane permeability and increases the energy requirement of the system. The overall aim is to study the proposed hybrid sorbent-ultrafiltration systems in terms of contaminant sorption capacity and membrane performance. The systems are tested under varying sorbent size (52-3000 nm for hormone, <38-500 µm for fluoride removal) sorbent concentration (1.7-84 mg/L for hormone, 1-50 g/L for fluoride removal), sorbate concentration (100 ng/L hormone and 5-500 mg/L fluoride) and solution pH (3-12). The thesis can be split into two parts: one part for hormones and the other for fluoride.

In the first part, a hybrid polystyrene nanoparticle-ultrafiltration system is investigated for hormone removal. Polystyrene nanoparticles are employed as they provide a large active surface area for the sorption and they can easily be manufactured in different sizes and with various functional groups. The results show that the system can only compete with the existing nanofiltration/reverse osmosis membrane systems if the sorption capacity of the polystyrene nanoparticles is increased. For this reason, carboxyl functionalized polystyrene nanoparticles were also tested. Contrary to expectations, even less hormone sorption is achieved with the functionalized particles. Further investigation of other functional groups such as amine/amidine for their hormone sorption capacity is recommended.

In the second part, laterite and bone char are selected as two sorbents for the hybrid sorbent-UF system for fluoride removal as they are locally sourced, low cost materials in parts of Ghana and Tanzania, respectively, where fluoride contamination is a major problem. The sorption capacity and the membrane fouling of the hybrid system with the two selected sorbents are compared. Fluoride sorption capacity of the bone char system is higher than the laterite system and this is attributed to the difference in the available surface area. The fouling of the membranes operated with laterite at high initial fluoride concentrations and alkaline solutions is linked to the precipitation of iron and aluminium complexes. With further system optimization, both hybrid laterite and bone char systems show the potential to be viable solutions for fluoride removal, noting that the bone char system is more feasible for high fluoride concentrations above 10 mg/L. Based on lab scale experimental results, two hybrid laterite-ultrafiltration systems are designed to be tested in Ghana. The two systems, one with submerged hollow fibre and the other with direct dead end tubular ultrafiltration membrane modules, are operated with real surface and ground waters. The findings indicate that the amount of sorption obtained in the field is lower than that which is obtained with laboratory experiments due to the presence of interfering co-ions in the real waters and differences in membrane systems. The systems also show the potential to remove arsenic, uranium and lead. The system with hollow fibre membranes can be suggested as an appropriate system for ground water applications as it did not experience any fouling and the investment cost could be lower compared to the tubular membranes. However, if the surface waters are to be treated with the proposed hybrid system, the tubular membranes offers a system with no fouling. The hybrid laterite-UF system shows to be a promising treatment technology for fluoride contaminated waters in Ghana.

Acknowledgment

The membrane research group members have accompanied me all the way through this PhD. Dr. Andrea Semião, thank you for sharing the experimental results obtained in Chapter 4, very useful scientific discussions, guiding me through the difficult parts of the PhD journey with your objective advice and all the whiskys we have shared. Dr. Annalisa De-Munari, thank you for proof reading the thesis, providing the stirred cell system photograph and all the laughs we have shared. Dr. Helfrid Schulte-Herbruggen is thanked for proof reading the thesis and her supportive hugs. Dr. Laura Richards, thank you for proof reading and encouraging me whenever I needed; we were the warriors. Payam Malek is thanked for all the scientific and social discussions; you were a great company, especially in the last weeks before the submission. Than Hieu, thank you for being enthusiastic about everything. Dr. Peta Neale, Dr. Laura Banasiak and Molly Partick are acknowledged for helping in the lab during the first months of my PhD. Helen Cope is specially thanked for assisting with surface charge analysis of laterite, helping to conduct some of the experiments in Chapter 7 and 8, analysis of the samples collected in Ghana. You have been a great support from the moment you have taken the desk next to me in the office. Thank you for sharing all the ups and downs, especially during and after the Ghana field trip. I guess the shooting is finally over. Thank you all for sharing and making this journey enjoyable, I have learned a lot from all of you individually and as a group.

Emad, Hala, Yousef, Kenan, Archana, Aman and Baba, thank you for your support, delicious meals, conversations and just being there for me when I needed. You have become like a family. I owe a lot to my friends; Leman, Ozlem, Nezire, Laden, Deniz, Nuray, Tugba, Els and Lucia who kept being there for me although they are settled all over the world. Florian, Freddy, Juan, Pas, Mihika, Bugs, Maria and all tango society people thank you for making my life even more fun and interesting especially during the final year of my PhD. Alexi and Anastaaaaasi, thank you for making a perfect flat and family environment.

Very special thanks go to Paris, I am very glad that you took the opportunity!

Finally, I would like to dedicate this thesis and thank to MOGI. Being a part of this family was essential for the completion of this thesis.

List of Publications and Presentation

Schäfer A.I., Akanyeti I. and Semião A.J.C. Micropollutant sorption to membrane polymers: A review of mechanisms for estrogens. *Advances in Colloid and Interface Science*, 2011. 164(1-2): p. 100-117

In Preparation

Akanyeti I., Ferrari M.C. *et al.* Hybrid sorbent-ultrafiltration system for fluoride removal from water. In preparation for *Environmental Science and Technology*

Akanyeti I., Kraft A., Ferrari M.C. *et al.* Hybrid polystyrene nanoparticle-ultrafiltration system for hormone removal from water. In preparation for *Journal of Membrane Science*

Akanyeti I., *et al.* Hybrid laterite-ultrafiltration system for fluoride removal from Ghanaian surface and groundwater. In preparation for *Environmental Science and Technology*

Conference Presentation

Akanyeti I., Semião, A.J.C and Schäfer, A.I. Hormone sorption on polymeric nanoparticle deposit on UF. Oral presentation at *International Congress on Membranes and Membrane Processes (ICOM)*, Amsterdam, 25 July 2011

Table of Contents

List of Figures

List of Tables

Abbreviations and Symbols

List of Abbreviations (In alphabetical order)

A: Arsenic

AFM: Atomic Force Microscopy

Al: Aluminium

AOP: Advanced Oxidation Process

B: Boron

BC: Bone Char

BE: Background Electrolyte

BET: Brunauer–Emmett–Teller

BJH: Barrett, Joyner & Halenda

CEL: Cellulose

DA: Dubinin-Astakhov

dpm: disintegrations per minute

DO: Dissolved Oxygen

DR: Dubinin Radushkevich

EC: European Commission

EPA: Environmental Protection Agency

E1: Estrone

E2: Estradiol or 17β Estradiol

F: Fluoride

F_A: Attractive forces

F_b: Brownian diffusion force

F_d: Drag (viscous) force

FE-SEM: Field Emission Scanning Electron Microscopy

F_l: Inertial lift force

F_R: Repulsive force

F_s: Shear induced forces

F_t: Tangential force

HDPE: Polyethylene High Density

HPLC: High Performance Liquid Chromatography

IC: Ion Chromotography

ICP-MS: Inductively-Coupled Plasma Mass Spectroscopies

ICP-OES: Inductively-Coupled Plasma Optical Emission Mass Spectroscopies

ISE: Ion Selective Electrode

KNUST: Kwame Nkrumah University of Science and Technology

L: Laterite

LOD: Limit of Detection

MF: Microfiltration

MIP: Molecularly Imprinted Polymer

Mn: Manganese

MW: Molecular Weight

MWCO: Molecular Weight Cut-Off

NF: Nanofiltration

ORP: Oxidation Reduction Potential

P: Progesterone

PA: Polyamide

PAC: Powdered Activated Carbon

Pb: Lead

PEN: Polyethylene Naphthalate

PES GF: Polyethersulphone Goodfellow

PES Radel: Polyethersulphone

PET: Polyethylene Terephthalate

PMMA: Poly(methyl methacrylate)

PP: Polypropylene

PPO: Poly(2,6 dimethyl 1,4-phenylene oxide)

PS: Polystyrene

PSu: Polysulphone

PSu U: Polysulphone UDEL

PVDF: Polyvinylidene Difluoride

RW: Raw Water

RO: Reverse Osmosis

SPE: Solid Phase Extraction

SW: Synthetic Water

T: Testosterone

U: Uranium

UF: Ultrafiltration

UK: United Kingdom

USA: United States of America

UV-Vis: Ultraviolet Visible

WHO: World Health Organization

WWTP: Wastewater Treatment Plant

XRD: X-Ray Diffraction

XRF: X-Ray Fluorescence

List of Symbols (In alphabetical order)

a: Langmuir isotherm coefficient, maximum contaminant mass adsorbed per mass sorbent (mg/g or mg/m^2 or ng/g or ng/cm^2)

A_m: Membrane area (m^2)

b: Langmuir coefficient describing the affinity of contaminant on sorbent

c: Solute concentration (kg/m^3)

c_b: Particle concentration in the bulk (g/L)

C_c: Contaminant concentrate concentration (mg/L or ng/L)

c_c: Particle concentration in the concentrate (g/L)

C_e: Equilibrium contaminant concentration (mg/L or ng/L)

C_f: Contaminant feed concentration (mg/L or ng/L)

c_f: Particle concentration in the feed (g/L)

C_{fi}: Contaminant concentration of filtrate sample (mg/L)

C_i: Initial contaminant concentration (mg/L or ng/L)

c_m: Particle concentration at the membrane surface (g/L)

C_p: Concentration of the contaminant in the permeate (mg/L or ng/L)

c_p: Particle concentration in the permeate (g/L)

C_{Pi}: Contaminant permeate concentration for specific sample identity (mg/L or ng/L)

C_s: Supernatant contaminant concentration (mg/L or ng/L)

D: Particle diffusion coefficient (m^2/s)

D_p: Diameter of the particle (m)

D_i: Diameter of the impeller (m)

F: Perrin shape factor (1 for a sphere)

$_i$: Identity number of permeate samples

J: Flux of membrane ($L/m^2.h$)

J_v: Permeate flux or velocity (m/s)

J_0: Initial membrane flux ($L/m^2.h$)

k: Freundlich empirical constant

K: Boltzmann constant (1.38×10^{-23} J/K)

K_{ow}: Octanol-water partition coefficient

k_s: Mass transfer coefficient (D/δ) of the particle and in the boundary layer (m/s)

k_1: First order rate constant

k_2: Second order rate constant (g/min.mg)

L_v: Permeability of membrane (L/m^2.h.bar)

L_{vo}: Initial permeability of membrane (L/m^2.h.bar)

M_{ads}: Contaminant mass adsorbed on sorbent (mg or ng)

m_{ads}: Contaminant mass adsorbed on the membrane (mg or ng)

$m_{ads(filter)}$: Contaminant mass adsorbed on syringe filter (mg)

$M_{ads(tube)}$: Contaminant mass adsorbed on centrifuge tube (ng)

M_d: Mass of the particles in the deposit layer (mg)

M_p: Mass of the particles in the deposit layer (mg)

N: stirring rate (revolution/s)

n: Freundlich empirical constant

$_n$: Number of the permeate samples

pH_{zpc}: Zero point charge of sorbents

pK_a: Dissociation constant

Q_e: Mass of contaminant adsorbed per mass of sorbent at the equilibrium (mg/g)

Q_t: Mass of contaminant adsorbed per mass of sorbent at the time (mg/g)

R: Removal (%)

r: Gas low constant (8.314 x 10^3 kg m^2/s^2 K kg mol)

R_a: Average roughness (nm)

R_{cp}: Resistance due to the concentration polarization (1/m)

R_d: Resistance of the particle deposit (cake) (1/m)

Re: Reynolds number

R_f: Foulant resistance (1/m)

R_m: Hydraulic resistance of the membrane (1/m)

r_p: Particle radius (m)

R_q: Root-mean square roughness (nm)

r_{sc}: Radius of the stirred cell (m)

Sh: Sherwood number

T: Absolute temperature (K)

t: Time (min)

V_B: Brownian diffusion velocity (m/s)

V_c: Volume of concentrate (L)

V_d: Volume of the particle deposit (L)

V_D: Viscous drag force velocity (m/s)

V_f: Volume of feed solution (L)

V_{fi}: Volume of filtrate sample (L)

V_i: Initial solution volume (L)

V_L: Inertial lift velocity (m/s)

V_p: Volume of the permeate (L)

V_{Pi}: Volume of sample permeate for specific sample identity (L)

V_S: Shear-induced diffusion (m/s)

z: Number of ions formed if the solute dissociates

List of Greek Letters

ρ: Density of water (kg/m^3)

ρ_p: Density of the particle (kg/m^3)

ε: Porosity (void)

δ: is the deposit thickness (m) and δ_d is the maximum deposit thickness (m)

δ_b: Boundary layer thickness (m)

δ_m: Membrane thickness (m)

α: Specific deposit (cake) resistance (1/m^2)

π: Osmotic pressure (Pa)

$\Delta\pi$: Osmotic pressure difference (bar)

ΔP: Trans-membrane pressure difference (bar)

ν: Kinematic solvent viscosity (m^2/s)

ψ: Function of the detailed flow characteristics

γ: Share rate (1/m)

μ: Solvent dynamic viscosity (Pa.s, N.s/m^2 or kg/m.s)

f(φ): Function of the particle volume fraction

φ: Particle volume fraction

1   Introduction

This thesis proposes two novel hybrid sorbent-ultrafiltration (UF) systems, based on the integration of specific sorbent materials into UF, in order to remove hormones and fluoride from drinking water.

Consumption of drinking water with fluoride concentrations exceeding World Health Organization (WHO) guideline, 1.5 mg/L, causes dental and skeletal fluorosis in humans, especially in infants [1, 2]. Fluoride is a worldwide problem occurring in many countries, most of which are developing countries [3, 4]. The scale of the problem is larger in developing countries as the drinking water sources are limited and there is no access to removal technologies for fluoride.

Hormones are detected in effluents of wastewater treatment plants (WWTPs) and surface waters in ng/L concentrations [5]. Even present at such low concentrations, hormones can interfere with the endocrine regulatory systems of humans and animals causing feminization of male fish [6, 7] or increased risk of cancer in humans [8, 9]. In near future, new water quality standards are expected to be introduced to regulate the hormone concentrations in effluent and drinking waters. In this regard, there is a need to explore efficient treatment technologies for hormone removal from water.

Current techniques available to remove hormones or fluoride from water either do not adequately remove these contaminants from water or require high energy supply. Worldwide increasing concern over water and energy scarcity drives the search for sustainable water treatment technologies especially in terms of energy consumption.

Sorption seems to be the most cost-effective removal technique for both contaminants. There are various sorbent materials with high sorption affinity. Nevertheless, large scale water treatment applications using these sorbent materials are limited to fixed bed reactors. Within the last decade, hybrid sorbent-low pressure membrane filtration systems are proposed as an alternative technology for the removal of trace contaminants such as arsenic [10], mercury [11], copper, cobalt,

nickel, zinc [12], lead [13], cadmium [14], soluble organics [15] and boron [16] from drinking water or wastewater.

A hybrid sorbent-membrane system has several advantages over a fixed bed sorbent reactor which are summarized here. A hybrid sorbent-membrane process gives the opportunity of using sorbent materials in the "powder" form which provides a large specific surface area for sorption. The usage of very fine sorbent particles in fixed bed reactors is not possible because of the increased pressure drop with smaller particle sizes [17, 18]. Pressure drop occurs in membrane systems as well, due to the particle deposition on the membrane surface. Nevertheless, the pressure drop can be much less with membrane systems if the thickness of the particle deposit on membrane surface is much smaller than the height of the fixed bed composed of particles. Additionally, by adjusting the operational parameters in a membrane system, the settling of the particles on the membrane surface and thus the pressure drop can be avoided. Koltuniewicz et al. [17] compared system performance in terms of pressure drop and cost for a fixed bed column and a sorbent-membrane system with the same size sorbent particle of 1 μm. The results show that the pressure drop in the membrane system is two orders of magnitude less than that in the fixed bed system. The difference in the pressure drop results in a total operational cost for the membrane system being three orders of magnitude less than the fixed bed system. In the same study [17], a comparative evaluation also shows that the membrane system is cheaper than the fixed beds for sorbent particles with a size equal to or less than 300 μm. The capital cost of a fixed bed reactor is likely to be less than the sorbent-membrane system as the membrane modules will add a considerable amount of cost, about \$1300-2000/m^2 [19] to the system. However, operational cost is expected to more than compensate the capital cost in long term application when particles less than 300 μm are utilized in the sorbent-membrane system. UF systems also give the possibility of removing suspended solids from water, if necessary. Moreover, unlike fixed bed reactors, ultrafiltration systems can disinfect water by removing bacteria and virus from water with the right pore size membranes.

Combination of activated carbon with membrane filtration is the only hybrid process proposed for the removal of hormones up to date. A powdered activated carbon (PAC)-Microfiltration (MF) process has been shown to be effective in removing estrone (E1), a steroid hormone, from water [20]. In another study, the removal of estradiol (E2), with a PAC-UF membrane is investigated in the presence of natural organic matter [21]. The source and characteristics of these hormones are detailed in Sections 2.1.1 and 4.2, respectively. The E2 removal with a PAC-MF system is hindered by the deposition of PAC on the membrane surface and the deposition is influenced by the intensity of mixing and the hydraulic retention time [22].

In this study, for the hybrid sorbent-UF system, polystyrene nanoparticles are selected as sorbent materials for the removal of hormones. The PS nanoparticles are employed because first they provide a large surface area and second they are uniform, non-porous, can easily be manufactured in different sizes and can be functionalized. Moreover, they are chemically resistant enabling regeneration of the used materials. Hormone sorption capacity of polystyrene nanoparticles is not known and polystyrene nanoparticle-UF system is a novel hybrid system which has not been studied before.

It is the first time that a hybrid sorbent-UF system is proposed and studied for fluoride removal in this study. Laterite and bone char are the two sorbent materials selected for this hybrid system. The selection of these sorbents is based on three criteria which are accessibility, cost and the possibility of regeneration of the sorbents with the prospect of system application in developing countries. Although these sorbents have been studied for their fluoride sorption capacity, filtration of these sorbents with UF membranes has not been systematically studied before.

For the design of such hybrid systems, determination of certain parameters is essential. These design parameters, which are studied in this study, are:

- sorbent sorption capacity
- optimal sorbent size/concentration

- optimal contact time

- contaminant concentration

- solution chemistry (pH) and

- the integration method of the sorbent.

Determination of some of these parameters is the main research challenge in this study. For example, the use of smaller size sorbent materials is desired as they provide a larger surface area for the contaminant sorption. On the other hand, smaller size particles are not desired in ultrafiltration as these particles are likely to cause larger hydraulic resistance in the system and thus influence the membrane performance adversely. Other design parameters such as sorbent concentration can cause similar paradox in the decision process of optimum process parameters. Therefore, determination of an optimum sorbent size or concentration for a hybrid system is one of the main objectives in this study. The solution chemistry is another parameter which can largely influence the chemical and physical properties of the sorbents as well as the membrane characteristics. The changes in characteristics of sorbent and membranes alters the sorbent-contaminant and sorbent-membrane interactions which are investigated within the scope of this study.

1.1 Sorption in a Nutshell

Sorption occurs when the molecules (sorbate) of a fluid bind to the surface of a solid material (sorbent) [23]. The following steps can summarize how sorption takes place for a porous sorbent (adapted from [24]):

- external mass transfer: the diffusion or transport of sorbate to the external surface of the sorbent from bulk solution across the boundary layer around the sorbent particle.

- intra-particle diffusion: the transfer of the sorbate ions into the porous structure of the sorbent

- sorption of the sorbate on the active sites of the sorbent by the means of ion exchange, molecular or intermolecular interactions

All these steps can be influenced by many factors, such as the chemistry of the sorbate, physical and chemical characteristics of the sorbents and operational parameters such as the solution pH, temperature, initial sorbate concentrations.

Determination of sorption equilibrium is very important as it provides an understanding of the sorption kinetics and the amount of sorbate accommodated by a sorbent [25]. Various sorption isotherms are used to describe the sorption equilibrium data of different sorbents and systems. Langmuir [26] and Freundlich [27] are the two commonly used isotherms. Sorption kinetics and capacity determine the efficiency of a sorbent material [25] and both can be influenced by many factors. Contaminant (sorbate) and sorbent characteristics influencing the physical and chemical interactions responsible for the sorption process are summarized in Table 1-1.

Table 1-1. Contaminant and sorbent characteristics influencing the sorption

	Characteristics	Important for/as
Contaminant	Hydrophobicity as octanol-water partition coefficient (K_{ow})	Intermolecular interactions
	Dipole moment as Debye (D)	Intermolecular interactions
	Available functional groups	Intermolecular interactions
	Disassociation constant (pK_a)	Intermolecular and mainly electrostatic interaction
	Solubility (g/L)	Above the solubility limit, sorption is hindered
	Molecular size/weight (nm or g/L)	Mobility and diffusivity into sorbent pores
Sorbent	Surface area or micro/macro pore volume (cm^2/g or mL/g)	The available active sites for sorption
	Hydrophobicity as contact angle (°)	Intermolecular interactions
	Available functional groups as group density	Intermolecular interactions
	Surface charge as zero-point charge (pH_{zpc})	Electrostatic interactions

1.2 Ultrafiltration

In an ultrafiltration (UF) process, a solution is pressurized along a membrane filter which is a selective barrier. This barrier restricts the transport of certain materials such as particles and colloids but allows the solvent to pass through. The restriction of the transport depends on the membrane properties and the physical and/or chemical characteristics of the materials in the solvent. Ultrafiltration processes are successfully used in water and wastewater treatment as well as industrial applications such as fruit juice production. The membranes can be made of organic or inorganic materials. Polymeric membranes are the most common membranes in waste/water applications [28].

Size exclusion, sorption and charge repulsion are the three main mechanisms playing a role in UF. UF membranes are classified based on their selectivity of particles or solutes of different size range. Depending on the preparation method, each membrane may have a single pore size distributed uniformly or a distribution of different pore sizes. In UF, membranes with an average pore size varying between 1 and 100 nm are used. UF membranes are usually identified with their Molecular Weight Cut Off (MWCO) in kDa units. The MWCO of a membrane indicates the molecular weight (MW) at which 90% of compounds are rejected by that membrane based on a size exclusion mechanism [28]. The compounds with MW smaller than the MWCO of the membrane are expected to pass through the membrane and appear on the permeate side.

UF membranes are generally used to separate the particles or solutes with MW ranging from 10^4 to 10^6 [28]. Particulates, macromolecules, bacteria and viruses can be removed from water by UF membranes due to their relatively large MW. Figure 1-1 presents the application range of UF membranes in comparison to other membrane processes. The figure also displays the size range of contaminants (hormones and fluoride), sorbent materials (PS nanoparticles, laterite and bone char) in comparison to MWCO of UF membranes used in this study. The MW of fluoride and hormones being 19 g/mol and 250-350 g/mol, respectively are too small

compared to the MWCO of the UF membranes (1-100 kDa: 1000-100,000 g/L) used in this study. Therefore, any retention of these contaminants by UF membranes based on size exclusion is not expected. The role of the sorbent materials integrated into UF system becomes significant as the removal is based on their sorption capacity for hormones and fluoride. Sorbent particles are expected to be fully separated with UF as the size of the sorbents is larger than the pore size of the membranes.

Contaminant/ Sorbent Size					
μm	0.001	0.01	0.1	1.0	10
nm	1.0	10	100	1000	10,000
MW (g/L)	100 200 1000 100,000	500,000			
Contaminants	Aq. salt / Metal Ion / F / Hormones	Virus / Proteins		Bacteria	
Sorbents			PS-Nanoparticles	Laterite and Bone char	
Membrane Process	Nanofiltration / PL-UF / Inge	Ultrafiltration / Zenon	Microfiltration		
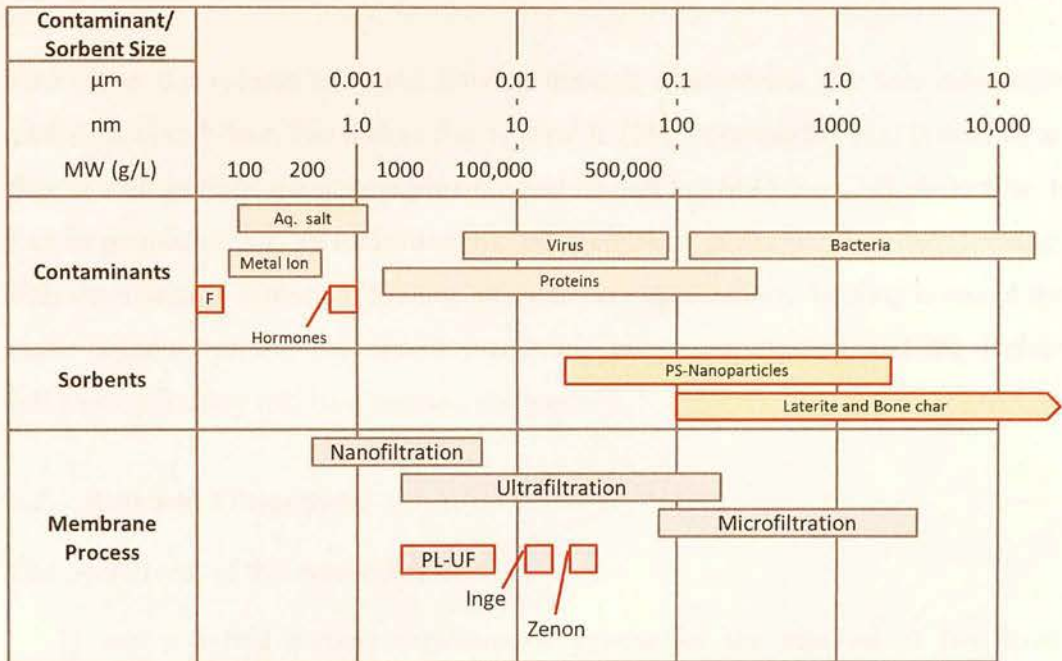
Figure 1-1 Application range of ultrafiltration in comparison to other membrane processes (modified from [28]. F: Fluoride ion, Membranes used in this study: PL-UF: PL series flat sheet UF membranes (1-100 kDa), Inge: dead-end UF module, Zenon: submerged UF module.

Besides the sorption on sorbent particles, UF membrane polymers can also act as a sorbent in the hybrid system. Sorption of hormones on UF membrane is reported in several studies [29-33]. To avoid any complexity, UF membranes made of regenerated cellulose are selected as minimal hormone sorption on such membranes is expected. Sorption of fluoride on membrane polymers has not been reported.

Selectivity and the liquid flow rate through the membrane are the two parameters determining the performance of a membrane process [28]. The selectivity of a membrane is usually expressed in terms of retention [28] which can solely be attributed to the size exclusion mechanism. In this study, the term removal is used

7

instead of retention, since the hybrid system relies on sorption rather than size exclusion of the contaminants. Contaminants removal percentage (R) is calculated as in Equation 1-1, where C_p and C_f are the contaminant concentrations (mass/volume) of permeate and feed, respectively.

$$R = \left(1 - \frac{C_p}{C_f}\right)100$$

1-1

Flux (J) is the volume of liquid flowing through a membrane per unit membrane surface area and time. The unit of flux is $L/m^2.h$. [28]. Permeability (L_v) is defined as flux at a given trans-membrane pressure and its unit is $L/m^2.h.bar$ [34]. A decline in flux or permeability is an indication that the membrane performance is deteriorating. This deterioration is termed `fouling` in membrane applications. Fouling is one of the major factors limiting the use of membrane processes. Fouling and the factors influencing fouling will be discussed in Chapter 2.

1.3 Aim and Objectives

The overall aim of this research is to:

1) test a hybrid sorbent-ultrafiltration system for the removal of two trace contaminants:

   - hormones
   - fluoride

2) evaluate the performance of each system in terms of its:

   - contaminant sorption capacity
   - membrane permeability

The overall system performance is evaluated by comparing:

   - the hybrid PS nanoparticle UF system for hormone removal to a NF/RO system

8

- the hybrid laterite-UF and hybrid bone char-UF systems for fluoride removal to each other.

1.4 Outline of the Thesis

The schematic outline of the thesis is presented in Figure 1-2. In Section 2.1 and 2.2 a comprehensive literature review is provided on the occurrence, adverse health effects and current removal technologies available for hormones and fluoride. In Section 2.3 and 2.4, fouling in UF is discussed in relation to the characteristics of the particles and membranes and operational parameters. General materials and methods used in the experimental study are identified and described in Chapter 3.
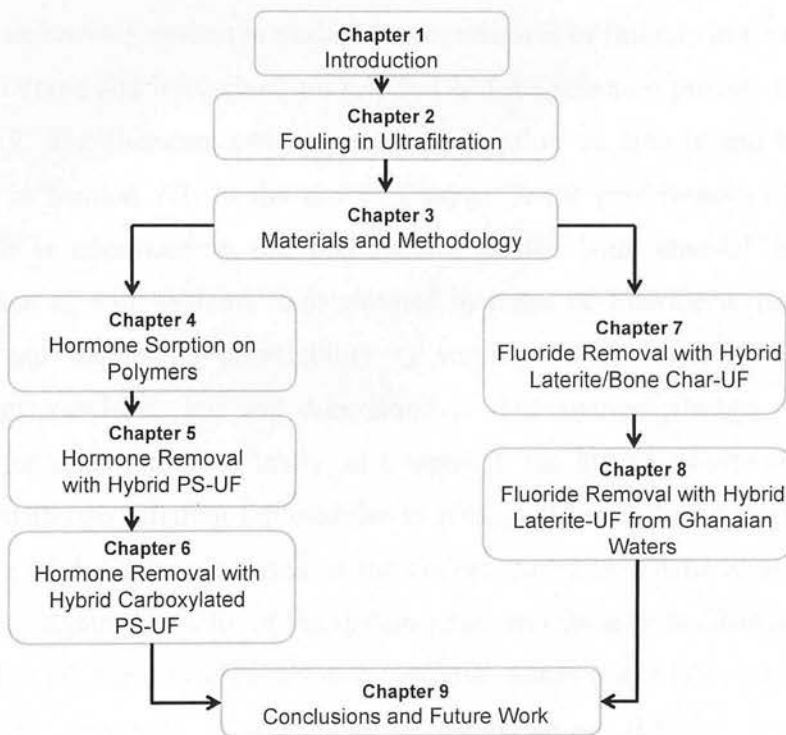
Figure 1-2 Schematic outline of the thesis

Considering the large differences in the nature of the contaminants (fluoride and hormones) and the sorbents which are selected for the removal of each contaminant, the thesis can be split into two parts: one part for hormones and the other for fluoride. The removal of hormones is explored in Chapters 4, 5 and 6 whereas Chapter 7 and 8 are devoted to fluoride removal.

Chapter 4 covers the literature on the sorption of hormones on polymeric materials as well as an experimental study on the comparison of various commercial polymers for their hormone sorption affinity. In Chapter 5, the performance of hybrid polystyrene (PS) nanoparticle-UF system in terms of hormone removal (sorption) and membrane permeability is investigated in terms of PS particle size, concentration, hormone type, solution pH and the integration method of PS nanoparticles. The selection of the PS nanoparticles is explained in Section 5.2. Chapter 6 elucidates whether the carboxylate functional groups of PS nanoparticles have an influence on the hormone sorption capacity and the membrane permeability of the hybrid system. The selection of the functional group for the PS particles is detailed in Section 6.2.

A hybrid sorbent-UF system is studied for the removal of fluoride in Chapter 7. Two sorbents, laterite and bone char, are selected and the selection process is detailed in Section 7.2. The literature covering fluoride sorption on laterite and bone char is compiled in Section 7.3. In the rest of Chapter 7, the performance of the hybrid laterite-UF is compared to the performance of the bone char-UF system. The performance of both systems is determined in terms of fluoride sorption kinetics, capacity and membrane permeability at varying initial fluoride concentration, solution pH, sorbent size and concentration. The optimal design parameter is obtained for each variable. Finally, in Chapter 8, the hybrid laterite-UF system is designed with two different UF modules to remove fluoride from Ghanaian waters. The design of the system is based on the optimal parameters determined in Chapter 7. Fluoride sorption capacity of the system tested in Ghana with Ghanaian waters is compared to the capacity obtained with synthetic waters under laboratory conditions in Edinburgh, Scotland. The removal of metals from Ghanaian waters is also investigated with the hybrid system and the removal percentages are compared for two different UF modules. Lastly the performance of the two different UF modules with Ghanaian surface and ground waters is studied in terms of membrane fouling.

2 Trace Contaminants-Fouling in Ultrafiltration

2.1 Trace Contaminants: Occurrence and Adverse Health Effects

2.1.1 Hormones

The hormones can be classified in two categories; one being the natural steroid hormones secreted by human and animal bodies and the second being the synthetic hormones manufactured chemically. Steroid hormones including progestogens, glucocorticoids, ineralocorticoids, androgens and estrogens, are biologically active compounds and secreted by adrenal cortex, testis, ovary and placenta in human and animal. Estrone (E1) is an example of estrogens and the daily excretion of E1 for males, menstruating females, menopausal females and pregnant women are given as 3.9, 8, 4 and 600 µg respectively [35]. Ethynylestradiol (EE2) and mestranol (MeEE2) are examples of synthetic steroids which are taken into body as contraceptives [36]. The excreted hormones end up in either wastewater treatment plants (WWTP) or directly in surface waters. The pathways of the hormones in environment reaching the surface and ground water sources are presented in Figure 2-1. Current wastewater treatment techniques are not able to remove hormones from water adequately. Hence, hormones are detected in WWTP effluents and surface waters in concentrations of nanogram per litre (ng/L) [5]. Even at such low concentrations, adverse effects on living organisms are possible [5]. Feminisation of male fish [6, 7], decrease in sperm counts, increasing risk of testicular cancer and male infertility in fish [9] has been linked to the intake of estrogens via food or drinking water.

The hormones are known to be one of the most dangerous trace contaminant groups as their potential to disrupt the endocrine activities of the living organisms is high [37]. The hormones with endocrine disrupting potential, are mainly estrogens and contraceptives including 17β-estradiol (E2), estrone (E1), estriol (E3), 17α-ethynylestradiol (EE2) and mestranol (MeEE2). Especially E1 and E2 are classified among the high priority trace contaminants; E1 being the metabolized form of E2. E1

and E2 are reported to have higher magnitude estrogenic activity compared to some other endocrine disrupters [38, 39].
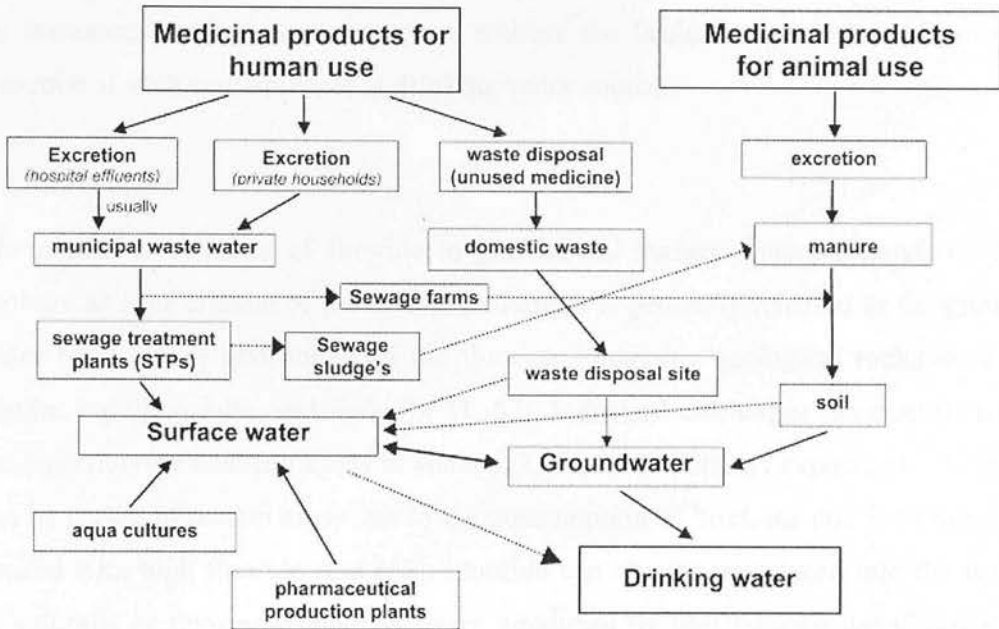
Figure 2-1 The pathways of hormones in environment (taken from [40])

The presence of hormones in water sources is a worldwide problem. The estrogenic compounds of 17β-estradiol (E2), 17α-estradiol, E1 and 17α-ethinylestradiol (EE2) were detected in Dutch surface waters up to 6 ng/L and in ng/L levels in WWTP effluents [41]. In China, E1 and E2 were found in concentrations up to 79 and 8 ng/L, respectively in river waters [42]. Steroids were detected in WWTP effluents in other countries at a range of concentrations up to 76 ng/L of E1 in UK [43], 70 ng/L of E1 in Germany, 64 ng/L of E2, 42 ng/L of EE2 in Canada [44], 18 ng/L of Estriol (E3) in Italy [45]. Synthetic oral contraceptives, which are a group of synthetic hormones were also detected in the WWTP effluents in many countries even at higher concentrations than natural steroids [46]. For example Norethisterone was found in concentrations up to 188 ng/L in Malaysia [47] and Mifepristone up to 195 ng/L in China [48]. Apart from the surface waters, the presence of steroids in ground water is a serious health concern considering that ground water is a direct source of drinking water in some countries. For example, E2 was detected in Arkansas aquifers in USA up to 66 ng/L [49].

Recent rise in public awareness resulted in more studies to develop treatment processes for removing endocrine disrupting compounds from water [50]. Exploring sustainable treatment processes and/or improving the efficiency of the existing ones for hormone removal is necessary to address the health concerns arise from the presence of such contaminants in drinking water sources.

2.1.2 Fluoride

The natural occurrence of fluoride in ground and surface waters depends on the geology and the climate of the location. Fluoride is generally released to the ground water by the slow dissolution of the fluorine containing geological rocks such as granite, basalt, syenite, and shale [3, 51, 52]. Industrial discharges can contribute to the high fluoride concentrations in water [53, 54]. Additionally, exposure to fluoride can be higher in certain areas due to the consumption of brick tea and food dried or cooked with high fluoride coal [55]. Fluoride can also be introduced into the water by rainfalls as fluorine containing gases, produced by coal burning can dissolve in rain water [3].

Fluoride concentration in drinking waters between 0.5 and 1.5 mg/L is the narrow range which is essential for healthy bones and teeth [1, 2]. Drinking water containing less than 0.5 mg/L fluoride can cause cavities in the teeth. Long term ingestion of high doses of fluoride (1.5-4 mg/L) results in mottling of the teeth called dental fluorosis. Fluoride concentrations above 4 mg/L can cause embrittlement of the bones which is called skeletal fluorosis and concentrations above 10 mg/L is linked to crippling fluorosis [1, 2]. The severity of the diseases depends on the age as well as the diet of the person. Apart from the dental and skeletal disorders, other health effects such as cancer, infertility, reproductive disorders, brain damage, and thyroid disorder have been linked to the excessive fluoride ingestion [56]. Considering the health effects, WHO set a guideline value of 1.5 mg/L in 1984 and since then the same value is used in WHO guidelines [55]. The regulation standards of a number of countries and organizations for fluoride concentrations in drinking water are given in Table 2-1.

Table 2-1 Fluoride regulation standards in drinking water (adapted from [3] except *[57])

Country/Organization	Guideline	Concentration (mg/L)	Comments
WHO	Guideline value	1.5	1984 guideline
U.S. EPA	Primary standard	4	Enforceable
U.S. EPA	Secondary standard	2	Not enforceable (for prevention of dental fluorosis)
EC	Maximum permissible value	1.5	1998 regulations
Canada	National standard	1.5	
India	National standard	1	Lowered from 1.5 mg/L in 1998
China	National standard	1	
Tanzania	National standard	8	Interim standard
Ghana*	National standard	1.5	

Water sources containing fluoride concentrations above the WHO standard (1.5 mg/L) have been located in many parts of the world including USA, Argentina, Canada, China, Israel, Japan, Norway, Nigeria and Saudi Arabia [3, 4]. The most of the worldwide locations where the fluoride concentrations in groundwater exceed the WHO standard (1.5 mg/L) is given in Figure 2-2.
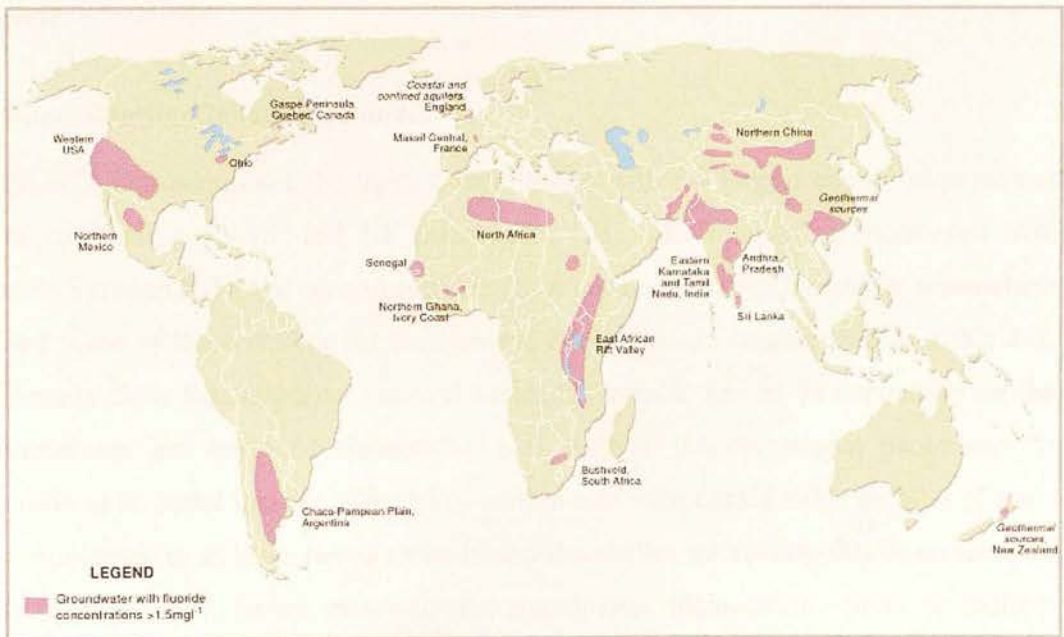
Figure 2-2 Groundwater sources which has fluoride above WHO Standards (1.5 mg/L) (taken from [3])

Although it is not very common, in some regions, surface waters also contain very high fluoride concentrations. For example, extremely high fluoride concentrations were detected in Kenyan and Tanzanian soda lakes up to 2800 mg/L [58] and 690 mg/L [59], respectively.

Considering that many water sources with fluoride concentrations above the WHO guidelines are within developing countries, local and sustainable solutions are needed to reduce the fluoride levels to the guideline value and prevent the related health effects.

2.2   Technologies to Remove Trace Contaminants from Water

2.2.1   Technologies for Hormone Removal

Hormones are physiologically active contaminants with small molecular weight and they occur in small concentrations (ng/L) in water. These characteristics cause challenges to remove hormones from water. Nanofiltration/reverse osmosis, advanced oxidation and sorption processes show potential to remove hormones from water effectively.

Nanofiltration/Reverse Osmosis

NF/RO membranes are the tightest membranes with the largest energy requirement in comparison to MF and UF membranes [28]. The removal of hormones with nanofiltration (NF) and reverse osmosis (RO) has been studied by several researchers and some of these studies for four natural hormones are summarized in Table 2-2. Results show that hormone removal varies between 8 and 99 % depending on the membrane and hormone characteristics as well as the operational parameters. It needs to be noted that the disposal of concentrate with considerable amount of trace contaminant is an issue raised recently and the studies addressing this issue are very limited [60, 61]. Reuse, removal of contaminants, incineration, direct or indirect discharge in surface water, direct or indirect discharge in groundwater and discharge on a landfill are the possibilities reviewed to treat or discharge the concentrate of the pressure driven membrane processes [61].

Although some of the NF/RO membranes can effectively eliminate specific hormones from water, energy requirement of these membrane systems is ~1 kWh/m^3 [62] which is relatively high in comparison to the energy requirement of UF systems (0.1-0.2 kWh/m^3) [63, 64]. Another advantage of an UF over NF/RO is that UF system offers a specific separation of target contaminants whereas NF/RO systems eliminates many divalent or single ions apart from the targeted trace contaminants depending on the pore density.

Table 2-2 Published data for E2, E1, T and P removal and membrane permeability for NF/RO systems,* taken from [65] as the permeability data is not provided

Hormone Type	Membrane	Hormone Removal (%)	Permeability (L/m^{2}hbar)	Reference
17β Estradiol (Estradiol, E2)	XLE (RO)	83	4	[66]
	SC-3100 (RO)	29	1	
	X20 (RO)	96	3	[67]
	TS 80 (NF)	37	5	
	NF 270	15	16	
	NF 270	85	15	[68]
	NF 200	64	4*	[69]
	ESNA (NF)	38	7	[32]
Estrone (E1)	NF 200	80	4*	[69]
	DL (NF)	15	3	[70]
	CK (NF)	8	8	[70]
	ESNA (NF)	42	7	[32]
	X20 (RO)	97	3	[67]
	TS 80 (NF)	39	4	
	NF270	19	21	
	TFC-ULP (NF/RO)	96	7	[71]
	TFC-S (NF)	98	11	
	TFC-SR1 (NF)	93	11	
	TFC-SR2 (NF)	79	15	
	X-20 (RO)	99	4	
	ACM-4 (RO)	86	5	
	XN-40 (NF)	73	9	
	TS-80 (NF)	83	5	
Testosterone (T)	NF 200	62	4*	[69]
	ESNA (NF)	60	7	[32]
Progesterone (P)	NF 200	98	4*	[69]
	ESNA (NF)	65	7	[32]

Advanced Oxidation Processes

Advanced oxidation/ozonation processes (AOPs) are suggested as a promising technology for the removal of endocrine disrupting compounds including hormones [50, 72] and have comparable energy consumption of ~0.1 kWh/m^3 [62] to UF systems. AOPs have been studied as a removal technique for both natural and synthetic hormones [73-85]. Studies show that undetectable concentrations for most of the hormones are achieved after the treatment depending on the ozone/hydrogen peroxide/ultraviolet dosage and the contact time. Nevertheless, investigation of the estrogenic activity of the treated water with AOPs was not conducted in many of the studies published [72]. Formation of by-products occurs during the oxidation reactions [73, 75, 86] and sometimes these by-products can be more toxic than the parent compound [87]. Due to the presence of these by-products, a residual estrogenic activity still remains in the treated water [50, 88, 89].

Sorption

Sorption of hormones on surfaces is very common. High affinity of polymeric materials for hormones is known especially because of the studies conducted on the removal of hormones by polymeric membranes [67, 90-92]. Adsorption is one of the mechanisms responsible for hormone removal in membrane filtration [93]. Characteristics of hormones and their sorption on polymeric materials will be reviewed and discussed in detail in Chapter 4.

Adsorption of hormones on novel sorbents has also been reported. Estrogens were found to sorb on carbon nanomaterials to a high extent [94, 95]. Cai *et al.* [96] suggested that multiwalled carbon nanotubes can extract endocrine disrupting compounds more efficiently than C_{18} which is very commonly used in solid phase extraction (SPE) of micropollutants. Implementation of such nanomaterials in real water treatment processes is currently not common as the materials have high capital cost and the separation of the materials from water is challenging due to their nano-size.

Studies using solely sorption mechanism as a removal technique for hormones are very limited. Adsorption with activated carbon columns has been proposed and the affinity of activated carbon for hormones is studied by several researchers [97-100]. The sorption capacity achieved for three different activated carbons with 100 ng/L initial E2 concentration is between 43 and 47 ng/g [97]. In another study, the sorption capacity of activated carbon for E1 and E2 is reported in mg/g values; such a high sorption capacity can be attributed to large initial hormone concentrations (mg/L) [98]. Although activated carbon has high affinity for hormones, its cost effectiveness needs to be studied further as the thermal regeneration of the activated carbon can be highly energy consuming [91]. Moreover, the presence of natural organic matter influences the hormone sorption capacity of activated carbon [91, 101].

2.2.2 Technologies for Fluoride Removal

NF/RO, electro/donnan dialysis, coagulation/precipitation and sorption processes are the main technologies which are used for defluoridation of water [53, 54, 102].

Nanofiltration/Reverse Osmosis

Several NF/RO systems can bring fluoride concentrations down to the values less than 1.5 mg/L [103-105]. The initial fluoride concentration range studied in these publications is within 1.5-5 mg/L. The removal of fluoride with NF membranes depend on applied pressure, solution flux and initial fluoride concentration [106]. Similarly, Tahaikt et al. [107] reported that membrane configuration and initial fluoride content can influence the fluoride removal efficiency in NF. The fluoride removal efficiency of NF membrane varied from 78 to 95 % depending on the nature of the solution treated [108]. At higher initial fluoride concentrations, NF/RO systems may not be as effective depending on the membrane type and operational parameters. For example, two different MWCO NF membranes, NF90 and NF400 were tested for their fluoride removal capacity with solutions containing four different concentrations varying between 1.8 and 20 mg/L [109]. NF90 membrane successfully brought the fluoride concentrations down to values less than 1.5 mg/L

for all initial concentrations studied whereas NF400 failed to achieve 1.5 mg/L for all initial concentrations except 1.8 mg/L. In another study with 460 mg/L initial fluoride concentration 98% removal was achieved with an RO system with permeate concentrations above 1.5 mg/L [110]. Additionally, implementation of such systems in developing countries is not sustainable due to the high energy requirement.

Electro/Donnan dialysis

Several studies performed on fluoride removal with electrodialysis show that it is an effective system which can bring the fluoride concentration down to less than 1.5 mg/L for a variety of initial fluoride concentrations of 20.6 mg/L [111], 10 mg/L [112] and 2.2 mg/L [113]. Defluoridation efficiency in electrodialysis is influenced by voltage, temperature, flow rate [114] as well as current density [112]. Similarly Donnan dialysis can remove fluoride bringing the concentrations down to the acceptable levels [115]. Initial fluoride concentration, pH and the presence of counter-ions seem to influence the fluoride removal with Donnan dialysis [116]. Similar to NF/RO systems, the high energy requirement limits the application of such a system.

Coagulation/Precipitation

Lime, alum, magnesium and barium oxide are the commonly used coagulants for fluoride removal [54, 117-119]. These coagulants react with fluoride and form insoluble fluoride complexes which precipitate out [102, 120]. Nalgonda technique, which involves combined use of lime and alum, is used in real applications in developing countries [121, 122]. Fluoride can also form soluble aluminium complexes which do not precipitate and this results in removal of only a small portion of fluoride [102]. Therefore, this process is usually not able to bring the concentrations down to the guideline values [102, 120].

Sorption

Sorption is one of the mostly used and studied defluoridation technique as it is cost-effective and highly accessible [54] especially in developing countries. The sorbents

which have a potential for defluoridation are activated alumina [53, 54, 120] and bone char [120]. Literature on fluoride sorption capacity of 102 sorbent materials is reviewed and compiled by Bhatnagar et al. [53]. A direct comparison of sorption capacity between the sorbents was challenging as the sorbent characteristics and operational parameter vary a lot depending on the study. The main findings of the literature review, conducted by Bhatnagar et al. [53], are given below:

- Fluoride adsorption by activated alumina is an established treatment technique and classified as the best demonstrated available technology by WHO and USA EPA. However, it is expensive and its performance is influenced by pH and the presence of other ions. The leachate of aluminium is a health concern as aluminium is a neurotoxin.

- Rare earth oxide-based adsorbents have high fluoride sorption capacity however in some cases they are considered as expensive materials.

- Sorption potential of carbon-based materials is relatively low however, information in terms of column operations and/or pilot scale is lacking.

- Clays are studied to a great extent among various natural materials. Difficulty in regeneration and low sorption efficiency with high fluoride concentrations are reported.

- The use of biosorbents, especially chitosan and its derivatives/composites, for defluoridation has been studied as chitosan is a natural, environmentally friendly and low cost sorbent material. However, the sorption capacity is limited and its performance is highly influenced by the solution pH.

- Waste materials containing metal oxides are seen as alternative low cost sorbents; however, the leaching of toxic metals from the materials requires a special attention.

- Recently studied sorbents such as synthetic layered double hydroxides/hydrotalcite-like compounds and nanosorbents show high defluoridation capacity, however information on their performance under continuous operation is limited.

- Detailed studies on the regeneration capacity of sorbent materials are required for the economic feasibility of the sorption process.

- Testing the materials under field conditions is highly necessary for the determination of the appropriate technology/sorbent media for real applications.

- Finally, the practical utility of promising sorbents on a commercial scale is open to exploration.

High capacity and selectivity sorbents are commonly used in fixed bed column reactors [120]. The strength of the particles is an important parameter for the design of the fixed bed reactors, as poor strength can result in occupation of the voids with crumbled particles. Similarly the particle size and shape plays a big role in the design of the fixed beds [123]. Generally, the sorbents are in the form of fine powder and cannot be applied in fixed bed columns as they are too small in size and not in granular shape [124, 125]. Having very fine particles in a fixed bed reactor can cause high pressure drops and undesired fluidization where a physical adsorption probably becomes negligible [18]. On the other hand granulation of the fine particles can be a solution for the application of fine sorbents in fixed bed reactors for fluoride removal [125]. Possible precipitation in the fixed bed reactors can result in accumulation of the precipitate in the voids of the bed and again high pressure drop. For example, in fixed bed reactors packed with granular calcite formation of lumps in a fixed bed is observed [126]. Moreover, the mass transfer coefficients is very poor due to the low liquid velocity [127].

Although various sorbents show a good potential for defluoridation of water, practical application of these sorbents for large scale applications is very limited.

2.3 Fouling in Ultrafiltration

This section describes the concepts and the parameters influencing membrane performance in terms of flux or permeability. The decline in these parameters is an indication that the performance is deteriorating. This deterioration is usually called

fouling which is one of the major factors limiting the use of the membrane processes. Membrane fouling occurs when there is a physical or chemical interaction between the particles and the membrane. These interactions are explained further in the following sections.

In this study, a hybrid sorbent-UF system is proposed for the removal of hormones and fluoride. Due to the small molecular size of contaminants relative to UF pore size, filtration of hormones and fluoride are not expected to cause fouling in the system; this is detailed in Section 1.2. In contrast, sorbent materials will possibly be the cause of fouling and influence the system performance. Hence, the literature is reviewed for colloidal particle ultrafiltration with the focus on nano/micro particles.

In a membrane process where a solution of particles is filtered, different phases can be observed in the time dependent flux decline. These phases are described differently by different researchers [128-131] but in general include:

- An initial flux decline due to the compaction of the membranes

- A sharp decline due to the concentrations polarization (if present)

- A long term steadier flux decline as the particles deposit on the membrane surface. Further decline can be observed due to the conformation of the particles on the surface.

2.3.1 Concentration Polarization

The rate of the particle transport in the bulk phase close to the membrane surface directly affects and determines the overall membrane performance. The convective transport of the particles to the surface occurs with the pressure driven fluid flow. If the particles are partially or fully retained by the membranes, they accumulate at the surface. Concentration polarization is the term given for this accumulation process and it is a consequence of filtration process with the membranes. As the particles accumulate a concentration gradient occurs between the bulk solution and membrane surface. The particle concentration increases from the one in bulk solution to the one in the solution at the surface of the membrane along concentration boundary

thickness. The concentration gradient along the concentration boundary thickness generates a diffusive back transport of the particles away from the membrane surface. Under steady conditions, a balance occurs between the convective and the diffusive particle transport rates and this balance results in the following Equation 2-1.

$$J_v = k_s \ln \frac{c_m - c_p}{c_b - c_p}$$
2-1

Where J_v is the permeate flux or velocity (m/s), k_s (D/δ_b) is the mass transfer coefficient of the particle and in the boundary layer (m/s), D is the particle diffusion coefficient (m^2/s), δ_b is the boundary layer thickness and c_m, c_p, c_b are the particle concentrations on the membrane surface, in the permeate and in the bulk, respectively. The mass transfer coefficient is the ratio of the diffusive solute flux at the membrane surface to the overall concentration driving force for diffusion. If the membrane is fully retentive for the particles, c_p is zero and then the equation becomes as in Equation 2-2.

$$\exp\left(\frac{J_v}{k_s}\right) = \frac{c_m}{c_b}$$
2-2

Knowing the particle concentration in the bulk, and the experimental flux at steady state, only the mass transfer coefficient needs to be calculated to be able to estimate the particle concentration on the membrane surface. The mass transfer coefficient can be obtained from the correlation of Sherwood number (Sh) that represents the ratio of convective to diffusive mass transport.

Concentration polarization effect can be eliminated or minimized by adjusting turbulence in the system with altering design and operational parameters such as stirring rate, cross-flow velocity or trans membrane pressure [34, 132].

2.3.2   Gel Polarization and Gel Precipitate Formation

The gel formation happens for solutes or molecules which are instable and have the potential to precipitate. The concentration of the solutes increases as they accumulate on membrane surface due to the concentration polarization or filtration. Once the concentration increases above the solubility limit, then the solutes can form gels or crystals by precipitation. This gel/precipitate layer exerts a hydraulic resistance and causes a flux decline [19, 34].

Calcium sulfate, calcium carbonate, calcium phosphate, silica, metal oxides and hydroxides (especially of iron and aluminium), colloidal sulphur and other inorganic particulates can cause serious fouling in UF membranes by precipitating on membrane surface or within the porous structure [34]. Temperature and the solution pH are very important parameters as they can influence the solubility of these precipitates.

As a result of concentration of the solutes (precipitates) on membrane surface, a transport of the solvent from the dilute permeate site to the concentrated membrane site may occur due to the osmotic pressure. Osmotic pressure, π (Pa) of a dilute solution can be estimated by the van't Hoff Equation 2-3 where z is the number of ions formed if the solute dissociates, c is the solute concentration (kg/m^3), r is 8.314 x 10^3 kg.m^2/s^2.K.kg.mol, T is the absolute temperature (K) and MW is the molecular weight (kg/kgmol).

$$\pi = \frac{zcrT}{MW} \qquad\qquad 2\text{-}3$$

The equation indicates that the osmotic pressure of particles decreases proportionally to the increase in the MW of the particles. Osmotic effect is higher for the particles with very small MW at high concentrations. For example, osmotic pressure of sodium chloride (NaCl) with MW of 58.50 g/L is two orders of magnitude larger than one of casein which is a milk protein with a MW of 25000 at 30 °C with 1% solutions [19]. On the other hand, the relationship between the solute size and the

osmotic pressure seems to be not proportional due to the different hydration density of the solutes at different ion radius [133].

2.3.3 Particle Transport and Deposition

Hydrodynamic forces active on a particle govern the deposition which is a non-equilibrium process. The important hydrodynamic forces acting on a particle are presented in Figure 2-3. Drag, shear induced and Brownian diffusion forces and the velocities associated with these forces are described in Appendix A.7.
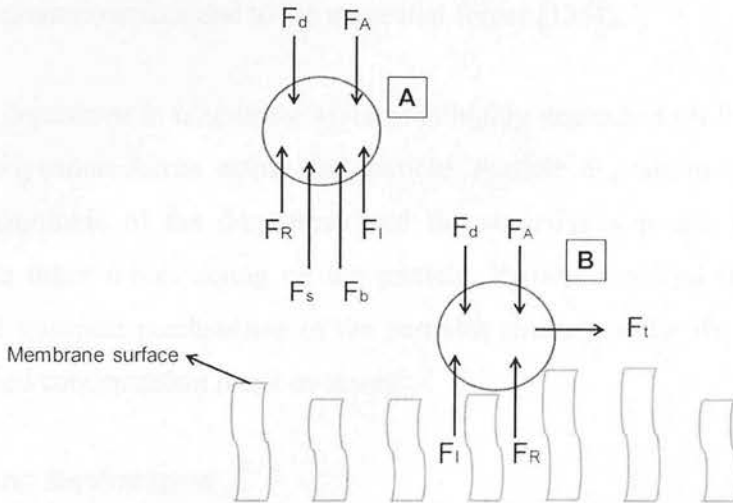
Figure 2-3 Hydrodynamic forces acting on a particle A) in solution and B) on membrane surface. F_d: Drag (viscous) force, F_R: Repulsive forces, F_A: Attractive forces, F_s: Shear induced forces, F_b: Brownian diffusion force, F_l: Inertial lift force, F_t: Tangential force (more likely for cross-flow systems) (adapted from [34])

Particle-particle and particle-membrane interactions due to the attractive and repulsive forces can contribute to the transport of the particles in membrane filtration systems. The particles in colloidal size can interact with each other by different mechanisms: electrostatic, van der Waals and short range forces [134]. Attractive forces between the particles or between the membrane and the particles would act on the same direction as the drag force, while the repulsive forces would act in the opposite direction moving the particles away from the membrane surface. These forces strongly depend on the surface characteristics of the particles and the membrane such as charge and functionality as well as the solution chemistry which influences these characteristics. In some cases, high repulsive forces act on

individual particles with large surface charge. These particles get close to each other and form a deposit layer only when the repulsive forces are overcome [134]. The repulsive and attractive forces between the particles can also influence the diffusional transport [135]. In highly turbulent systems surface transport mechanisms such as tangential shear forces become effective, especially when there is a flow parallel to the membrane surface. Due to this parallel flow, particles tend to flow along the surface because of the tangential force applied on them and the growth of deposit can be arrested. Non spherical particles like clay, would sit on their long sides and would be exposed to drag force more due to the larger surface area and would not be moved along the membrane surface due to the tangential forces [136].

The particle deposition in membrane systems is highly dependent on the magnitude of the hydrodynamic forces acting the particle. Particle deposition happens only when the magnitude of the drag force and the attractive van der Waals forces overcome the other forces acting on the particle. Particle size and the shear rate influence the transport mechanisms of the particles strongly while the influence of changes in feed concentration is not as strong.

2.3.4 Fouling Mechanisms

There are several mechanisms which are responsible for the fouling of the porous membranes with particles. These mechanisms include pore constriction, pore blockage and cake filtration [34]. Pore constriction usually occurs when particles (solutes) enter into to the porous structure of the membrane and constrict the pores via either accumulation in the pores or adsorption to the pore wall. Pore constriction is usually valid when the particle size is smaller than the pore size of the membranes. When the particle size is equal or comparable to the pore size the blockage of the pore entrance is likely to happen. For very large particles, a deposit (cake layer) forms on the membrane surface which causes a resistance. The deposit layer can be formed of the individual or aggregates of the particles present in the suspension. The cake filtration mechanism also applies for the fouling caused by gel (precipitate) layer formation. If a membrane is considered as a porous structure, any possible pore

constriction or blockage changes the membrane porosity and directly influences the membrane resistance (R_m) with a significant flux drop [130].

2.3.5 Resistance Model

In membrane systems, the relationship between permeate flux and the pressure is described with Darcy's law in Equation 2-4, where J is the flux of membrane ($L/m^2.h$), ΔP is the trans-membrane pressure difference (bar), μ is the dynamic viscosity (converted into bar.h) of water at the experimental temperature and R_m is the membrane resistance ($1/m$).

$$J = \frac{\Delta P}{\mu(R_m)} 10^3$$ 2-4

Membrane has an intrinsic resistance which depends on many factors such as the membrane thickness, membrane morphology, membrane material and the membrane pore size. The resistance increases with increasing thickness and decreasing pore size and number density [136].

When particle filtration starts happening in the system additional resistances can cause a decline in permeate flux. During ultrafiltration particles accumulate and form a deposit layer on membrane surface. Formed deposit layer creates an additional hydraulic resistance to the solvent flow which is called deposit (cake) resistance [34, 136]. Deposit resistance is one of the most important hydraulic hindrance for high permeate fluxes in ultrafiltration and the factors influencing this resistance still need to be better understood because of its complexity. Osmotic resistance is another resistance which can play a role in flux decline as the osmotic pressure increases due to the accumulation of the particles on the membrane surface.

Darcy's law can be modified for particle filtration to include the osmotic and deposit resistance and this is given in series resistance relationship in Equation 2-5 where $\Delta \pi$ is the osmotic pressure difference, R_d is the resistance of the particle (solute) deposit ($1/m$).

$$J = \frac{\Delta P - \Delta \pi}{\mu(R_m + R_d)} 10^3 \qquad\qquad 2\text{-}5$$

A term (R_{cp}) for the resistance due to the concentration polarization can be added to the equation if R_{cp} is very large in the system. Usually the resistance caused by the concentration polarization is much less than the deposit resistance and in this case R_{cp} can be neglected [137].

Osmotic effect is usually ignored since the osmotic pressure of the solutes at low concentration is negligible. The only case where osmotic pressure can be significant is when the particle concentration becomes very large due to the concentration polarization. At very high concentrations second and third "virial coefficients" may become important and result in increased osmotic resistance [19]. However, this is rarely the case in UF as the size of the particles is large and the feed concentrations is low [34, 138]. Ignoring the osmotic pressure effect the permeate flux can be described by Equation 2-6 [139].

$$J = \frac{\Delta P}{\mu(R_m + R_d)} 10^3 \qquad\qquad 2\text{-}6$$

According to deposit (cake) filtration theory, the resistance of the deposit can be calculated with the Equation 2-7 [34, 138] where α is the specific deposit resistance per unit thickness ($1/m^2$), δ is the deposit thickness (m) and δ_d is the maximum deposit thickness (m).

$$R_d = \int_0^{\delta_d} \alpha d\delta \qquad\qquad 2\text{-}7$$

The specific deposit resistance per unit thickness (α) can be estimated with Carman-Kozeny equation 2-8 assuming the following [140]:

1) the deposit is formed of uniform spherical particles
2) the flow is laminar
3) validity of Darcy's law

$$\alpha = \frac{180(1-\varepsilon)^2}{D_p^{\ 2}\varepsilon^3}$$

2-8

where ε is the porosity (void) and D_p is the diameter of the particle (m). The particle size, the deposit porosity and thickness are the important parameters affecting deposit resistance. The deposit resistance is expected to increase in proportion to the deposit thickness and to decrease with the increase in particle size and deposit porosity.

The Carman-Kozeny equation is valid only if the deposit porosity is less than 0.5 [141] and the deposit is incompressible [136]. Highly compressible deposit materials such as clay, and microbial cells causes a decrease in porosity and thus in deposit resistance. Variation in the applied pressure needs special attention as the increased applied pressure may result in enhanced compressibility and thus decreased porosity [136]. With more compressed deposit layer, a larger flux decline can be observed due to the reduction in porosity [142].

It is also important to note that the Carman-Kozeny equation can determine the permeability of relatively compact deposit where aggregation of the particles is not expected and they would pack uniformly on the membrane surface. Porosity of the cakes is expected to increase if the particles tend to aggregate before the deposition [143]. The void fraction of a randomly packed deposit is ~0.4 [136]. The porosity is usually considered to be not dependent on the particle size but dependent on the packing density; however, some studies disagree with this. Lee and Clark [142] shows that the deposit porosity is underestimated for small particles and overestimated for large particles forming the deposit layer when calculated with Carman-Kozeny equation. Differences in the estimation and the experimental data were attributed to the changing interaction forces between the particles as the particle size varied.

If the deposit layer is assumed to be homogenous then the Equation 2-7 becomes as in Equation 2-9:

$$R_d = \alpha\delta$$

2-9

The deposit thickness can be expressed as in Equation 2-10 where M_p is the mass of the particles in the deposit layer, ρ_p is the density of the particle/solute (kg/m^3) and A_m is the membrane surface area.

$$\delta = \frac{M_p}{(1-\varepsilon)\rho_p A_m}$$

2-10

Equation 2-10 assumes a minimum back transport of the particles and thus the particles in the concentration-polarization layer to be negligible and the deposit homogenous. Equation 2-11 is obtained by combining specific deposit resistance (Equation 2-8) with the deposit thickness (Equation 2-10) in Equation 2-9.

$$R_d = \left[\frac{180(1-\varepsilon)}{\rho_p D_p^{\,2} \varepsilon^3}\right] \cdot \frac{M_p}{A_m}$$

2-11

In dead-end filtration, a continuous increase of deposit mass (M_p) is expected. Equation 2-11 allows us to directly relate the deposit resistance to the particle mass in the deposit and to the feed particle concentration. At the end of the filtration process, the deposit layer can be washed off and the initial permeate flux can be retained. Harmant and Aimar [134] suggested that there is a threshold above which the particles form irreversible deposit layers. This threshold is called "critical mass" and is shown to be dependent on the flux and ionic strength of the solution.

The deposit layer is assumed to be homogenous for particle filtration in unstirred cell systems [142]. Shear rate is an important parameter which determines the formation of the deposits. In systems with high shear rates, the homogeneity of the deposit thickness is questionable. The heterogeneity of the deposit thickness and porosity depending on the wall shear rate is confirmed by Gaucher et al. [144]. Glover and Brooker [145] examined the deposit layer of proteins on membrane surface and observed an asymmetric deposit layer.

A direct correlation between the physically measured deposit thickness and experimentally calculated deposit resistance is difficult to make as it is challenging to get an accurate thickness of the deposits by characterisation methods without

disturbing the deposit layer [142]. It is even more challenging to measure the thickness of a non-homogenous deposit layer.

2.4 Parameters Affecting Fouling

The parameters which can strongly influence the particle-particle and particle-membrane interactions and thus the extent of the membrane fouling can be classified as membrane and particle characteristics, solution chemistry and operational parameters.

2.4.1 Membrane Characteristics

The characteristics of UF membranes such as pore size (or MWCO), hydrophobicity, surface charge and roughness influence fouling.

The surface charge of the polymeric membranes is generally measured as zeta potential with streaming potential methods. The charge interactions between the membrane and the charged particles can play a significant role in membrane fouling. In general membranes with a more negative zeta potential are less likely to foul by negatively charged particles [14].

The relative flux decline is proportional to the ratio of resistance of the fouling layer to the resistance of the membrane. Therefore, the membranes with smaller pore size, thus higher intrinsic hydraulic resistance experience less flux decline due to the colloidal fouling compared to the ones with lower resistance [146]. In UF membranes, although a nominal pore size is usually presented, there is a distribution of pore sizes [28]. Larger pores are likely to experience higher degree of concentration polarization and pore plugging compared to the smaller pores as water flow is biased towards the larger pores [130]. Similarly the fouling of the larger pore size membranes due to the pore constriction or pore blockage is more likely compared to the ones with smaller pore size. Filtration of very small silver nanoparticles showed a larger flux decline with larger pore size membranes [143] and this is due to the fact that the particles deposited within the membrane structure

as they had more access to the internal voids. In another study, when nanoparticles are filtered with two different MWCO UF membranes, 100 kDa membrane experienced a larger flux decline compared to 5 kDa membranes [14]

Although a different pore size is used for the filtration of the same size PS particles, no difference in critical flux is observed. This is attributed to the fact that the drag force applied is the same and thus the particle deposition for all pore size membranes as the system is operated at the same permeate flux for all pore sizes [147].

The surface energy of the membranes influences the membrane-particle interactions which plays an important role in membrane fouling [148]. Less fouling is observed with hydrophilic membranes compared to the hydrophobic ones [130]. The deposition of the particles on rough membrane surfaces is more likely compared to the smooth ones due to the lower interaction energy created in the valleys of the rough surfaces [149].

2.4.2 Particle Characteristics

The particle size, surface charge and feed concentration are the main characteristics which influence particle-membrane and particle-particle interactions and thus membrane fouling.

Particle size is an important parameter determining the deposit resistance which can cause a severe flux decline UF applications. Looking at the Carman-Kozeny equation (Equation 2-8), the deposit resistance is inversely proportional to the square of particle size (d_p^2) meaning the decrease in permeability is larger as the particle size decreases. Lee and Clark [142] observed larger flux decline as the size of polystyrene particles forming the deposit is decreased. No flux decline is observed when a mixture of TiO_2 particles with a size range of 0.1-10 µm is filtered by a UF membrane. This is attributed to the possibility of the cake layer being porous enough not to exert any resistance [150].

The surface charge interactions determine the formation of the deposit layers and are influenced by the particle size. For example, [142] suggested that the deposit porosity is larger for smaller size particles and this was attributed to the larger ratio of the double-layer thickness to particle size for smaller particles if it is assumed that the double-layer thickness does not change with the size of the particles.

The dependence on the transport mechanisms on the particle size is also known. Shear-induced diffusion theory predicted the long-term flux decline the best for the latex (polymeric) particles of 0.64, 0.95 and 1.39 μm in diameter [151].

The influence of particle size on flux is also studied in terms of the determination of critical flux. An empirical approach for the definition of critical flux is taken by [152] as "a flux below which a decline of flux with time does not occur; above it fouling is observed". In order to have an accurate analysis on the influence of particle size on the flux decline, particles with different size but the same surface properties are required [132]. A decrease in critical flux is reported when the size of the polystyrene nanoparticles is increased from 0.1 to 0.46 μm while the critical flux increased with increase in particle size from 0.46 to 11.9 μm [147]. In the study of Harmant and Aimar [134], the results show that there is a minimum critical flux at a certain particle size which is within the size range of 10-100 nm. A similar trend is observed in the study of [153] where a decline in flux is observed when the particle size is increased from 0.025 μm to 0.125 μm and the flux increased when the particle size is changed from 0.125 to 5 and 20 μm. In all studies the change in the flux decline trend with different size particles is attributed to the fact that for smaller particles Brownian diffusion is dominant and for the larger size range shear-induced and inertial lift play a significant role in particle transport. In another research where the influence of particle size on the permeability of one deposit layer is studied, 60 nm is found to be the size for the minimum permeability [154]. However, in the study of Petsev et al. [154] higher permeability at lower particle size is attributed to the larger voids created due to the larger repulsion forces between the small particles.

Belfort et al. [136] studied these mechanisms under typical conditions and predicted the influence of these parameters on the long term flux. It is suggested that the dominating mechanisms are Brownian diffusion for particles less than 1 µm, shear-induced diffusion for particles with a size range of 1-30 µm and inertial lift for larger particles >40 µm. Zeman et al. [34] adapted the mechanisms from [136] and suggested slightly different size ranges being <0.1 µm for Brownian diffusion, 1-10 µm for shear-induced diffusion and >100 µm for inertial lift.

Most of the colloids and particles are negatively charged in nature; this is an advantage as negatively charged particles are repelled by the membranes which have a fixed negative surface charge [136]. A decrease in flux is observed for gold nanoparticles as the zeta potential of the particles is increased due to the increased pH [155]. The zeta potential of the particles is changed by varying the pH and a minimum flux was observed as the zeta potential of the particles increased. [156]. Large flux values are attributed to the electro-kinetic enhancement of the back diffusion for the particles with larger zeta potential and to the formation of deposit layers with smaller specific resistance due to the particle aggregations for the particles with low zeta potential. Critical flux studies generally show that an increase in pH above isoelectric point results in an increase in critical flux [132]. The influence of pH related surface charge on critical flux is studied and generally an increase. The critical flux with silica particles increased as pH is increased from 3 to 5 [157].

Increased feed concentration generally causes an exponential decline in permeate flux as predicted by concentration polarization theory [19, 158]. Increase in the feed concentration of polystyrene nanoparticles resulted in flux decline in unstirred dead-end filtration [142]. The flux decline was attributed to the increase in the deposit mass and the deposit layer thickness while no influence was observed on specific deposit resistance. It is more likely that there will be more particles depositing on the membrane surface at higher feed concentrations [159]. The feed particle concentration may also play role on the hydrodynamic forces affecting the deposition of the particles [147].

2.4.3 Solution pH and Ionic Strength

Solution pH and ionic strength are two very important factors influencing the stability of the colloidal particles. The dissociation of the functional groups on particles as well as the membrane surface can result in significant changes in charge and charge interactions. The attractive and repulsive charge interactions between the particles influence the formation of the deposit and thus the deposit resistance. pH is a also very important factor for the formation of precipitates and thus gel layer deposition. Low stability of the solutes can be seen as the underlying mechanism for the formation of the precipitates and the crystallisation [132].

The ionic strength of the solution can influence the physical characteristics of the deposit layer and thus the flow rate [160]. Similarly, Faibish et al. suggested that a denser deposit layer is formed at higher ionic strength [161]. This is because the ionic strength influences the shape and the charge of the colloids such as proteins [130].

2.4.4 Turbulence in the System

The turbulence created in the system influences the accumulation of the particles as well as the concentration polarization. Stirring, recirculation or moving the membranes determines the turbulence. Turbulence can be expressed as recirculation rate, velocity, shear rate, pressure drop or Reynolds number [19]. Determination of the Reynolds number (Re) is a common way of defining the flow regime in the systems. The Reynolds number for the stirred vessels can be calculated using Equation 2-12 where ρ is the density of water (kg/m^3), N is the stirring rate (revolution/s), D_i is the diameter of the impeller (m), μ is the dynamic viscosity of water (kg/m.s) [162, 163].

$$Re = \frac{\rho N D_i^2}{\mu} \qquad \qquad 2\text{-}12$$

The higher stirring rates causes higher Re numbers and higher shear rate at the membrane surface. It needs to be noted that most fluid mechanical analyses are based

on laminar flow in open channel. This severely limits their application to real membrane systems, which often operate under turbulent flow conditions [34].

In stirred cell systems, the stirring plays a big role in concentration polarization and particle deposition. Stirring the solution just at the membrane surface can prevent or minimize the concentration polarization. The rate of stirring also contributes to the inertial lift and shear induced forces. For example Fane [153] observed larger flux with stirring compared to unstirred conditions while filtering nanoparticles with UF. Larger flux is obtained when 50 nm gold colloidal particles were filtered by UF under stirred conditions compared to unstirred conditions [155]. In the study of Madaeni [155] for 10 nm gold particles, larger flux is obtained for unstirred condition and this is attributed to the increased aggregation of the small particles due to the lack of stirring.

The turbulence can differ a lot depending on the system configuration. The turbulence and the shear rate created in cross-flow system are very different from stirred dead end filtrations. In cross-flow systems a shear is created parallel to membrane surface and it changes along the membrane. Stirring is the cause of the shear in stirred cell systems where the rate is more likely to be higher at the outer circle and close to the middle of the circle. In unstirred dead-end filtration, the formation of deposit continues to grow until the process is stopped whereas in systems where tangential flow affects the deposit growth such as in cross-flow systems under certain shear rates the deposit growth is arrested [136].

3 Materials and Methodology

3.1 Membranes and Membrane Characterisation

3.1.1 Membranes

Commercially available polymeric flat sheet UF membranes were supplied by Millipore (Bedford, US) and were made of a regenerated cellulose active layer on a nonwoven polypropylene support layer. Prior to use for experiments and characterisation, the membrane coupons were soaked in 0.1 M sodium hydroxide (NaOH) (Fisher, UK) solution for 30 minutes to remove the glycerine preservative present on the surface. Afterwards they were rinsed with plenty of tap water followed by 2.5 L of ultra-pure water. The list of the flat sheet UF membranes and the chapters where each membrane was used are given in Table 3-1.

Table 3-1 The list of flat sheet UF membranes

Product code	MWCO (kDa)	Operating Pressure (bar)	Used in
PLAC	1	5	Chapter 5
PLBC	3	5	Chapter 5
PLCC	5	5	Chapter 5
PLGC	10	5	Chapter 5
PLTK	30	1	Chapter 5
PLHK	100	0.5	Chapter 5 and 6
PLHTK	100	0.5	Chapter 7

3.1.2 Surface Charge

The streaming potential of some of the flat sheet membranes was measured over a pH range (2-14) using an electro-kinetic analyser (Anton Paar KG, Gratz, Austria). The instrument consisted of an autotitrator for pH adjustment, a pump to circulate the solution through the system and a measuring cell where the Ag/AgCl-electrodes (SE 4.2, Senortechnik Meinsberg, Waldheim/Sa., Germany) were connected. The instrument was connected to a PC which had a programme controlling the titration, measurement and recording the results.

The membrane was cut into two pieces (7.5 cm x 2.5 cm) and each piece was attached to a microscope slide with a double sided sticky tape. The membrane pieces were soaked in 20 mM NaCl and 1 mM NaHCO$_3$ background electrolyte solution overnight. The background and titration solutions were prepared with the same chemicals and at the same concentrations as the solutions used for the filtration experiments. The system was rinsed with ultra-pure water for five times until the conductivity was stable at 1.15 Ms/cm and pH was between 5 and 6. The ultra-pure water was discharged from the system and the tubes. The membrane slides were assembled in the cell and the cell was connected to the instrument as well as the electrodes. The system was flushed with the background electrolyte solution for three times. Afterwards, it was rinsed with the background electrolyte solution for 30 minutes and the conductivity, pH and especially the voltage were monitored for the stabilization. The pH adjustment was conducted in two steps with an autotitrator: step one, by adding 0.1 M hydrochloric acid (HCl) (AlfaAesar, USA) and step two, by adding 0.1 M NaOH (Fisher, UK). Six measurements were taken at each pH and the average value was taken with the variability based on the standard deviation. Between each pH adjustment step, the system was rinsed with ultra-pure water for five times until the conductivity was stable at 1.15 Ms/cm and pH was between 5 and 6.

3.1.3 Surface Roughness

Membrane surface roughness was estimated using an atomic force microscopy (AFM) instrument (Bruker Corporation, formally Veeco, USA). Measurements were performed in a liquid contact mode with a silicon probe (Mikromasch CSC38/AL BS type C). The probe had a force constant of 0.005-0.21 N/m, a resonance frequency of 6-23 kHz, nominal tip radius of 8 nm and cantilever length of 300 μm.

The roughness analysis considers that the membrane surface occupies a x-y plane area, which in this study mostly had size of 2.5 x 2.5 and 1.0 x 1.0 μm. The cantilever tip measures the relative height z at each x, y location. The surface roughness was measured as the average roughness, Ra, and the root-mean square

roughness, Rq. Ra is the average of the measured z-values, while Rq describes the standard deviation of the z-values. The average of two measurements for both Ra and Rq was presented in this study.

3.2 Sorbents

Various materials were used as sorbent for the trace contaminants. Polymers, plain polystyrene and carboxylated polystyrene nanoparticles were employed for the sorption of hormones while for fluoride sorption, laterite and bone char were studied.

3.2.1 Polymers

Commercially available polymers; polysulphone (PSu), polypropylene (PP), polyethylene high density (HDPE), polyamide (PA), polystyrene (PS), polyethylene terephthalate (PET), polyethylene naphthalate (PEN) and polyethersulphone (PES GF) were purchased from Goodfellow (Huntingdon, UK) in the form of 2-3 mm granules. Polysulphone UDEL (PSu U) and polyvinylidene difluoride (PVDF), polyethersulphone (PES Radel) were obtained from Solvay (Brussels, Belgium) in granular form and cellulose (CEL), poly(methyl methacrylate) (PMMA) and poly(2,6 dimethyl 1,4-phenylene oxide) (PPO) were purchased from Sigma Aldrich (Gillingham, UK) in powder form. Polymers in granular form were with Retsch Ultra Centrifugal Mill ZM 200 (Leeds, UK), in three stages using sieves with 1.00, 0.75 and 0.50 mm openings. The final size of the polymers used in the experiments were less than 500µm for PA, PSu, PP, PEN, PS, PET, PVDF, HDPE, PES GF, PSu U and PES Radel, 15µm for CEL, ~5µm for PPO, 36µm for PMMA.

The grinding process of the polymers in granular forum was rather challenging. As a result of strong rotation of the mill, a large amount of heat was produced and this heat caused the polymers to melt and deform. Melted polymer pieces stacked on the rotating units and caused interruption in the operation of the mill. In order to prevent the polymers to melt, polymers samples and each component of the rotating unit which had a contact with the polymers such as the blade and the sieves were immersed in liquid nitrogen for about half a minute prior to the grinding process. A

very small amount of granules (4-5 pellets) was placed in the rotating unit at a time. For some of the polymers which have a very low melting point, cooling process with liquid nitrogen had to be repeated several times until all the samples could be grinded and a single pellet was placed in the rotating unit at a time.

3.2.2 Polystyrene Nanoparticles

The plain (non-functionalized) (52, 81, 465 and 3000 nm), non-functionalized fluorescent (43 nm) and carboxyl-functionalized (48 nm) polystyrene (PS) nanoparticles were purchased from Polysciences, Inc. (Eppelheim, Germany). Prior to experiments and instrumental analysis, the nanoparticle solutions were sonicated for 5-10 seconds with 150 W ultrasonic cleaner (Sonic Wave, UK) to break any possible aggregates.

3.2.3 Laterite

Laterite (LA) was extracted in Bongo, Upper East Region, Ghana (GPS: N10.89522 W0.77871). Laterite was air-dried and the larger fragments were crushed with a hammer (inside a bag). An orbital grinder (TEMA, Italy) was used to grind the materials. Grinding time was changed between ten seconds and a minute depending on the size fraction required.

Sieves were used to separate the laterite into the following size fractions: 500-710 μm, 250-500 μm, 125-250 μm, <125 μm, 63-125 μm, 38-63 μm, <38 μm. Grinding/sieving was an iterative procedure to get the desired size fractions. Laterite was not washed or treated prior to any characterisation analysis or experiment.

3.2.4 Bone char

Bone char (BC) was collected on December 2010 from Ngurdoto Defluoridation Research Station, Arusha Region, Tanzania, where it was treated and prepared. The detailed description of the treatment is given in the study of Mjengera and Mkongo [164]. Duration of the ignition depends on the size of the kiln and thus the amount of the raw bones treated such as 6, 8, 24 hours (including cooling time), respectively in

10, 20 and 150 kg kilns. The kilns were fuelled by about 1 kg of wood charcoal with a controlled air supply. The treatment temperature changed between 400 and 550 °C. A ratio of charcoal/raw bone used was 8%.

The same grinding and sieving methods used for laterite were applied to bone char. For some of the bone char experiments <63 and <150 μm size fractions were used exceptionally. The other size ranges tested were exactly the same ones used for laterite. Bone char was not washed prior to any characterisation analysis or experiment.

3.3 Sorbent Characterisation

3.3.1 Particle Size Analysis

The size of the sorbents was analysed with two different instruments depending on the sensitivity of the instrument for the size range.

The effective diameter of the PS nanoparticles was determined by Zeta Plus and 90Plus/BI-MAS Particle Size (Brookhaven Instruments, New York, USA) by taking the mean of 10 measurements. The size of the 52 nm plain PS nanoparticles was measured for three samples prepared at different times and the relative variability obtained was used for all other nanoparticle sizes. The instrument is effective for the particle size range of 2 nm to 2 μm. The size of the PS nanoparticles was measured in experimental background solution of 1 mM $NaHCO_3$ and 20 mM NaCl unless stated otherwise.

The particle micro size distribution of the laterite and bone char samples, ground and sieved with different mesh sizes, was measured using LS230 Particle Size Analyser (Beckmann Coulter, UK). 0.3 g laterite/bone char was mixed into 25 mL ultra-pure water and was stirred for five minutes prior to the analysis.

The particle size distribution of the polymeric particles was analysed using program Image J_1.40 on FE-SEM images assuming a spherical shape for the particles. The

microscopic imaging of the polymeric particles was detailed in Section 3.3.4. The particle size distribution of six selected polymers was presented in Appendix A.3 and the data is used to calculate the average particle diameter.

3.3.2 Surface Charge Analysis

Titration Method

The zero point charge of laterite and bone char was determined by using titration method adapted from Wang and Reardon [165]. 0.2 g of sorbent and 0.1 M KCl was added into 10 mL ultra-pure water. 150-212 μm and < 38 μm size ranges were used for bone char and laterite, respectively. The solution pH was adjusted using 1 M HCl and 0.1 M NaOH and the reading was recorded after 15 minutes, while swirling. The solutions were mixed for one hour in a shaker at 25 °C and 200 rpm. The solution pH in each bottle was recorded. 0.5 mL of 2 M KCl was added into each bottle and the pH was recorded for the last time while swirling the solution.

Zeta Potential Analysis

Zeta potential measurement was performed with Zeta Plus (Brookhaven Instruments, New York, USA) by taking the mean of a set of 10 measurements. 1.5 mL sample was placed in a 3 mL sample cuvette. The temperature of the samples was let to equilibrate in the machine at least for five minutes. The measurements were conducted in the experimental background electrolyte solution of 1 mM $NaHCO_3$ and 20 mM NaCl, unless otherwise stated. The pH of the solutions was adjusted with 1M HCl and 1M NaOH.

The concentrations of ~0.60 % v/v for fluorescent (43 nm), carboxylated (48 nm), plain (52 and 81 nm) and 0.15 % v/v for plain (465 and 3000 nm) size were used for the zeta potential measurements of PS nanoparticles. The influence of the pH on the surface charge was studied varying the pH of the solution.

The laterite samples were measured in the concentration of 0.01% v/v. After the pH adjustment the solutions were mixed and let to settle for 10 minutes.

3.3.3   Chemical Composition

X-Ray Diffraction

X-Ray Diffraction (XRD) was used to characterize the crystalline phase of laterite and bone char. For the measurements, <125 µm particle size was used. To carry out the XRD analysis, D8-Advance X-ray Diffractometer (Bruker AXS, Germany), which employs a 2-theta configuration in which the X-rays are generated by a Cu-anode x-ray tube operating at 40KV and a tube current of 40mA, was used. The scanning range of the samples was 2θ=2-60° at a scanning rate of 0.01°/sec. EVA analysis package was used to compare the diffractogram results with the 2012 issue of the International Centre for Diffraction Data (ICDD) diffractogram database library.

X-Ray Fluorescence

X-Ray Fluorescence (XRF) method was used to determine the major element composition of laterite and bone char. For the measurements, <125 µm particle size was used. Before the samples were analysed with PW2404 automatic XRF spectrometer (Philips, the Netherlands) with a Rh-anode X-ray tube, they were fused with a lithium borate flux containing La_2O_3 as a heavy absorber by a method similar to that of Norrish and Hutton [166].

3.3.4   Sorbent and Deposit Morphology

The morphology and the size of the sorbents and the thickness of sorbent deposit on membranes were analysed using Scanning Electron Microscopy (SEM). The scale, magnification, beam accelerating voltage (kV) and working distance (WD) are provided on each image in the results sections.

Morphology of Polymeric Particles

The size and the shape of the polymeric particles were analysed imaging the samples with 4700 II cold field emission SEM (FE-SEM) (Hitachi, UK). Each polymer sample was mounted on Leit conductive double-sided carbon adhesive disc (Agar Scientific, UK) which was stuck on SEM specimen stub (Agar Scientific, UK). The

edges of the disc and the specimen were painted with conductive carbon cement (Leit C) (Agar Scientific, UK). The samples were coated with about 8nm of 60% gold/40% palladium alloy (Testbourne, UK) before imaging. The particle size distribution of the polymers was analysed using program Image J_1.40 on SEM images assuming a spherical shape for the particles.

Thickness of PS Nanoparticle Deposit

The membranes with nanoparticle deposit layers were preserved in a petri dish on a wet cotton tissue to prevent the membranes and the deposit from drying out. FE-SEM imaging with freeze drying technique was conducted at DRIAM facilities in Manchester University using Supra 40V field emission SEM (Carl Zeiss, UK) with a freeze drying unit (Quorum Technologies, UK). The freeze drying technique was required due to the nature of the membrane samples. Once the membranes were soaked in aqueous solution, they could not be air dried as this would interfere with the membrane structure and the regenerated cellulose active layer would come off the support layer. By freeze drying the membrane sample with means of liquid nitrogen prevented such damage to the membrane structure. Additionally imaging of the regenerated cellulose membranes was required to be under low beam accelerating voltage as regenerated cellulose is a very unstable material [167]. Hence, for the characterisation of the nanoparticle deposits on membranes, a beam voltage of 1 kV was used. A rectangular piece of membrane was cut from the middle of the membrane coupon prepared with deposited nanoparticles. Three square membrane samples with the size of about 5 x 5 mm were cut with a spatula from different locations of the rectangular piece. All three samples were placed between two silicon plates and the silicon plates were clamped perpendicular to the sample holder so that the cross sections could be imaged. The sample holder was connected to a transfer rod which had a unit where the sample holder could be enclosed. The samples together with the sample holder were immersed in liquid nitrogen for about half a minute. The temperature on the holder was between -80 and -100 °C. It was then transferred to the freeze drying unit. The sample holder was placed in the unit without any contact to the air. In the freeze drying unit, the samples were let to dry at

low temperature under the vacuum pressure of ~0.02 torr (2.67 Pa). The drying process lasted for about 2.5 hours. When the samples were warmed up to 3-5 °C, the samples were transferred into the imaging chamber. The samples were imaged without coating the samples. The deposit thickness was measured using program Image J_1.40 on FE-SEM images.

Morphology of PS nanoparticles

The size and the shape of 52, 81 and 465 nm PS nanoparticles deposited on regenerated cellulose membranes were imaged with analytical field emission SEM (FE-SEM) (Carl Zeiss, UK). The sample preparation and imaging method was the same as the one described above for deposit thickness measurements. The beam voltage used for these measurements was ≤5 kV. The size of the particles was measured using program Image J_1.40 on FE-SEM images.

Morphology of Laterite and Bone Char

The morphology of laterite and bone char was determined using an analytical SEM (Carl Zeiss, UK). Each powder sample (not washed) was placed on a sticky carbon disc attached to aluminium specimen sub (Agar scientific, UK). The sample was not coated and was imaged under high vacuum using secondary electron imaging (SE2).

3.3.5   Total Surface Area and Micropore Volume Analysis

The specific surface area analysis of laterite and bone char was performed using Multi point BET analysis with an Autosorb-iQ (Quantachrome (USA) and nitrogen. For the BET method [168], the weight of the nitrogen adsorbed at a relative pressure (P/Po) was determined usually for a pressure range of 0.05-0.30. A sample of laterite and bone char with the size range of <125 μm was used. The average of the measurements of three different samples was used and the largest difference between a single measurement and the average was used as the variability. For micropore analysis, a lower P/Po range was used whereas for mesopore analysis a larger P/Po range is required. The Dubinin-Astakhov (DA) method, proposed for materials with heterogenous micropores, was used to determine the micropore size distribution and

volume. Micropore analysis was performed with Dubinin Radushkevich (DR) method as well to have a confirmation of the DA method. For both methods a pressure range of 7.64×10^{-5}-0.075 P/Po was used. Barrett, Joyner & Halenda (BJH) method which takes the P/Po range of >0.35 was used to determine the mesopore volume of the samples.

3.4 Chemicals

Analytical grade chemicals were used for the preparation of the experimental solutions, the pH adjustment and buffer solutions for analytical measurements. All solutions were prepared with ultra-pure water (conductivity: 18.2 Ms/cm) obtained from a laboratory purification system (Elga LabWater, UK).

Tritium labelled [2, 4, 6, 7-3H] estrone (2.449 TBq/mmol), [2,4,6,7-3H] 17β-estradiol (2.59 TBq/mmol), [1, 2, 6, 7-3H] testosterone (2.7 TBq/mmol), and [1,2,6,7-3H] progesterone (2.74 TBq/mmol) with a radioactive activity of 37 MBq/mL was obtained from Perkin Elmer (Beaconsfield, UK). Non-labelled estrone ($\geq$ 98% purity) was purchased from Sigma Aldrich (Gillingham, UK).

Sodium fluoride (NaF) (>99 % Sigma Aldrich, UK) was dissolved in ultra-pure water to the required fluoride concentration to prepare a fluoride stock solution of 1000 mg/L. The required fluoride concentrations were diluted from this stock solution.

Hydrochloric acid (HCl) (Fisher, UK) and sodium hydroxide (NaOH) (Fisher, UK) were used to prepare the solutions for pH adjustment. For the characterisation, batch and filtration experiments, the pH was adjusted with 1 M and 0.1 M HCl and 1 M and 0.1 M NaOH.

Unless stated otherwise, all the solutions for batch and membrane filtration experiments were prepared in a background electrolyte solutions of 1 mM sodium bicarbonate ($NaHCO_3$) (Fisher, UK), 20 mM sodium chloride (NaCl) (Fisher, UK) using ultra-pure water.

3.5   Analytical Instruments and Equipment

The analytical instruments are presented in this section. The calibration curves of hormones and fluoride determined for scintillation counter, ion selective electrode and ion chromatography are displayed in Appendix A.1.

3.5.1   pH, Conductivity, Oxidation Reduction Potential and Dissolved Oxygen Meter

pH, conductivity, oxidation-reduction potential (ORP) and dissolved oxygen (DO) of the samples were measured with pH/Cond 340i meter (WTW, Germany) using the corresponding probe. The probes; SenTix 41 (WTW,UK), TetraCon 325, Cellox 325 (WTW, Germany) and Elit ORP 31 C (NICO 2000, UK) used for pH, conductivity, DO and ORP respectively. The pH probe was calibrated every 2-3 days with pH buffer solutions at pH 4, 7 and 10 (Fisher Scientific, UK) and the conductivity probe was calibrated when required with 0.01 M KCl (Fisher Scientific, UK). ORP electrode was calibrated every 2-3 days, using buffer solutions of pH 4 and 7. DO probe was calibrated every 2-3 days with its Oxical-SL calibration and storage vessel.

3.5.2   Alkalinity meter

Alkalinity of the samples were analysed with alkalinity test kit AL-DT, digital titrator with reagent kit (Hach Lange, UK). For the analysis total alkalinity method was used for a range of 10-4000 mg/L as $CaCO_3$. Total alkalinity included carbonate, bicarbonate and hydroxide and was determined by titration to a pH between 3.7 and 5.1.

3.5.3   Turbidity meter

The turbidity of the samples was measured with portable turbidimeter TN-100 (Eutech Instruments, USA). The turbidimeter was calibrated daily with the standards provided by the manufacturer. The sample was placed in the instrument and the turbidity value was recorded once the reading was stable.

The turbidimeter TN-100 was also used to determine the PS nanoparticle concentration in feed, permeate and concentrate samples. A calibration curve was prepared by measuring the turbidity of PS nanoparticle solutions with 2.0, 7.9, 16, 31, 50 and 79 mg/L concentrations and determining a correlation between the PS concentration in mg/L and turbidity (ntu).

3.5.4 Scintillation Counter

The radioactivity of the tritium labelled hormones was measured in disintegration per minute (dpm) with Beckman LS 6500 scintillation counter (Fullerton, USA) after mixing 0.5 mL of sample with 3.5 mL of Ultima Gold LLT (Perkin Elmer, UK) in 20 mL scintillation vials (Perkin Elmer, UK) . Each sample was counted three times, each 10 minutes and the average value was used. The instrument was calibrated each time a new hormone stock solution was prepared. A calibration curve was prepared with solutions of 0.1, 1, 10, 100 and 100 ng/L hormone concentrations and used to convert dpm into ng/L. The detection limit of the instrument for the hormones was 1 ng/L.

3.5.5 Ion Selective Electrode

Fluoride concentration in the samples was determined using an ion selective electrode (ISE) for fluoride in conjunction with an Ag/AgCl reference electrode connected to an ion meter 826 (Ion Meter, Metrohm, UK) was immersed in well mixed 2.5 mL of samples and 2.5 mL of TISAB (total ionic strength adjustment buffer) solution. The conductance of the fluoride ions was measured in millivolt (mV) and the value was recorded after one minute once the reading on ion meter was stabilized. A calibration curve was prepared daily with standard fluoride solutions of 0.1, 0.3, 1, 3, 10, 30 and 100 mg/L and used to convert mV into mg/L. Calibration solutions were prepared for each fluoride stock solution separately. The detection limit for fluoride electrode was 0.1 mg/L.

TISAB was prepared by adding 57 mL glacial acetic acid (99+%) (Fisher, UK), 58 g NaCl (99.9%) (Fisher, UK) and 4 g of 1,2-cyclohexanedinitrilo-tetraacetic acid (CDTA) (98%) (Anachemia, UK) into approximately 500 mL ultra-pure water. The

solution was stirred until a homogenous solution was obtained and the solution temperature cooled down to room temperature. 5 M NaOH (Fisher, UK) was added until pH was adjusted to 5-5.5 and then the solution was completed to 1 L.

The pH, ionic strength and the presence of metals, especially aluminium in the samples are very important parameters which may interfere with the fluoride measurements with ISE. In order to eliminate these interferences TISAB must be used and must include CDTA.

3.5.6 Ion Chromatography

Anion concentrations in the samples were measured with a Basic Plus Ion Chromatography 883 (IC) (MetrOhm UK). The samples were introduced to the instrument with an eluent, reagent solutions and ultra-pure water as a rinsing solution. Eluent solution was composed of 3.2 mM sodium carbonate (Na_2CO_3) (Fisons Scientific, UK) and 1 mM sodium bicarbonate ($NaHCO_3$) (Fisher, UK). Reagent solution included 150 mM sulphuric acid (98%) (Fisher, UK), 100 mM oxalic acid (BDH Chemicals, UK) and 5% acetone (Fisher, UK).

Standard solutions of sodium bromide (NaB), sodium fluoride (NaF), sodium nitrate ($NaNO_3$) and sodium chloride (NaCl) all from Fisher Scientifics (UK), sodium phosphate ($Na_2PO_4.7H_2O$) and sodium sulfate (Na_2SO_4) both from Acros Organics (UK) prepared with ultra-pure water were used to calibrate the IC. The concentrations of the standard solutions used for calibration were 0.1, 0.3, 1, 3 and 5 mg/L for fluoride, bromide and phosphate, 2, 6, 20, 60 and 100 mg/L for nitrate and sulfate and 10, 30, 100, 300 and 500 mg/L for chloride. The calibration curve for fluoride is given in Figure A 1-2 in Appendix A.1. Calibration curves were generated with the instrument software for each anion. The correlation coefficient (r^2) of the calibration curves for each anion was 0.999 or better. The limit of detection (LOD) was calculated using the Equation A 2-1 in Appendix A.2 and is given for each anion in Table 3-2. The LOD was calculated using the slope (m) of the full calibration curve.

Table 3-2 LOD for anions with IC

Specie	Symbol	LOD (mg/L)
Fluoride	F$^-$	0.05
Bromide	Br$^-$	0.77
Chloride	Cl$^-$	0.23
Nitrate	NO$_3^-$	0.20
Sulfate	SO$_4^{-2}$	0.15
Phosphate	PO$_4^{2-}$	0.62

Prior to the analysis of the samples, the accuracy of the calibration was determined by analysing a certified standard IC anion solution (10 mg/L F, Cl, Br, NO$_3$, SO$_4$, PO$_4$) (Sigma Aldrich, UK). One of the standard solutions and blank (ultra-pure water) were analysed about every eight samples in order to control for any drift during analysis.

3.5.7 Inductively-Coupled Plasma Optical Emission and Plasma Mass Spectroscopies

For calcium, potassium and magnesium, inductively coupled plasma-optical emission spectroscopy (ICP-OES) (Perkin Elmer Optima 5300 DV, USA) was used since the concentrations were mostly higher than 1 mg/L. For the rest of the cations the samples were analysed with inductively coupled plasma-mass spectroscopy (ICP-MS) (Agilent 7500ce, Japan). The details of the instruments and the methodology of the inorganic analysis are given in Appendix A.2.

3.6 Experimental Protocols

3.6.1 Batch Sorption Protocol for Polymers

60 mL of 100 ng/L 17β-estradiol solutions were prepared in 100 mL glass bottles. 2.5 g of each polymer was added into each estradiol solution and the solutions were mixed in a Certomat BS-1 UHK-25 shaker (Göttingen, Germany) at 200 rpm and 25 °C. Samples of 1 mL were taken with 1 mL syringes at certain time intervals and filtered through 0.7 μm glass microfibre filters (Fisher, Loughborough, UK) which was placed in Millipore Swinnex filter support (Ireland). Based on the results of preliminary experiments where glassfibre filters were chosen due to their lowest sorption of estradiol, after the third sample filtration, the filter reached saturation and

the adsorption calculated was due to polymer adsorption. Experiments were stopped after about 8000 minutes.

3.6.2 Batch Sorption Protocol for Nanoparticles

Hormone solutions are prepared in 100 mL glass bottles and the solution pH was adjusted before the addition of nanoparticles. Following the addition of the particles, the solution was mixed for an hour at 200 rpm at 20 °C in an Certomat BS-1 orbital shaker (Sartorius, Germany). Sorption equilibrium for PS particles was expected to be reached within an hour. The solution was then ultra-centrifuged for 4 hours at 686700 m/s^2 (70,000xG) and 20 °C in 16 mL polycarbonate centrifuge bottles (Beckman Coulter, UK). Samples were taken from the initial and supernatant solutions after the centrifugation and analysed for hormone concentration.

Fluorescent non functionalized PS particles were used to determine the required centrifugation time for the >95 % of the nanoparticles to settle. The UV absorbance of fluorescent PS nanoparticles was scanned over a wavelength range between 200 and 800 nm using a Cary 100 Scan UV visible spectrophotometer (Palo Alto, USA) and the result is presented in Figure 3-1, on the left.
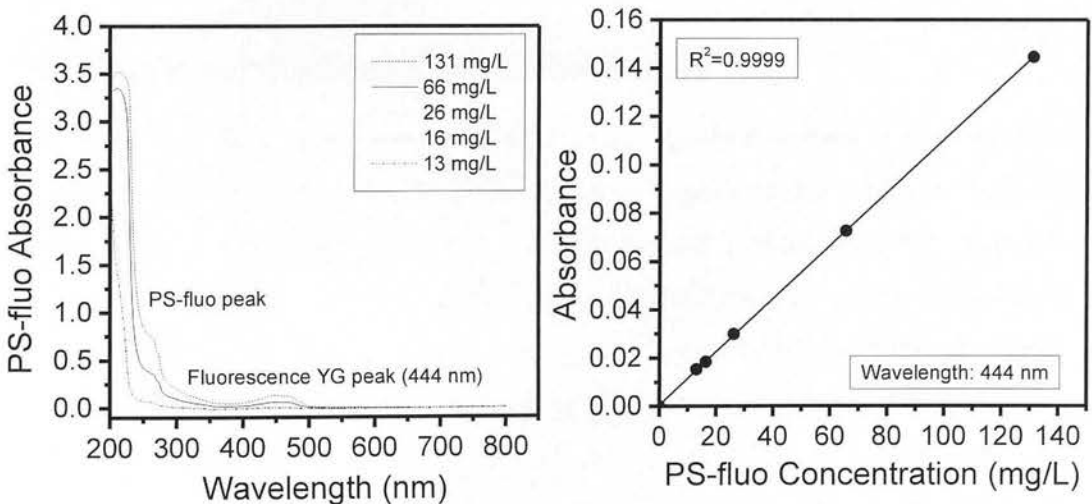
Figure 3-1 Left: Scan of the fluorescent polystyrene nanoparticles, Right: Absorbance of YG dye on fluorescent nanoparticles with changing particle concentration

The peak absorbance for the yellow green (YG) dye of the fluorescent particles was measured at the wavelength of 444 nm and this wavelength was used for the determination of the PS nanoparticle concentrations. The absorbance was measured at different fluorescent PS concentrations and a correlation curve, presented in Figure 3-1 on the right, was obtained between the PS particle concentration (mg/L) and the YG dye absorbance. Initial and supernatant PS concentrations were calculated using this curve.

3.6.3 Batch Kinetic Protocol for Laterite and Bone Char

Laterite or bone char was added into 400 mL of fluoride solution which was stirred on a magnetic stirrer at 300 rpm and room temperature (22±2 °C). The solutions were prepared in a background solution of 1 mM $NaHCO_3$ and 20 mM NaCl. pH of the solution was monitored, recorded and adjusted (if required) throughout the experiments by adding 1M NaOH or 1M HCl. 10 mL samples were taken with a 20 mL polypropylene syringe at certain time intervals and the sorbent was filtered with 0.45 µm disposable syringe filters (CA, Sartoris). Fluoride concentration in both feed and the filtrates were measured. The sorption equilibrium was considered once the last two consecutive filtrate samples had the same fluoride concentration. Initial and final pH and conductivity of the solution were measured.

3.7 Membrane Filtration System: Stirred Cells

The dead end filtration experiments with flat sheet membranes were conducted using stainless steel stirred cells. A photograph of the cells is given in Figure 3-2. Each cell had a volume of 990 mL, a diameter of 70 mm and a magnetic stirrer assembly (Millipore, Watford, UK). The dimensions of the stirring unit were provided in Figure 3-3. The membrane coupons were cut to the size required to fit into the stirred cells. The membrane surface area exposed to the pressurized solution was 0.0033 m^2. The cells were placed on a magnetic stirrer (Fisher Scientific, Loughborough, UK) which was adjusted to 300 rpm for all experiments to minimize the concentration polarization effect.
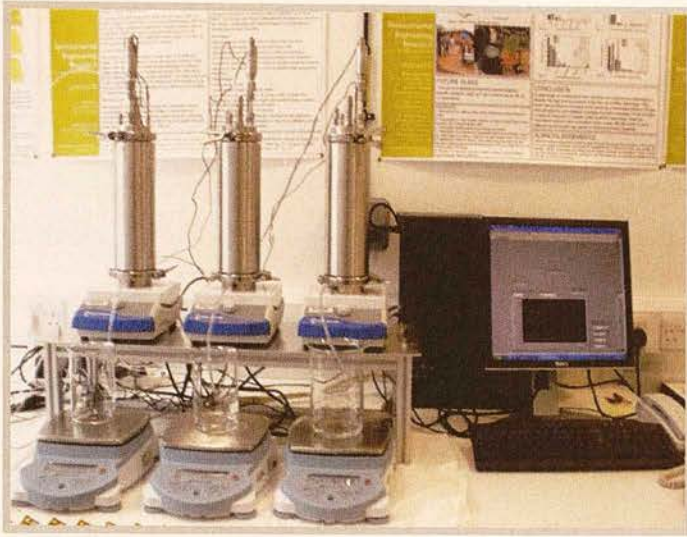
Figure 3-2 Photograph of the stirred cells connected to the computer system

Each permeate line had a valve to control the flow. Permeate of each cell was collected in a beaker placed on a balance (Fisher Scientific, Loughborough, UK) and the weight and hence the volume of the permeate was monitored continuously.
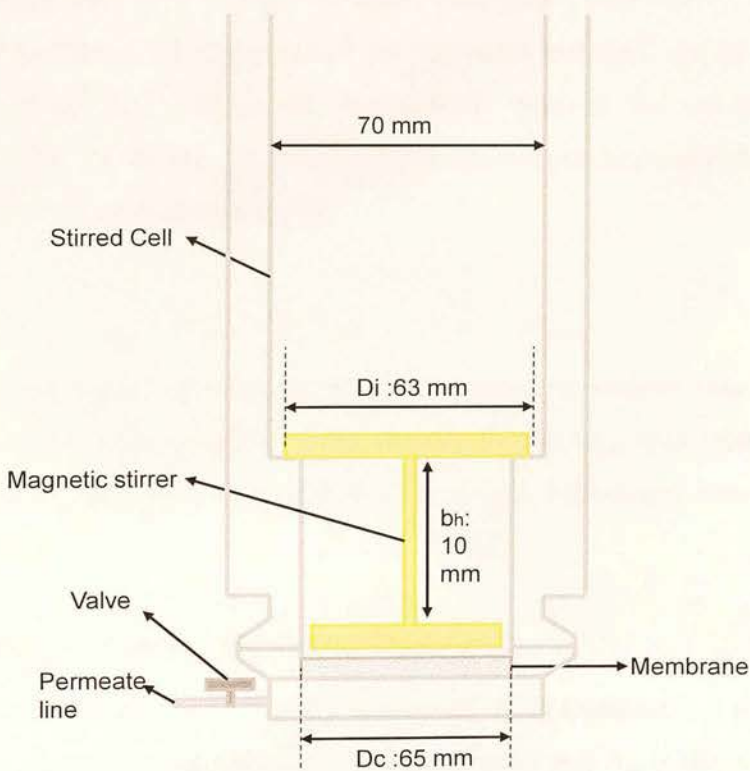
Figure 3-3 Schematic of the stainless steel stirred cells and the magnetic stirrer (not to scale), D_i: impeller diameter, D_c: stirred cell diameter, b_h: height of the blade

The cells contained a pressure transducer and a thermocouple which were connected to a data acquisition system (OMB-DAQ-56), all purchased from Omega Engineering (Irlam, UK). The data from the acquisition system and the balances were transferred to the computer and processed using the program Labview 8.0 (National Instruments, Newbury, UK). The filtration protocols are described individually in the material and methods section of each chapter.

3.8 Data Analysis

Standard calculations used for the data analysis in all chapters are given in this section.

3.8.1 Calculation of the Contaminant Mass Adsorbed

The contaminant (sorbate) mass adsorbed (M_{ads}) in milligram (mg) for fluoride and nanogram (ng) for hormones was calculated with Equation 3-1 where V_f, V_{Pi} and V_c are the volume (L) of feed, sample permeate, concentrate, respectively, C_f, C_{Pi} and C_c are the contaminant concentration (ng/L for hormones and mg/L for fluoride) of feed, sample permeate and concentrate, respectively, m_{ads} is the contaminant mass adsorbed on the membrane, $_i$ is the identity number of permeate samples and $_n$ is the total number of the permeate samples.

$$M_{ads} = V_f.C_f - \sum_i^n V_{p_i}.C_{p_i} - V_c.C_c - m_{ads}$$ 3-1

m_{ads} was determined with blank experiments, where no sorbent was added to the system, using the same Equation 3-1 but substituting the M_{ads} with zero. An example of the E1 mass adsorbed is calculated in a sample experiment was presented in Appendix A.4.

3.8.2 Flux, Permeability and Deposit Resistance

Membrane water flux (J) ($L/m^2.h$) was calculated using Equation 3-2 where dV/dt is the volume of the permeate in a specific time interval and A_m is the surface area of the membrane exposed to the solution. A_m is 0.0033 m^2 for the stirred cell system.

$$J = \frac{dV}{dt}\frac{1}{A_m} \qquad\qquad 3\text{-}2$$

The permeability (L_v) (L/m^2.h.bar) was calculated with Equation 3-3 where ΔP is the operational pressure (bar). The sorbent deposit resistance (R_d) (1/m) was determined using the same equation where μ is the dynamic viscosity (converted into bar.h) of water at the experimental temperature, R_d is the resistance of the sorbent deposit (1/m) and R_m is the membrane resistance (1/m). R_m was calculated from the data obtained from ultra-pure water filtration using the same Equation 3-3 by substituting R_d with zero.

$$L_v = \frac{J}{\Delta P} = \frac{1}{\mu(R_m + R_d)}10^3 \qquad\qquad 3\text{-}3$$

The flux data was corrected for the average experimental temperature (21±2 °C) for some experiments where the temperature was lower or higher than the experimental standard deviation (±2), using the corresponding viscosity data and replacing it in the Equation 3-3. The dynamic viscosity corresponding to the average temperature was calculated using the Vogel Equation 3-4 where μ is dynamic viscosity (Pa.s) and T is the temperature (K) [169].

$$\mu = e^{\left(-10.5 + \frac{530}{T-146}\right)} \qquad\qquad 3\text{-}4$$

3.9 Experimental Quality Control and Assurance

The practices employed to assure and control the experimental quality are described in this section. The methodology used to estimate the variability in the experimental results is also explained.

It is known that polymeric materials have sorption affinity for organic compounds while inorganic compounds chemically interact with glass materials. In order to prevent analyte sorption on laboratory equipment, for hormone sorption experiments, glass and for fluoride sorption, plastic equipment was used. Similarly appropriate cleaning agents were used for organics and inorganics. Solutions of acetic acid (8% in volume) were used to rinse the equipment utilized for fluoride experiments.

Equipment used with radiolabelled hormone was de-contaminated with solution of RBS® (Sigma Aldrich, UK) while NaOH (5% in weight) was used to clean the non-labelled hormone contaminations. After cleaning with the appropriate cleaning solutions all equipment was rinsed with ultra-pure water and dried either with hot air in ambient conditions.

All chemicals used were of analytical grade, stored in appropriate conditions, dated once opened and discarded when outdated. The instruments were calibrated regularly or on a daily basis depending on the specific requirement with the appropriate standard solutions and a references standard was measured prior to the sample analysis to confirm the accuracy. A standard solution and blank samples with only ultra-pure water were regularly analysed to monitor if any analyte carry-over or contamination happened in the instrument. Limit of detection was determined for each analyte and the instrumental results were presented accordingly.

Analyte sorption on sorbent materials was quantified taking the equipment and membrane sorption into account. Prior to both batch adsorption and filtration experiments with the sorbents, blank experiments where no sorbents were added to the system were performed in order to quantify the sorption on equipment and the system. The mass of analyte sorbed on membranes or equipment was subtracted from the final mass adsorbed to quantify the sorption only on sorbent materials. Attaining the sorption equilibrium was an important parameter for the comparison of the analyte mass sorbed especially for filtration experiments conducted with hormones where the duration varied depending on the MWCO of the membrane. The sorption equilibrium is confirmed by monitoring the consecutive permeate samples.

For interpretation of the experimental results accurately, estimating the error is mandatory. In this study, sorption and the membrane permeability are the main experimental results presented and the estimation of the error for these results was challenging. Several estimation methods were tried and an example is presented for a single experiment for permeability in Table 3-3.

Table 3-3 Relative permeability data and estimation of error and variability for the data point

	Error propagation based on the error in each measured data	Variability estimation based on variability in each measured data	Variability of experimental data repeated 5 times
Experiment Permeability/ Initial Permeability (L_v/L_{vo})	0.34±0.009	0.34±0.02	0.41±0.07

When a quantity is a function of measured quantities and each measured quantity has its own uncertainty (error), an error for the function can be propagated using individual errors. The analyte (contaminant) mass sorbed is a function of measured contaminant concentration and volume of the feed, permeate and concentrate samples. Permeability is a function of measured volume of permeate, time and the membrane surface area. Error was propagated for both sorption and permeability using individual error in each measured data. Error propagation for permeability of a single data point was conducted and was based on the instrumental error in measured water flow with balance (±0.2 g) and pressure in the stirred cell measured with pressure transducer (±0.001 mV). Calculated error (±0.009) is presented in the second column in Table 3-3 and was less than the other two uncertainties (variability) calculated with different methods, this is not surprising as other variables can influence the permeability of sorption. For example, permeability depends on the variability in pressure and temperature while variability in initial contaminant concentration can influence the sorption to a great extent.

A variability approach, similar to the one of De Munari [170], was used to determine the variability of each parameter influencing the sorption or permeability. Overall variability in sorption or permeability was estimated (propagated) using variability in each parameter. Estimation result for a single experiment for permeability (±0.02) is presented in the third column in Table 3-3. Although the presented variability estimation (±0.02) is larger than the propagated error (±0.009), it is still smaller than the variability based on the repeated experiments.

In membrane science, sometimes each data point is repeated twice or three times and the error is estimated using the standard deviation. In this study, each data point could not be repeated three times as the available membrane coupons were limited.

For sorption and permeability, an experimental variability was calculated for each data series where a single parameter was varied. In each data series, a single experimental data point was repeated at least three times. Instead of standard deviation, variability is estimated for that specific point by taking the largest difference among individual experimental data and the mean value. Variability in permeability (±0.07) calculated from five repeated experiments of a single data point is presented in the last column in Table 3-3 and is the largest compared to the other estimation results of the other methods. Therefore, estimated variability based on repeated experiments was used as an absolute variability for the rest of the data points in the specific series. In some data series, variability was estimated for additional data points and was presented individually. The additional data points were selected due to the experimental complexity and the expectancy of additional variability.

For deposit or foulant resistance data, it was observed that there was a linear correlation between the magnitude of the resistance and the magnitude of the specific variability, therefore a relative variability rather than absolute was used for resistance data series throughout the thesis.

4 Hormone Sorption on Polymers

4.1 Introduction

This chapter aims to provide a literature review on the polymeric materials which have hormone sorption affinity and the factors responsible for the hormone sorption on polymers. Additionally an experimental study on hormone sorption affinity of commercial polymers is conducted to enrich the discussion of the review.
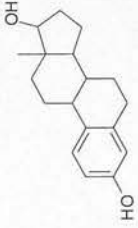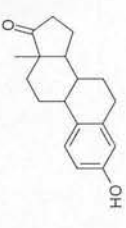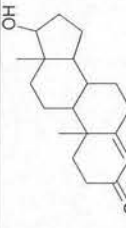
The experimental study is conducted by testing the hormone sorption affinity of various commercial polymers with known surface area. Considering its high endocrine disrupting potential [38, 39], E2 is selected as the representative hormone for this experimental study.

4.2 General Characteristics of Hormones
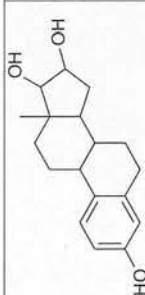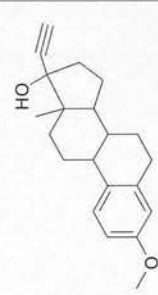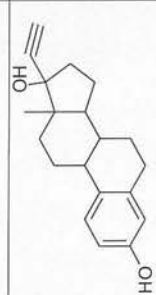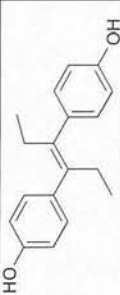
The physical and chemical characteristics of the selected hormones are given in Table 4-1. Although it is known that the characteristics contribute to interaction mechanisms, no direct correlation between a single characteristic of the hormone and its sorption behaviour could be made. A major difficulty in removing hormones from water is not only the small concentration in which they occur and are physiologically active, but also their small size or molecular weight (MW). The MW of the hormones is very similar, varying between 268 and 315 g/mol.

The Log K_{ow} parameter measures the hydrophobicity of the hormones by partitioning between octanol and water. As a general rule of thumb, compounds with Log $K_{ow} > 2.5$ are expected to accumulate in solid phases instead of being soluble in the aqueous phase. The Log K_{ow} values for the hormones given in Table 4-1 are above 2.5.

Table 4-1 Characteristics of selected hormones (taken from [171])

Compound	Molecular Formula	CAS No.	Molecular Structure	MW (g/mol)	Solubility in water (mg/L)	pK_a	Log K_{ow}	Dipole moment (Debye)	Solvent Accessible Molecular Surface Area[t] (Å)	H bond capacity
Estradiol (E2)	$C_{18}H_{24}O_2$	50-28-2		272	3.6, 82 [b,f,s]	10.23 [c]	4.01 [g]	2.2 [h]	390	Strong OH donor and acceptor; π weak acceptor (benzene)
Estrone (E1)	$C_{18}H_{22}O_2$	53-16-7		270	13, 147 [f,l,s]	10.34 [c]	3.13 [g]	2.1, 3.36 [h,o]	396	Strong OH donor and acceptor; Strong =O acceptor; π weak acceptor (benzene)
Testosterone (T)	$C_{19}H_{28}O_2$	58-22-0		288	24, 68 [m,s]	17.4 [s]	3.32 [g]	3.53 [e]	378	Strong OH donor and acceptor; Strong =O acceptor
Progesterone (P)	$C_{21}H_{30}O_2$	57-83-0		315	5, 8.8 [m,s]	NA	3.87 [g]	3.50, 4.58 [e,o]	418	Strong =O acceptor

4. Hormone Sorption on Polymers

Estriol (E3)	$C_{18}H_{24}O_3$	50-27-1		288	13, 441 [l,r,s]	10.25, 10.4 [n,s]	2.60 [l]	1.71, 3.22 [o,r]	394	Strong OH donor and acceptor; π weak acceptor (benzene)
Mestranol (ME2)	$C_{21}H_{26}O_2$	72-33-3		310	0.3, 3.5 [l,s]	-	4.10 [l]	-	471	Strong OH donor and acceptor; Strong -O- acceptor; π weak acceptor (benzene)
Ethinylestradiol (EE2)	$C_{20}H_{24}O_2$	57-63-6		296	4.8, 116 [r,s,l]	10.25, 10.5 [n,s]	3.67 [l]	2.64 [r]	405	Strong OH donor and acceptor; π weak acceptor (benzene)
Diethylstilbestrol (DES)	$C_{18}H_{20}O_2$	56-53-1		268	12 [r]	-	5.07 [r]	1.62, 2.2 [q,r]	475	Strong OH donor and acceptor; π weak acceptor (benzene)

a [172], b [66], c [173], d [174], e [175], f [176], g [176], h [177], i [178], j [179], k [180], l [181], m [182], n [183], o [184], p [185], q [186], r [67], s [187], t estimated using MarvinBeans 6.0.4 program

The water solubility and the dipole moment can also give an indication on the hydrophobicity of the molecule although they are not strong indicators like the parameter K_{ow} [188]. Less soluble and less polar molecules are unlikely to interact with water molecules and thus show hydrophobic properties.

Estrogen solubility in water (0.3 to 441 mg/L) has a remarkable variability in published data but is relatively low. Low solubility usually indicates larger sorption coefficients [189]. Dipole moments give an indication on the polarity of the molecules and vary from 1.6 to 4.6 Debye. The molecules with larger difference between positive and negative electrical charges have a higher dipole moment values [190]. Dipole moments of the molecules are important considering that considerable attractive interactions may occur because of the alignment of one dipole molecule with another [191].

Other characteristics considered have been molecular shape and size [66, 192-194]. The diffusivity of the molecules changes depending on its molecular weight. Enhanced sorption can be achieved if the molecules can diffuse into the polymeric material and interact with the internal active sites and this mostly the case for porous sorbents such as activated carbon [100]. Molecular shape can be exploited to prepare molecular imprints in polymers to create specific sorption sites [195]. Information on molecular surface area of hormone molecules (given as solvent accessible surface area) gives an indication on the number and mass of hormone molecules sorbed on polymeric sorbents with a known surface area, based on mono or mutli-layer coverage.

Proton donor and acceptor characteristics are further characteristics that may affect interaction with polymers, in particular the ability to form hydrogen bonds. H-bonding has been attributed to play a predominant role in the transport of hormones in biological systems [29, 196-200]. Electronegative atoms with a lone pair of electrons (as an acceptor) and hydrogen atom, which is bonded to an electronegative atom such as nitrogen (N) or oxygen (O), (as a donor) are the indications of the capability of hydrogen bonding [191]. The hydrogen bonding capacity of the

estrogens has been reported before. It is suggested that some hormones with hydroxyl groups, such as 17β estradiol [201] are able to make hydrogen bonding [202]. Nghiem et al. [176] reported results indicating that the oxygen atoms at the first ring of E1 and E2 have predominantly the potential to be involved in hydrogen bonding with membrane polymers. The hydrogen bonding capacity of progesterone with its electronegative oxygen atom acting as hydrogen acceptor in hydrogen bonding is also reported [203]. The similarity in the chemical structure of testosterone with the other hormone molecules and the existence of electronegative oxygen and a hydroxyl group indicate that T may have hydrogen bonding capacity as well. Hormones such as E1 and E2 possess a phenol group which is electron-rich [204] and can therefore form π-π bonding with electron deficient phenyl groups [191].

The pK_a shows the acid dissociation constant at which the hormones loose a hydrogen atom and become negatively charged. The hormones that have a phenolic hydroxyl group all dissociate in the same pH range; between 10.2 and 10.5. When the solution pH increases above the pK_a, the hormone molecules deprotonate and become negatively charged and this can influence their charge interaction with the polymeric sorbents. Dissociation may also cause loss of H-bonding capacity of hormones.

The given characteristics of the hormones indicate that sorption has a potential to be used as an efficient process for the removal of the hormones from water.

4.3   Hormone Sorption on Polymeric Materials

Sorption of hormones on polymeric materials was first noticed due to the interactions with laboratory equipment. For example, Petri dishes (PVC) were found to adsorb significant amounts of hormones and results were verified with grinded PVC [205]. One study established that polystyrene plastic ware adsorbed 38% and 43% of 17β-estradiol and progesterone, respectively [206], while another study reported that parathyroid hormone sorbed to borosilicate glass tubes, polycarbonate and cellulose

nitrate [207]. Sorption to polypropylene tubes was lower and equilibrium was reached within 4 hours [207]. Packaging materials equally have an adsorption capacity for hormones. Results using granular materials found very high adsorption capacities for polystyrol (6 ng/cm²), for glass (18 ng/cm² and 105 ng/cm² depending on the glass type), for polypropylene (60 ng/cm²), for polyethylene (PE, 75 ng/cm²), for Lupolen (low density polyethylene, 180 ng/cm²) and for Cellidor (Celluloseacetobutyrat, more than 420 ng/cm²) [208]. While concentration values were not provided in the study with packaging materials, the high adsorption most likely indicates a relatively high concentration of contaminants used.

Sorption has also been observed for filters used in sample preparation resulting in significant losses of analytes. Different types of filter materials were tested for estradiol adsorption and the results showed that cellulose acetate and cellulose nitrate adsorbed the most estradiol compared to glass fibre and paper materials [208]. Adsorption of up to 50% of feed estradiol concentration on a cellulose acetate filter was observed [209].

Sorption interactions are exploited for analytical purposes for example in chromatography as well as sample preparation. Solid phase extraction (SPE) is used for the concentration of analytes in samples. The most widely used SPE sorbents for micropollutants are alkyl-bonded silicas (C18 silica, C2 silica), copolymer sorbents such as cross-linked polystyrene divinylbenzene, and hydrophilic lipophilic balanced polymers. Each has specific contaminant applications [210, 211]. C18 resins and other polymeric sorbents have been used in several studies, separate or in combination, for purification and determination of pesticides, estrogens and progestogens with SPE [44, 212]. Solid phase micro-extraction (SPME) sorbs a fraction of the analyte and can be used for the quantification of analytes and analyte interactions with other dissolved molecules. Polyacrylate has been used for the detection of estrogens in water and their interactions with organic matter [213, 214]. Polydimethylsiloxane (PDMS), divinylbenzene (DB), polyacrylate (PA), as well as Carboxen (CAR; a carbon molecular sieve) and Carbowax (CW; polyethylene glycol) are other commonly used coating polymers for SPME of organics [215].

Recently developed molecularly imprinted polymers (MIPs) show potential for specific adsorption of hormone molecules, especially estrogens [195, 201, 202, 216-219].

Sorption is studied as one of the mechanisms which are responsible for the removal of hormones from water in polymeric membrane filtration. Hormone sorption on membrane polymers are known for both large MWCO membranes (UF and MF) and dense membranes (NF and RO).

Sorption of hormones on UF membranes is highly dependent on the membrane polymer material. For example, >34% of 17β estradiol is adsorbed on a UF membrane [220]. Adsorption of estrone, progesterone and testosterone is determined as ~45, 55 and 30% on ultrathin polyimide coated sulfonated polyethersulfone UF membrane respectively [32]. In another study on recovery of 6-α-methylprednisolone (a type of steroid) from heat-treated cell suspension of *Arthtobacter simplex*, UF membranes are used and results show that 27% and 31% of hormone is adsorbed on two different MWCO UF polysulfone membranes respectively [30]. The solution pH also plays an important role on the sorption process. Bisphenol A (BPA) is recognized as an artificial estrogen with similar characteristics [221]. Lyko *et al.* demonstrated that there was no removal of bisphenol (BPA) with UF membrane at pH>5 while 36% removal was achieved at pH 5. Schäfer *et al.* state 30% BPA adsorption at pH values 4-9 [29, 31]. Considering that BPA has a pK_a values of 9.28, charge repulsion due to dissociation is potentially hindering the adsorption process at higher pH values.

Sorption on polyamide NF and RO membranes is stated as a main mechanism responsible for removal of hormones such as estradiol, 17β estradiol, estriol, estrone, 17α ethynyl estradiol, testosterone and androstenedione in several studies [67, 90, 91]. The sorption of 17β-Estradiol on polyamide NF membrane is estimated as 0.12 μg/cm^2 by McCallum 2008 [68]. The results suggested that the adsorption of E2 is mainly occurring on the polysulfone layer of the membrane rather than the polyamide and the adsorption mechanism is suggested to be hydrophobic. The

sorption is found to be influenced strongly by the operating conditions and the water quality. In another study, the retention of E1 and E2 on porous membranes is found to be less due to the decreased adsorption compared to the denser NF/RO membranes [176]. This can be due to the portioning of the trace contaminants on membrane surfaces and diffusion into the dense membrane structure as it is the case for E1 [222]. The adsorption of E1, E2, T and P on NF membranes with polyamide active layer and polysulfone support layer is reported [223]. 22-46% of adsorption occurred for progesterone, testosterone, 17α-ethinylestradiol, estriol and estradiol on polyamide NF membrane [69] and similar sorption rates of 27% is reported for estrone on polyamide NF membrane by Hu et al. [70].

The literature review shows that polymers have a sorption affinity for hormones and the affinity depends on hormone and polymer type as well as the solution chemistry.

4.4 Hormone Sorption on Polymer Surface Area

The surface area of the sorbents gives an indication on the availability of active sites for the sorption of hormones. The importance of the active surface area for hormone sorption on polymeric materials is studied in membrane filtration and adsorption. The membrane adsorption is usually presented in hormone mass adsorbed per unit surface area (ng/cm^2) and the area in the unit usually refers to the top surface area of the membrane. However, the internal surface area of the membrane structure is expected to influence the adsorption as well. The retention of hormones by different membrane material and MWCO is given in the following increasing order of adsorption: X20 (MWCO <200 Da, polyamide) > TS80 (MWCO <200 Da, polyamide) > NF270 (MWCO 400 Da, polyamide) > UE10 (MWCO 10000 Da, polysulphone) [224]. Results show that the membrane which has the highest retention has the smallest pore size and at the same time has the lowest adsorption indicating that the adsorption is larger for the membranes with larger pore. However, the difference can be attributed to both the differences in material type as well as the pore size of the membranes. Semião [93] studied the influence of pore size on E2 adsorption with the same membrane NF270 but different batches which have

different pore sizes and showed that larger pore size membrane has a larger amount of hormone adsorbed. This was attributed to the larger amount of hormone having access to the internal active sites of the membrane. It is also noted that for the membranes with similar pore size, the membrane providing a larger internal surface area adsorbs more hormone [93]. The membranes are usually made of several polymeric materials and the internal surface area can vary a lot due to its physical characteristics such as thickness, pore size and porosity. Therefore, investigating the influence of surface area on the hormone sorption on polymeric membranes is challenging.

A simpler and systematic study is required for understanding the influence of surface area on the hormone sorption by polymeric materials as particles. Besides the available surface area of the polymer, type of polymeric material plays a significant role on the extent of adsorption and this is due to the various intermolecular interactions happening between specific polymers and hormones.

4.5   Intermolecular Interactions in Hormone Sorption on Polymers

Sorption of hormones on polymeric materials is commonly exploited in the application of chromatography and solid phase extraction (SPE) beyond membrane filtration. Hydrophobic effect, dipole-dipole, dipole-induced dipole and dispersive interactions, hydrogen bonding and ionic interactions are the mechanisms mentioned to be playing role in the adsorption process for these applications [225].

Looking at the intermolecular interactions three main mechanisms are considered to be playing a role in the adsorption of hormones on polymer materials. These mechanisms are hydrophobic interactions, hydrogen (H) bonding and π-π stacking and illustrated in Figure 4-1. The strength of the interactions between the hormone molecules and the sorbent materials can change significantly depending on the solution chemistry [226].

Hydrophobic molecules, in this case hormone and polymers, in water tend to agglomerate as they are squeezed out of the way of the strong interactions between the water molecules.

A) Hydrophobic interaction

B) Hydrogen bonding

C) π-π interaction (stacking)
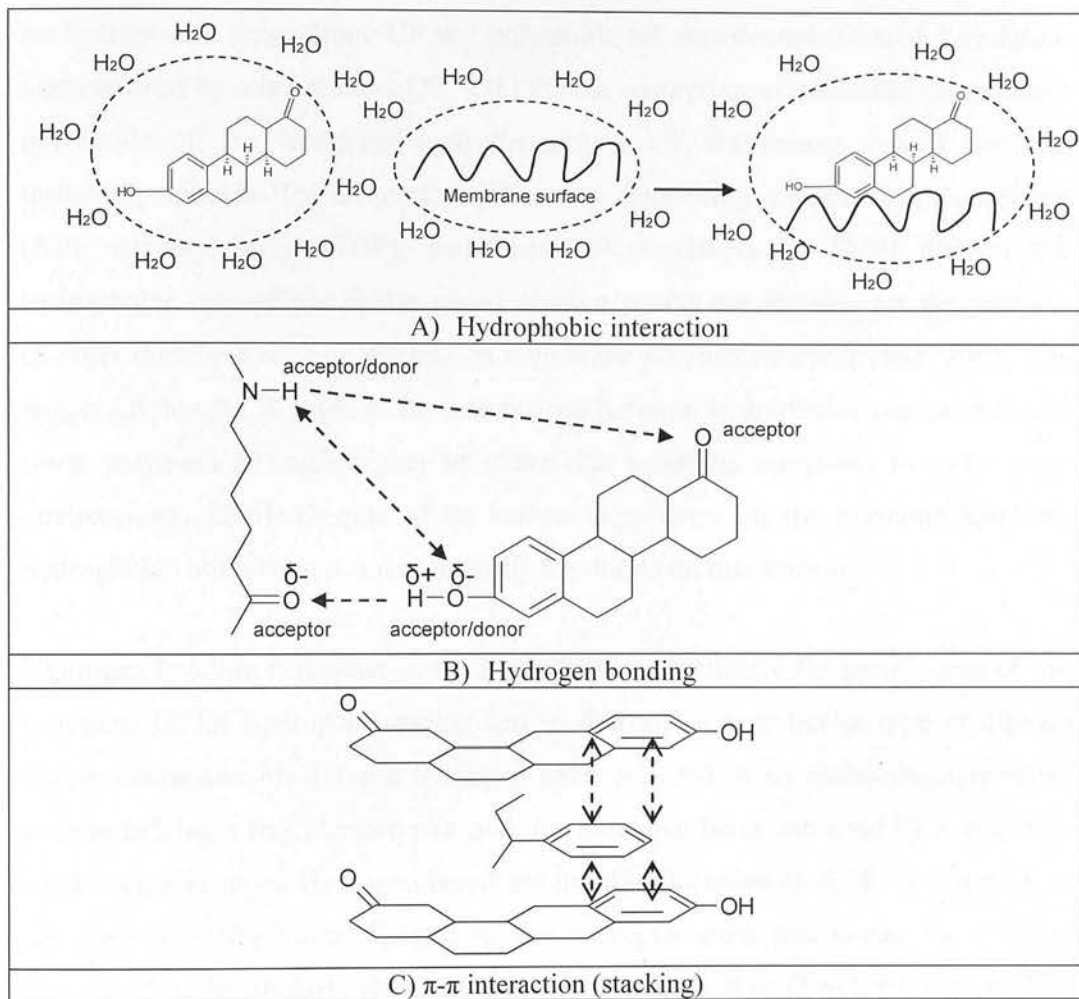
Figure 4-1 Selected possible intermolecular interactions between hormones and polymers. A) hydrophobic interaction between polypropylene (PP) and estrone (E1), B) hydrogen bonding between polyamide (PA) and estrone (E1), C) π-π interaction between aromatic rings of polystyrene (PS) and estrone (E1). Interaction mechanisms adapted from [191]

This hydrophobic effect can resemble an attraction between two hydrophobic molecules. With hydrophobic interactions, the molecules tend to form a host guest complex instead of forming individual "holes" in the structure of bulk water and this results in a lower overall free energy with an entropic gain [191].

Hydrophobic molecules and polymers are expected to interact with each other when they are found in aqueous solution. The adsorption of the estrogens on MIPs is

attributed to the hydrophobic interactions and it is suggested that the estrogens with higher K_{ow} has higher possibility of sorption due to the enhanced hydrophobic interactions [219]. Camerton et al. [227] reported a correlation between the K_{ow} of 17α estradiol, 17β estradiol, estriol, estrone, 17α ethynyl estradiol and their sorption on hydrophobic polysulfone UF and polyamide NF membranes. Similar correlation was obtained by other authors [33, 228] for the adsorption of hormones on aromatic polyamide NF or sulfonated polyethersulfone UF membranes coated with an ultrathin polyimide. The adsorption of hormone mimicking compounds, nonylphenol (NP), tertbutylphenol (TBP), and bisphenol A (BPA) by [229] due to the hydrophobic interactions is also stated. Similar results are obtained for the sorption of other dissolved organic matters on membrane polymers as well [188, 230]. It is suggested that the strength of the interactions between hydrophobic compounds and some polymers is much higher in water rich solutions compared to water poor environments [226]. Despite of its known importance on the hormone sorption, hydrophobic interaction is not necessarily the dominant mechanism.

Hydrogen bonding is another interaction which can influence the partitioning of the estrogens [231]. Hydrogen bonding can be defined as a particular type of dipole-dipole interaction involving a hydrogen atom attached to an electronegative atom usually bearing a free electron pair and this hydrogen being attracted by a similarly electronegative atom. Hydrogen bonds are usually illustrated as X-H...Y where X is the electronegative atom attached to the hydrogen atom and acting as a donor whereas Y is the similarly electronegative atom such as N or O as the acceptor. The strength of normal hydrogen bonds changes typically between 4 and 60 kJ/mol. Hydrogen bonding can be classified into three categories being strong, moderate and weak. Hydrogen atoms shared between electronegative atoms and π electrons of aromatic rings or C-H groups is an example of weak hydrogen bonding [191]. Nghiem et al. [176] reported that hydrogen bonding can form between the 3-oxygen atoms of the first ring of estrone and estradiol and membrane polymer. The sorption of E1, E2, EE2 and BPA on polyamide MF membranes is attributed to the hydrogen bonds forming between the amide groups of PA and proton-donating moieties of the estrogens [232].

The self-assembly of the estrogens used as a template for MIPs was based on hydrogen bonding mechanism considering that these molecules have predominantly carbonyl and hydroxy groups [195]. Specific functionalization of the MIPs with groups which may have high hydrogen bonding capacity with hormones is under investigation. For example, it is observed that MIPs functionalized with amide groups have a stronger hydrogen bonding capacity compared to carboxyl groups [233]. Buszewski et al. [217] suggested that the hydrogen bonding is a dominant interaction between the MIP and 17β Estradiol. The solvent seems to be playing an important role on the strength of these hydrogen bonds [217, 233, 234]. It is suggested that the hydrogen bonding capacity of the molecules can be higher in non-polar solvents as non-polar solvents favour hydrogen bonding whereas in water, hydrogen acceptors and donor becomes surrounded by water molecules which lead the hydrophobic interaction to be dominant [191]. Sanbe and Haginaka [201] also reported that hydrogen bonds formed by hormones are more important (compared to hydrophobic interactions) in the absence of the water.

The importance of hydrogen bonding for the retention of the estrogenic compounds on polymers in high performance liquid chromatography (HPLC) applications is also reported and it is suggested that the bonding can form between the diethylamino groups on a MIP and the weakly acidic phenolic groups on the estrogens [216].

Both interaction mechanisms, hydrophobic and hydrogen bonding, are held responsible for the adsorption of hormones on membrane polymers in membrane filtration [176, 222, 223]. In the case of the MIPs, the electrostatic interactions are the main driving force while hydrogen bonding and hydrophobic interactions are considered to be contributing to the binding, especially in water rich environments [226]. The relatively high adsorption of E1, E2, EE2 and BPA onto MIPs can be explained by the hydrophobic properties of both the estrogens and MIP itself. Hydrogen bonding through carbonyl, carboxyl groups and the phenolic groups as well as van der Waals forces are also contributing to the adsorption [235]

In addition to hydrophobic interactions and H-bonding, π-π interaction is a possible mechanism to be considered. The difference between the π densities of the adsorbent and the corresponding adsorbate determines the stability of the π-π interaction. π density is determined by electron rich and deficient aromatic fragments [236]. π-π interactions and strong hydrophobic interactions are involved in the sorption mechanisms of methylene and phenyl groups to hypercrosslinked polystyrene [236]. Sychov et al. [237] states that π-π interactions between the hypercrosslinked polystyrene and the molecules with π-systems of electrons such as aromatic rings, carboxyl groups and alike governs the retention mechanisms in HPLC application with non-polar solvents. In fact, hypercrosslinked polystyrene has a strong π-electron donating-accepting ability in non-polar organic solvents. This ability results in high sorption capacity of compounds which contain aromatic π-systems or functional groups with free electron pairs in HPLC application [238]. Sorbents used in SPE with phenyl groups (such as polystyrene divinlybenzene) have the capacity to interact with steroids through π-π interactions. The number and positioning of phenyl groups in this phase determine the level of π-π interactions and the sorption capacity. It was suggested that the π-π interaction between the phenyl phase and the steroid occurs when the double bonds of steroid and phenyl group overlap [238].

The reasons why specific polymers have higher affinity for certain hormones are still not understood completely. Beyond the uncertainty in active surface area due to variability in material size, shape and porosity the responsible intermolecular interactions need to be clarified.

In this study, several commercially available polymers are purchased and tested for their sorption capacity in order to enrich the discussion on the hormone sorption on polymeric materials based on the literature review. For the comparison the polymer particles are reduced to the similar size by grinding process except for the few that could only be purchased in small sizes. Having similar particle size for the polymers has provided a relatively more reliable comparison in terms of available surface area.

4.6   Materials and Methods

The supplier, preparation method and the final particle size of the 13 polymers used in this chapter were given in Section 3.2.1. The surface morphology and the size of the polymer particles were analysed and measured with field emission electron microscopy (FESEM) as described in Section 3.3.4.

17β-estradiol (E2) was selected as the representative hormone for the experimental study in this chapter and tritium labelled E2, [1, 2, 6, 7-3H] was used to prepare the solutions. No background electrolyte was used in order to prevent its interference on hormone sorption on polymers. The characteristics of the E2 are given in Table 4-1.

The batch adsorption protocol is described in Section 3.6.1. The hormone concentration in feed and filtrate samples were measured with scintillation counter as described in Section 3.5.4.

4.7   Characteristics of the Polymers
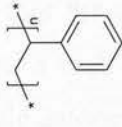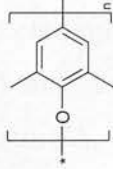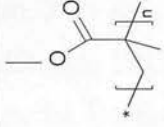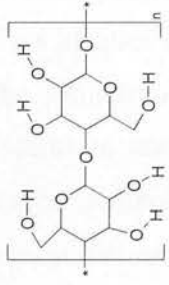
The chemical and physical properties of the polymers are compiled in Table 4.2. The chemical structure gives an indication about the kind of interaction each polymer can make with E2. The contact angle is usually measured with a water droplet and it is the angle where a water interface meets a solid surface. The solid surfaces with contact angle larger than 90° are considered hydrophobic whereas the hydrophilic surfaces usually have values less than 90° [28]. As the surface characteristics highly depend on the manufacturing process, the contact angle values obtained from the literature may not necessarily describe the specific polymer properties well.

PES Radel A, PS, PP and HDPE are hydrophobic polymers. PPO can be considered both hydrophobic and hydrophilic as it has a contact angle very close to 90°. Cellulose seems to be the most hydrophilic polymer with a contact angle of 24°. The rest of the polymers have similar contact angle values and show hydrophilic characteristics.

Table 4-2 The physical and chemical properties of the polymers

Polymer Name	Supplier	Structure	Monomer MW (g/mol)	Density [a] (g/cm³)	Refractive Index (-)	Contact Angle (°)	Average Particle Size (µm)
Polysulphone (PSu), (PSu UDEL)	Goodfellow & Solvay		442	1.24	1.63[m]	77[c]	224
Polyester; Polyethylene Teraphthalate (PET)	Goodfellow		192	1.35	1.58-1.64[b]	79.09[d], 81[e], 70[f]	244
Polyester; Polyethylene Naphtalate (PEN)	Goodfellow		242	1.36	1.65-1.90	80[f]	226
Polyamide Nylon, 6 (PA)	Goodfellow		113	1.14	1.53[b]	70[e]	202
Polyethersulphone (PES)	Goodfellow		232	1.37	1.65[b]	56[g], 72[f]	310
Polyethersulphone (PES Radel A)	Solvay		324	1.37	1.65[b]	127[h]	232
Polyvinylidene fluoride (PVDF)	Solvay		64	1.78	1.42[m]	71[i]	164

4. Hormone Sorption on Polymers

Polymer	Source	Structure					
Polystyrene (PS)	Goodfellow	[structure]	104	1.05	1.59-1.60[b]	91[e]	198
Polypropylene (PP)	Goodfellow	[structure]	42	0.9	1.49[b]	95[f]	194
Polyethylene (HDPE)	Goodfellow	[structure]	28	0.95	1.54[b]	93-94[f]	202
Poly(2,6 dimethyl 1,4-phenylene oxide) (PPO)	Sigma	[structure]	120	1.06	1.57[m]	88[j]	71
Polyacrylate; Poly(methyl methacrylate) (PMMA)	Sigma	[structure]	100	1.2	1.49[m]	73[f]	204
Cellulose	Sigma	[structure]	324	1.55	1.47[l]	24[k]	11

[a] Materials Safety Data Sheet, [b][239], [c][240], [d][241], [e][242], [f][243], [g][244], [h][245], [i][246], [j][247], [k][248], [l][248], [l][249], [m][250],

4.8 Estradiol Sorption on Polymers

E2 sorption is studied for various commercially available polymers in order to provide a better understanding of the underlying mechanisms governing the sorption. The sorption affinity of the polymers for E2 is presented in Figure 4-2. The affinity is presented in two different ways by normalising the E2 mass adsorbed (ng) by first mass of polymer (g) and second by the polymer surface area (cm^2). The surface area of the polymer was calculated from the particle size distribution data obtained from FE-SEM. It needs to be noted that this measurement takes only the external surface area into account and the possible internal surface area due to the polymer porosity is neglected. If a polymeric surface can be measured including the pores then the surface area related sorption can be evaluated better.

Mass and surface area normalized affinities (ng/g and ng/cm^2) are presented in Figure 4-2A-B and Figure 4-2C-D, respectively. The results show that PA has the largest affinity (2.30 ng/g) for E2 with relatively fast kinetics. Fast kinetics of PA indicates that the sorption is a surface phenomenon. PES R is the second polymer which has a high affinity (1.50 ng/g) for E2. Although PPO seems to adsorb a comparable amount of E2 (2.29 ng/g) with PA, when the sorption is normalized with surface area, the sorption affinity of PPO (0.001 ng/cm^2) is one of the smallest among the other polymers. Similarly, E2 sorption is the smallest for PVDF (0.22 ng/g), however when normalized with surface area, its sorption affinity (0.006 ng/cm^2) is comparable to most of the polymers. Cellulose (0.001 ng/cm^2) and PMMA (0.001 ng/cm^2) are the other two polymers besides PPO which have almost no sorption affinity for E2. There is not an obvious difference among the rest of the polymers for E2 sorption. The difference between the mass and surface area normalized affinity show that the surface area is a very important parameter playing role in the hormone sorption on polymers.

Hydrophobic interactions are considered to be one of the main mechanisms responsible for the hormone sorption on polymeric materials. Surprisingly polymers, which have a larger contact angle indicating high hydrophobicity such as HDPE

(0.61 ng/g), have less sorption affinity for E2 compared to hydrophilic polymers such as PA (2.30 ng/g).
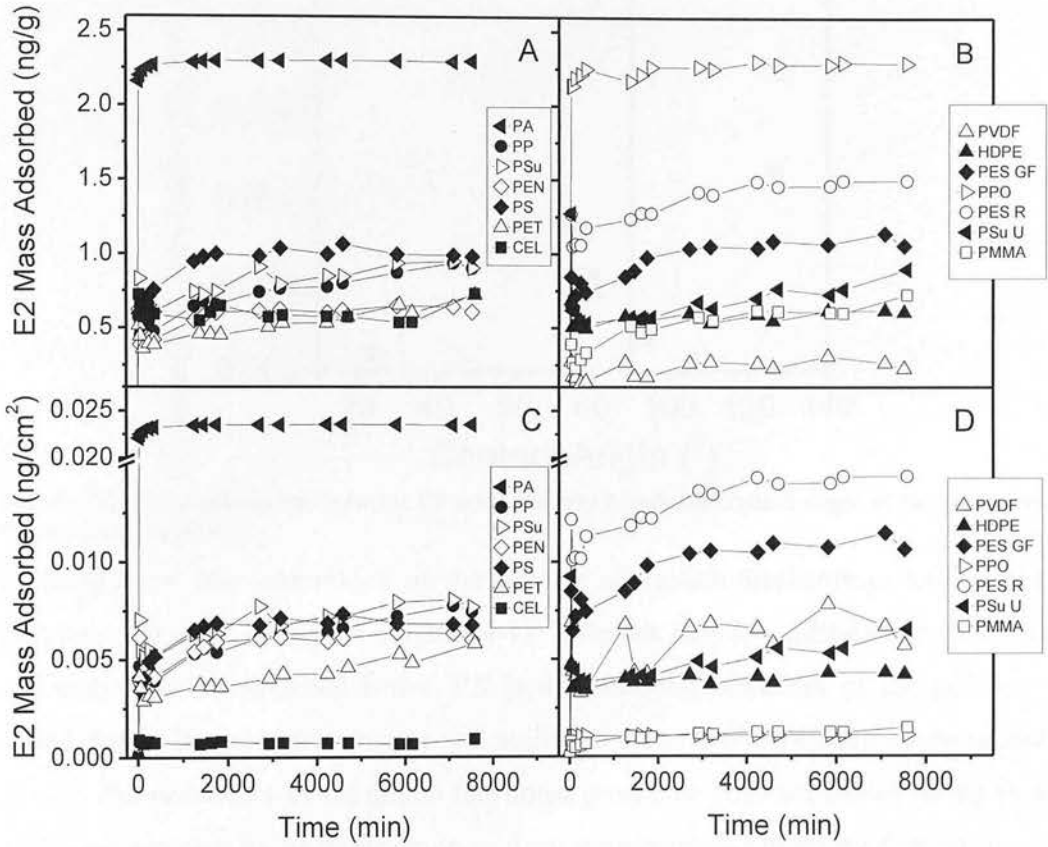
Figure 4-2 Estradiol (E2) adsorption on different polymers. A-B: E2 mass adsorbed/polymer mass, C-D: E2 mass adsorbed/polymer surface area. 2.5 g of polymer in 60 mL of 100 ng/L E2 solution

In order to find out if there is a correlation between the hydrophobicity of the polymers and the E2 affinity, E2 mass adsorbed is plotted against the contact angle of the tested polymers in Figure 4-3. It is observed that there is no correlation between the experimental sorption results and the hydrophobicity of the polymers.
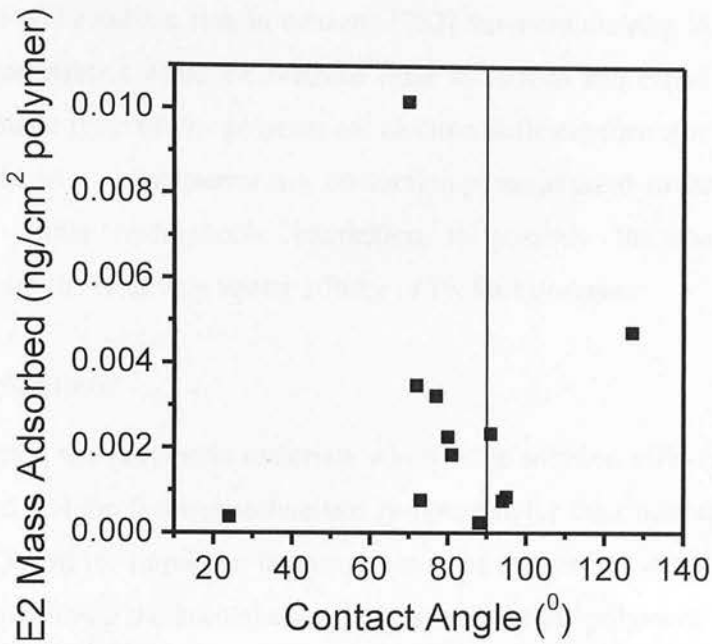
Figure 4-3 The relationship between E2 mass adsorbed and the contact angle of the polymers (taken from Table 4-2)

Looking at the literature review on the possible interaction mechanisms between the polymers and the hormones (Figure 4-1), different sorption affinities by various polymers can be explained better. PA is the strongest adsorbent of the polymers tested due to its quite polar nature and ability to act as both hydrogen acceptor and donor. The possibility of the amide functional groups on polymer chains acting as a hydrogen acceptor for phenolic compounds or steroids is also mentioned by Saitoh et al. [251]. High hormone sorption capacity of membranes with polyamide active surface agrees with the observed result. PVDF is known to dislike interactions with either hydrophobic or hydrophilic compounds. The adsorption on PVDF is indeed relatively low. Polysulphone and polyethersulphone radel (PES R) have similar functional groups but the hormone sorption onto these polymers is very different. This difference can be explained by the fact that polysulphone has more diluted functional groups in the structure compared to PES R. The sulphone group of PES R makes the polymer polar and available for H-bonding. Although cellulose has a high capacity for H-bonding it does not like to H-bond with other molecules which is confirmed with the estrogen results. It does, however, interact with its own functional groups. After PA and PES, PS is one of the polymers which have a relatively high sorption capacity. As the distribution of the π electrons is even around the top and

bottom face of the carbon ring in benzene [252] the aromatic ring in PS is expected to be electron neutral while the benzene rings in estrone and estradiol are electron rich. If aromatic rings on the polymer are electron deficient then π-π stacking would be expected. As a consequence π-π interaction is anticipated to be a contributing mechanism while hydrophobic interaction is possibly the main mechanism responsible for the relatively strong affinity of PS for estrogens.

4.9 Conclusions

In this chapter, the polymeric materials which have sorption affinity for hormones are reviewed and the factors/mechanisms responsible for their hormone sorption are discussed. One of the important factors seems to be the surface area of the polymeric particles determining the hormone sorption capacity of the polymers. The size of the polymeric particles as well as the microporosity (if exists) and pore size determines the available area for the sorption to take place, thus influences the sorption capacity of the polymers.

As important as the polymeric surface area, intermolecular interactions seem to influence the hormone sorption capacity of polymers. As stated in the literature, the interaction mechanisms are governed most likely by molecular and supramolecular interactions such as hydrophobic interactions, hydrogen bonding, π-π interaction, ion-dipole and dipole-dipole interactions. Type of polymer, hormone characteristics and solution chemistry can influence these interactions to a great extent. Determination of the dominant interaction mechanism responsible for the hormone sorption on polymeric materials is rather challenging. Experimental results in this chapter show that there is no correlation between the hydrophobic properties of several polymeric materials and their E2 sorption capacity indicating that hydrophobic interaction is not the dominant mechanism. In parallel, it is observed that a hydrophobic polymer such as PP has a much smaller hormone sorption capacity than a polymer such as PA which is hydrophilic.

Polyamide is experimentally shown to have the highest sorption capacity for E2 among the tested polymers and in the literature this strong affinity is attributed to the ability of polyamide forming hydrogen bonding with hormone molecules. Literature suggests that hydrophobic interactions are expected to be dominant in comparison to hydrogen bonding and π-π stacking between hormone molecules and polymeric particles in polar solvents like water. Nevertheless, strong affinity of hydrophilic PA for hormones in comparison to hydrophobic polymers indicates the importance of hydrogen bonding as an interaction mechanism for the sorption, especially in the case of PA.

In order to provide a better understanding of the dominant sorption mechanisms for a specific polymer, quantification of the interaction energies is required. However, a systematic quantification of the contribution of each interaction is challenging given the low energies of the interactions, the complexity of the system and the possibility of several interactions taking place simultaneously. Such an investigation within the scope of future work will be very valuable.

5 Hybrid Polystyrene Nanoparticle-Ultrafiltration System for Hormone Removal

5.1 Introduction

A hybrid polystyrene (PS) nanoparticle-UF system is proposed for the first time to remove hormones from water in this research. The aim of this chapter is to:

- study the fundamental design parameters of a hybrid PS nanoparticle-UF system to remove hormones from water and

- evaluate the performance of the hybrid system in comparison to NF/RO system in terms of hormone removal and membrane permeability.

The PS nanoparticles are employed as the sorbent in the hybrid system because firstly they provide a large surface area and secondly they are uniform, non-porous, can easily be manufactured in different sizes and be functionalized. Cross-linked polystyrene divinlybenzene (PS-DVB) is one of the widely used sorbents in solid phase extraction (SPE) for concentration of the trace contaminants [210, 211]. Sorption of steroids on PS-DVB has been reported [238]; however, hormone adsorption capacity of the plain PS nanoparticles at environmental hormone concentrations has not been studied before.

E1 and E2 are reported to have higher magnitude estrogenic activity compared to many other endocrine disrupters [38, 39]. The concentrations of estrogens detected in WWTP effluents and surface waters are in ng/L [5]. Therefore, E1 and 100 ng/L are chosen as the representative hormone and hormone concentration to be studied.

Finding an optimum nanoparticle size and concentration is the biggest research challenge of the system design as there is an expected trade-off between adsorption and membrane permeability. It is expected that smaller particle size or higher particle concentration will result in higher hormone sorption. However, the limitations of the sorption onto PS nanoparticles in the hybrid system are not known. In contrast,

smaller particle size or higher particle concentrations are likely to cause fouling and decrease the permeability of the UF membranes.

The adsorption is highly influenced by the hormone type and the solution chemistry such as pH [171, 199, 253]. Simultaneously, solution pH is an important parameter for particle stability and thus permeability since the amount of particles deposited and deposit porosity can be influenced by pH [155, 158, 254]. Therefore, the influence of variation in solution pH is required to be studied for a better understanding of the system operation.

The chemical and physical characteristics of the hormone determine the interaction mechanisms responsible for the sorption. Studying the sorption capacity of the PS particles for different hormones is essential to investigate whether the system is applicable for a wider range of hormones rather than one specific one. For this specific investigation, E2, T and P are selected besides E1.

The method that the PS nanoparticles are integrated into the hybrid system is very important as it can influence hormone sorption as well as the membrane permeability. In this study, PS nanoparticles are pre-deposited on UF membrane surface in order to provide a systematic, controlled study of the membrane fouling. Nevertheless, E1 sorption capacity is studied with two integration methods for PS nanoparticles: pre-deposited and pre-mixed, to elucidate whether the method has an influence on the sorption.

The sorption capacity of PS nanoparticles is studied with changing particle size, concentration, solution pH and hormone type as well as the permeability of ultrafiltration membranes with molecular weight cut off ranging between 1 and 100 kDa. Based on the experimental results obtained, a model has been developed to predict the hormone mass adsorbed and the permeability with changing PS particle size and the feed concentration. The potential of the proposed system for practical application is discussed for each changed parameter.

5.2 Selection of the Sorbent

In order to make a selection of the polymeric sorbent material for the proposed hybrid sorbent-UF system for hormone removal, the availability of the surface area is chosen as the main selection criteria. The importance of the surface area for hormone sorption on polymeric materials is detailed in Section 4.4 and 4.8.

Nanomaterials are considered as a new research area for water purification processes considering they provide large surface area and their enhanced reactivity and selectivity for specific compounds [255]. The chemical stability of polymeric nanoparticles could allow the regeneration of the particles for large scale application. While there are no studies where polymeric nanomaterials are used as sorbent materials for hormones, they have been applied to the removal of dissolved organic matter and other trace contaminants. One of the applications of polymeric nanoparticles in water treatment is using the particles as a pre-adsorption process prior to the membrane filtration. Polysulfone nanoparticles are used in a pre-adsorption process prior to the membrane filtrations and found to be very effective in removing the natural organic matter fraction which is responsible for membrane fouling [256]. Application of non-polymeric nanoparticles for micropollutant removal also exists and the importance of the nano-sizes for these applications is emphasized. Jawor and Hoek [14] studied the cadmium sorption capacity of polymeric and non-polymeric nanoparticles. Zeng et al. [257] stated that the adsorption affinity of nanosized hematite particles for uranium increased as the particle size decreased. In another study with microscale adsorbents, the metal uptake of tree fern particles increased per unit mass of sorbent with a decrease in the particle size [258].

Among the available polymeric nanoparticles, the PS nanoparticles are the most commonly and cheaply manufactured particles. Beyond the cost and availability, PS nanoparticles are very uniform, non-porous and easily adjustable in size and surface functionality. The uniformity and availability of a wide size range enable a systematic and fundamental investigation of the hormone adsorption in correlation

with the available surface area. As the particles are non-porous, the sorption will be mainly governed by adsorption on the particle surface. Moreover, commercial availability of the particles with various functional groups make it possible (if necessary) to study whether the sorption capacity of the particles can be increased by enhancing the intermolecular interactions between the particles and the hormone molecules. Therefore, PS nanoparticles are selected as the sorbent material for the hybrid polymeric sorbent-UF system.

5.3 Materials and Methods

5.3.1 Nanoparticles and Characterisation

Plain PS nanoparticles of 52, 81, 465 and 3000 nm and fluorescent PS nanoparticles of 43 nm from Polysciences were employed in the experiments. The effective diameter and the zeta potential of the particles were measured as it is described in Section 3.3.1 and 3.3.2 respectively. The size of the 52, 81 and 465 nm particles as well as their morphology was studied with FE-SEM analysis. The average diameter of the 15 different particles measured on a sample image was taken as the effective diameter. Methodology used in microscopic analysis is detailed in Section 3.3.4. A turbidimeter was used to measure the nanoparticle concentration in the samples as explained in Section 3.5.3.

FE-SEM was used to image the nanoparticle deposit on membrane surface in order to analyse the homogeneity and thickness. The methodology is described in Section 3.3.4.

5.3.2 Solution Chemistry

Radiolabelled [2, 4, 6, 7-3H] estrone (E1), [2, 4, 6, 7-3H] 17β-estradiol (E2), [1, 2, 6, 7-3H] testosterone (T), and [1, 2, 6, 7-3H] progesterone (P) and non-labelled E1 were used to prepare the hormone solutions. The chemical and physical characteristics of the estrogens are given in Table 4-1. All hormone solutions were prepared in a background electrolyte solutions of 1 mM $NaHCO_3$, 20 mM NaCl and the solutions were adjusted to pH 7 with 1 M HCl and 1 M NaOH unless stated otherwise.

Hormone concentration in the samples was analysed with a scintillation counter as described in Section 3.5.4.

5.3.3   Batch Adsorption Protocol

For the sorption isotherm, batch sorption experiments were conducted with 16 mg/L plain PS (52 nm) particles at varying concentrations of E1 solution (50, 100, 500 and 5000 ng/L) and solution pH of 5, 7 and 12. E1 concentrations higher than 500 ng/L radio labelled E1 was mixed with non-labelled E1. For determining the E1 adsorption capacity at varying PS nanoparticle concentration, a range of 1.6-7.9 mg/L of 52 nm PS particles was added into 100 ng/L radiolabelled E1 solutions. The adsorption experiments for E1, E2, T and P were performed with 16 mg/L of fluorescent (43 nm) and plain (52 nm) PS particles and 100 ng/L hormone solution. The experiments for all hormones were also conducted with 100 mg/L of fluorescent (43 nm) PS particles. The protocol is detailed in Section 3.6.2.

5.3.4   Membranes and Characterisation

The list of the ultrafiltration membranes used in this chapter is presented in Section 3.1.1. The surface charge characterisation was conducted with streaming potential method as described in Section 3.1.2 and the surface morphology was studied with Atomic Force Microscopy (AFM) (Section 3.1.3).

5.3.5   Membrane Filtration Protocol

The stirred cell system, described in Section 3.7 was used for the filtration experiments. Flat sheet UF membranes were compacted for 30 minutes and then pure water flux was recorded for an hour.

PS nanoparticles were mixed into 100 mL ultra-pure water and the solution was filtered until there was no water left in the cell and all the particles were deposited on the membrane surface. Following the deposition, the ultra-pure water flux of the membrane with nanoparticle deposit was recorded for an hour. For all the membrane filtration experiments, 450 mL of 100 ng/L hormone solutions were filtered until 50

mL of concentrate was left in the cell. During this filtration, 8 samples of 50 mL permeate were collected in glass bottles. The pressure applied for different MWCO membranes are given in Table 5-1. Membrane sorption (blank) experiments were performed using the same protocol without nanoparticle deposition. Hormone concentration in feed, permeate and the concentrate samples were analysed.

For the premixing experiments, the PS particles were added into 100 ng/L of hormone solution and the solution was mixed for 3 hours at 300 rpm in a glass bottle on a magnetic stirrer at room temperature (21±2 °C) prior to the filtration.

5.3.6 Kinetic Experiment Protocol

The kinetics of the E1 sorption on PS nanoparticles was determined by static filtration experiments using 3 kDa membranes. Unlike continuous filtration experimental set up, manually controlled valves were used to control the sampling of the permeate samples (see Figure 3-3). 450 mL of 100 ng/L E1 solution was placed in the stirred cell. Two different concentrations of 16 and 31 mg/L of 52 nm PS nanoparticles were added into hormone solutions and stirred at 300 rpm by magnetic stirrer. The valves were kept closed throughout the experiments except when 6 mL of samples were collected from the permeate line at certain time intervals. Kinetics of the membrane (3 kDa) sorption was determined with the same protocol without particle addition.

5.3.7 Data Analysis

For the batch (centrifuge) experiments in order to calculate the hormone mass adsorbed, M_{ads} (ng) on PS nanoparticles, a simple mass balance (Equation 5-1) was used where V_i is the initial volume (L), C_i and C_s are the initial and supernatant E1 concentrations (ng/L) respectively, $m_{ads(tube)}$ is the mass adsorbed onto the centrifuge tube.

$$M_{ads} = (C_i - C_S)V_i - m_{ads(tube)} \qquad 5\text{-}1$$

$m_{ads(tube)}$ was determined conducting blank sorption experiments where no nanoparticles were added in the tube. Based on these blank experiments, a correlation

between the equilibrium hormone concentration and the $m_{ads(tube)}$ was obtained. This correlation is presented for all hormones in Figure 5-1. In order to calculate the E1 mass adsorbed (M_{ads}) on PS nanoparticles during the filtration experiments, Equation 3-1 was used where n is equal to 8.
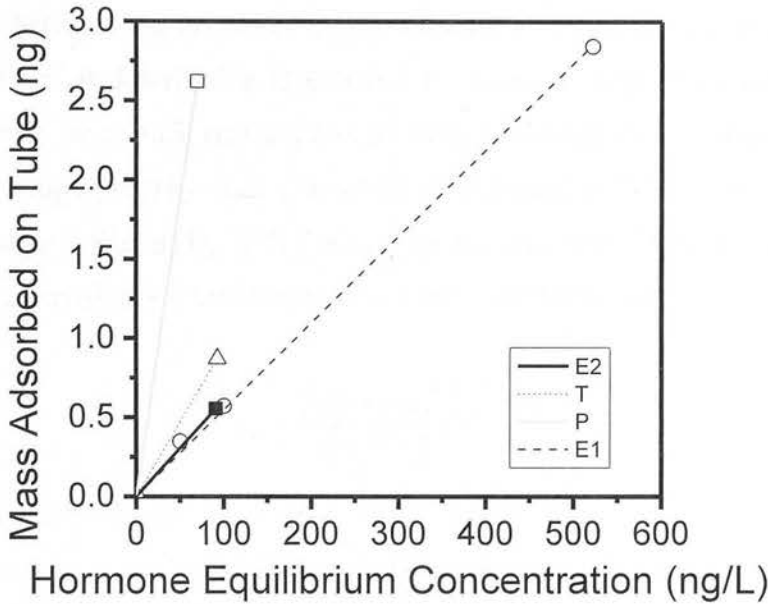
Figure 5-1 Hormone sorption isotherm onto centrifuge tubes: batch experiment, hormone solution with 1 mM NaHCO₃ and 20 mM NaCl background electrolyte, pH 7

The PS surface area available was calculated using Equation 5-2 where, c_f is the particle feed concentration (g/L) which can be replaced by c_i for batch adsorption experiments, V_f is the volume of the feed solution (L) which can be replaced by V_i for batch adsorption experiments, ρ_p is the particle density (g/cm³) and D_p is the diameter of a particles (cm)

$$SA_{PS} = \frac{6c_f V_f}{\rho_p D_p}$$

5-2

The mass of the particles in the deposit (M_d) was calculated using Equation 5-3, where c_f, c_p, c_c are the concentrations of the nanoparticles in the feed, permeate and the concentrate respectively and V_f, V_p, V_c and V_d are the volume of the feed, permeate, concentrate and particle deposit on the membrane surface. For the deposition experiments, the amount of PS particles in the concentrate was assumed to be

negligible, thus c_c is equal to zero since all the particles were deposited on the membrane before the solution filtration.

$$M_d = c_f V_f - c_p V_p - c_c (V_c - V_d)$$

5-3

Deposit resistance of the PS nanoparticles (R_d) was calculated using Equation 3-3. The relationship between the R_d, specific deposit resistance (given by Equation 2-8) and deposit thickness is described in Equation 5-4 where ε is the porosity (void) and D_p is the diameter of the particle (m) and δ is the nanoparticle deposit thickness (m). In this study, an average porosity was calculated with Equation 5-4, using R_d determined experimentally, replacing D_p with the average nanoparticle diameter measured and δ with average deposit thickness determined with FE-SEM images.

$$R_d = \frac{\left[180(1-\varepsilon)^2\right]}{\left[D_p^2 \varepsilon^3\right]} \cdot \delta$$

5-4

The deposit thickness (δ) determined with FE-SEM images was compared to the deposit thickness value calculated with Equation 5-5, where M_d is the mass of particles in the deposit (kg), ρ_p is the density of the nanoparticle (kg/m^3), A_m is the membrane surface area (m^2) and ε is the porosity (void).

$$\delta = \frac{M_d}{\rho_p A_m (1-\varepsilon)}$$

5-5

5.4 Membrane Characteristics

The operational conditions and the characteristics of the flat sheet UF membranes are given in Table 5-1. Regenerated cellulose membranes with their hydrophilic properties have shown relatively minimal organic sorption [158, 259]. Moreover, regenerated cellulose membrane is reported as one of the membranes which have minimal hormone sorption among many tested MF membrane made of different polymers [260]. As the hormone sorption capacity of the PS nanoparticles is the focus of this study, regenerated cellulose UF membrane with minimal hormone sorption affinity was selected. For particles larger than the membrane pore size, the penetration of the particles into the pores can be ignored [147]. The MWCO of the

membranes were chosen considering that the particles will not penetrate through the membranes. The internal fouling with particle sizes of 52-3000 nm is unlikely as the smallest particle size is at least 2 times larger than the largest average pore size.

Table 5-1 UF membrane characteristics and operational conditions

MWCO	Pore Radius[a]	Operating Pressure	Average Pure Water Flux	Pure Water Permeability	Clean Membrane Resistance[b]	Rq	Ra
kDa	nm	Bar	L/m².h	L/m².h.bar	1/m	nm	nm
1	0.94	5	22±4	4	8.27E+13		
3	1.42	5	39±5	8	4.69E+13	0.85	0.67
5	1.91	5	56±9	11	3.24E+13	1.2	0.93
10	2.59	5	109±9	22	1.68E+13	1.3	1.0
30	4.81	1	326±19	326	1.07E+12	2.8	2.2
100	9.1	0.5	433±55	865	4.30E+11	2.2	1.8

[a] **taken from [167] calculated after [261],** [b] **calculated using average operation temperature (21 °C), the viscosity is calculated using Equation 3-4, R_q: root-mean square roughness, R_a: average roughness**

The streaming potential measurements of the membranes (presented in Figure 5-2) indicate that 30 and 100 kDa membranes are negatively charged within the pH range of 3-13.
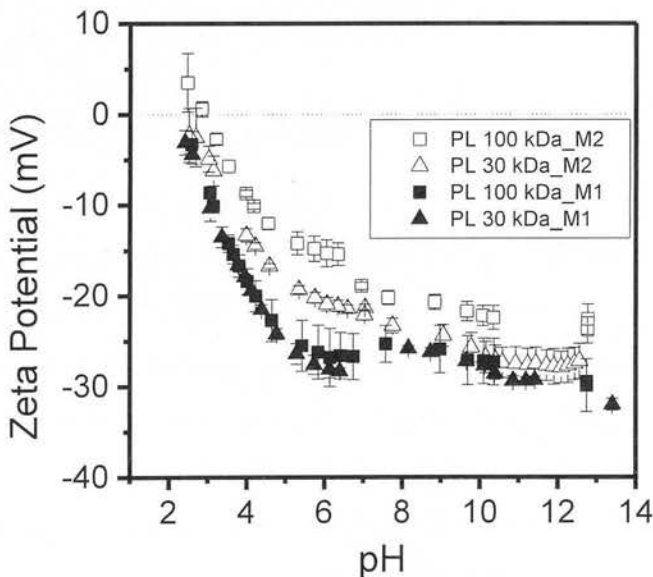
Figure 5-2 Surface zeta potential of UF membranes with changing pH in 1 mM NaHCO₃ and 20 mM NaCl background electrolyte solution

The surface charge analysis was only conducted for 30 and 100 kDa membranes as they have a higher potential of fouling compared to the smaller MWCO membranes due to their lower intrinsic membrane resistance. The isoelectric point of the membranes is found to be between pH 2 and 3 which agree well with the literature [167, 262]. There is not an obvious difference between the surface charge of 30 and 100 kDa membranes. A difference in zeta potential between different coupons of the same MWCO membrane is observed at pH between 3 and 7. Larger absolute zeta potential values for 30 and 100 kDa_M1 are attributed to the higher ionic strength of the background electrolyte solution at pH between pH 4 and 7. The nominal value for the zeta potential of the membranes is higher than the results obtained by Schäfer [167], who studied exactly the same membranes but in a different background electrolyte solution of 1 mM KCl. This difference can also be attributed to the influence of the ionic strength and the type of the ions present in the solution on the measured surface charge [263].

AFM results for surface roughness of 3-100 kDa membranes show that average roughness, Ra is changing between 0.67 and 2.2 nm depending on the MWCO of the membranes. Roughness data for UF membranes is usually changing between 1 and 20 nm [264] which agrees with the results obtained in this study.

5.5   PS Nanoparticle Characteristics

The size of the particles is important for the availability of active sites for the sorption to take place. Information on the surface charge gives an understanding of the possible physical interactions between the hormones and the particles. Moreover, the extent of membrane fouling can be influenced by the particle size and charge in comparison to membrane pore size and surface charge. The size, surface charge and the polydispersity of the particles are presented in Table 5-2. The measured size values in ultra-pure water and in background electrolyte solution as well as the ones obtained with FE-SEM analysis are comparable to each other confirming the values provided by the manufacturer. Therefore particle sizes provided by the manufacturer are used this study. The polydispersity data for 465 nm particles being smaller than

0.02, suggests that the particles are monodisperse. For the other size particles, values between 0.020 and 0.080 indicate a narrow distribution of particles. The microscopic images of 52, 81 and 465 nm particles confirm that the particles are spherical, uniform and have a narrow size distribution (Figure 5-3).

Table 5-2 Characterisation of the PS nanoparticles

	43±5.9 (fluorescent)	52±7.9	81±10	465±11	3000±65
Diameter[a] (nm)	43±5.9 (fluorescent)	52±7.9	81±10	465±11	3000±65
Diameter[b] (nm)	49.3±2.5	51.1±2.6	78.0±4.0	495.5±25.2	–
Diameter[c] (nm)	49.1±2.5	49.0±2.5	71.8±3.7	469.8±23.9	–
Polydispersity	0.064±0.006	0.046±0.005	0.074±0.005	0.007±0.002	–
Diameter[d] (nm)	–	49.4±9.8	73.3±17.7	476.1±17.9	–
Zeta Potential[b] (mV)	-46.79±6.0	-49.3±6.3	-56.6±7.3	-74.4±9.6	-87.6±11.3
Zeta Potential[c] (mV)	-62.7±8.0	-52.2±6.7	-64.1±8.2	-106.7±13.7	-92.9±11.9

[a] according to the manufacturer, [b] measured at pH 7 in pure water with size analyser, [c] measured in 20 mM NaCl and 1 mM $NaHCO_3$ with size analyser, [d] size obtained from FESEM images (Figure 5-3) with Image J program

Zeta potentials measured in solutions with or without background electrolyte (Table 5-2), show that the absolute surface charge of the larger particles (465 and 3000 nm) is higher compared to 43, 52 and 81 nm particles. Elimelech 1990 [265] reported similar results; zeta potential of 121 nm PS nanoparticles was measured as approximately -60 mV while for 378 and 753 nm particles, approximately -80 mV was obtained. Higher zeta potential of the larger particles in this study can be attributed to the higher surface charge density [266].
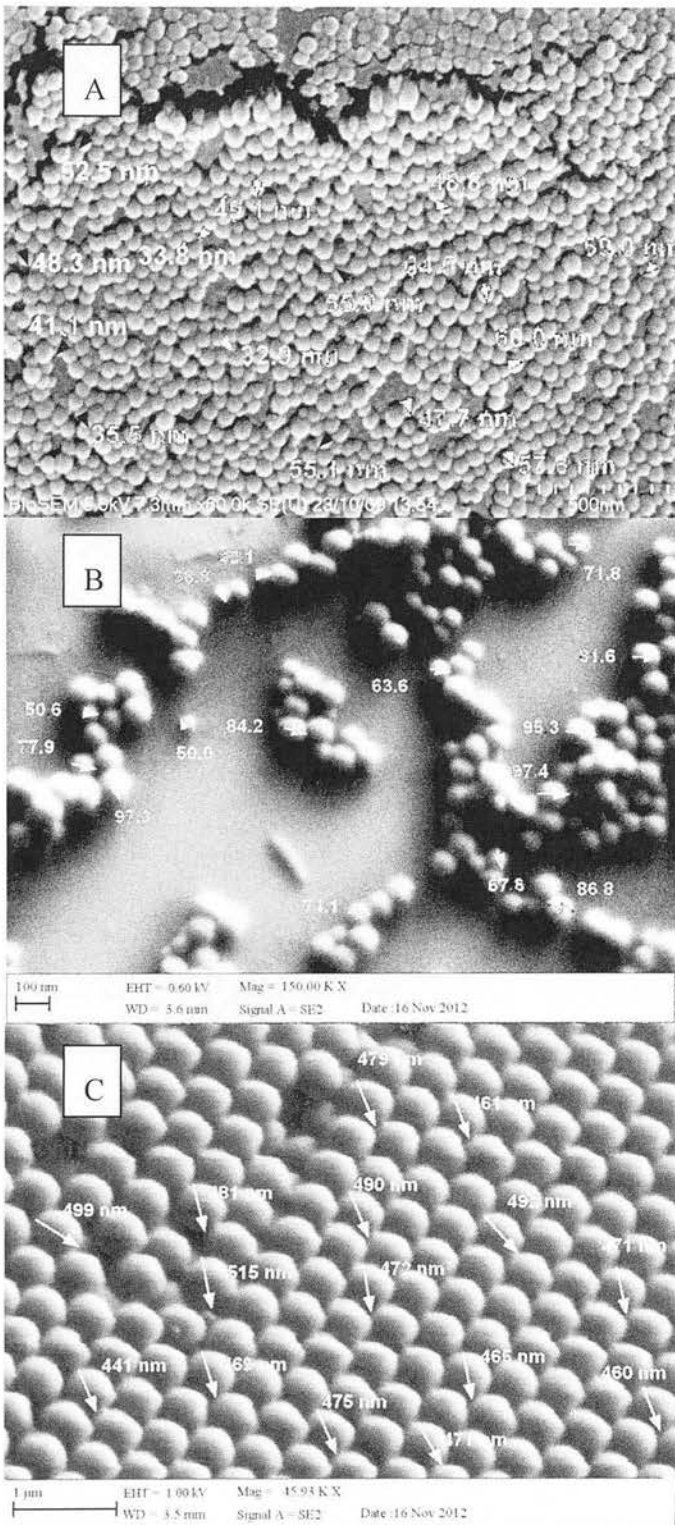
Figure 5-3 FE-SEM images of A) 52, B) 81 and C) 465 nm PS particles

Comparable zeta potential values for 52 nm PS nanoparticles, presented in Figure 5-4, imply that solution pH between 3 and 12 does not influence the surface charge

of the particles. Stable zeta potential of PS nanoparticles in solution with pH between 4 and 6 [266] and 3.5 and 10 [265] was reported and agree well with the findings of this study.
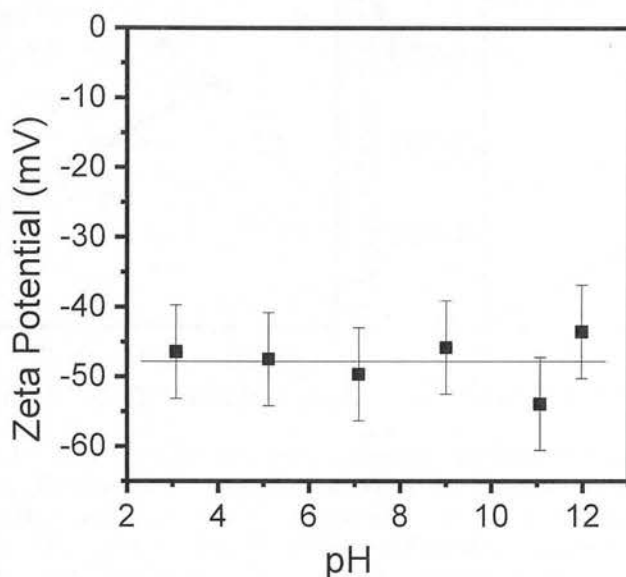
Figure 5-4 Zeta potential of PS particle in background electrolyte solution of 1 mM NaHCO₃ and 20 mM NaCl with varying pH, line represents the mean of the zeta potential values.

5.6 E1 Adsorption Capacity of PS Nanoparticles

Prior to studying the hormone adsorption in the proposed hybrid PS nanoparticle UF system, E1 sorption only on PS nanoparticles was studied with batch experiments in order to understand the limitations of the adsorption. Determining the adsorption capacity of PS particles enables a better explanation of the sorption results which are obtained with the hybrid system in the following sections.

Adsorption capacity is studied by varying E1 concentration to elucidate whether PS surface area is limited for the sorption at higher concentrations. E1 adsorption isotherms for PS particles at pH 5, 7 and 12 are given in Figure 5-5, on the left. The adsorption capacity at 100 ng/L initial E1 concentration (0.001 ng/cm^2) is the same at pH 5 and 7 however; it declines to 0.00002 ng/cm^2 as the solution pH is increased to 12. This decline is attributed to the disassociation of the E1 at pH 12 which is above the pK_a of E1 (10.23) and becoming negatively charged. At pH 12, PS nanoparticles

are also negatively charged as it can be seen in Figure 5-4. Negatively charged E1 is repulsed by negatively charged particles and therefore the sorption is hindered.
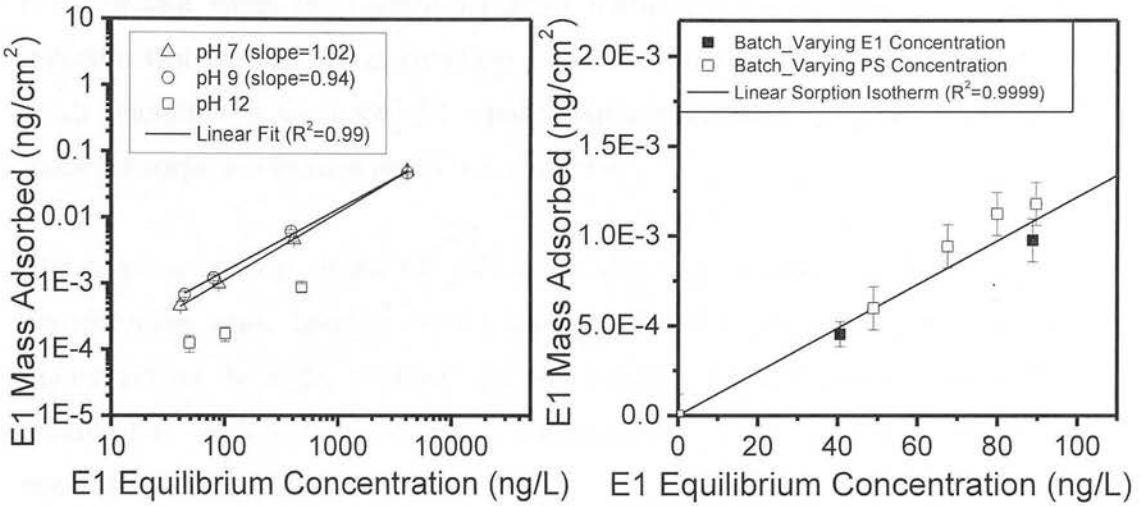
Figure 5-5 Left: E1 sorption isotherms of PS nanoparticles at pH 7, 9 and 12: batch experiments with 16 mg/L PS (52m) particle concentration, Right: E1 mass adsorbed on PS nanoparticles at varying PS particle concentration in comparison to sorption isotherm at pH 7: batch experiments with 7.9, 16, 31, 50 and 79 mg/L plain PS (52 nm) particle concentration, 100 ng/L E1 solution with 1 mM NaHCO$_3$ and 20 mM NaCl background electrolyte, pH 7

The adsorption capacity increases linearly with the hormone concentration at pH 7 and 9 studied. This linearity indicates that the active sites of the PS nanoparticles do not reach saturation within the E1 concentration range of 50-5000 ng/L. The surface area is not a limiting factor for the studied E1 concentration range at 16 mg/L PS particle concentration. The linear isotherm is given in Equation 5-8, where Q is the E1 mass adsorbed on PS nanoparticles (ng/cm^2), C_e is the equilibrium E1 concentration and k is the sorption constant, 1.22×10^{-5} obtained from the linear fit to the experimental data obtained at pH 7 in Figure 5-5, on the left.

$$Q = kC_e \qquad\qquad 5\text{-}8$$

In order to check the availability of the PS surface area in comparison to the molecular surface area of E1, the mass of E1 forming a monolayer on PS surface particles at the concentration of 16 mg/L is calculated in Appendix A.8. Theoretical E1 mass adsorbed based on a monolayer coverage is compared to the E1 mass adsorbed data obtained experimentally at the same given PS particle concentrations for increasing initial E1 concentration. The results, presented in Table A 8-1, indicate

that E1 sorption estimated based on monolayer coverage is an order of magnitude larger than the one determined experimentally, even at the highest E1 equilibrium concentration when the highest E1 mass adsorbed is achieved. This difference indicates that the monolayer coverage is not achieved and thus PS particles do no reach saturation at the tested E1 equilibrium concentration range, confirming the linear E1 sorption isotherm on PS nanoparticles.

The sorption capacity of the PS particles is also studied under varying PS particle concentration while keeping the E1 concentration the same. Results presented in Figure 5-5 on the right, confirms that the sorption capacity (ng/cm^2) has a linear relationship with E1 equilibrium concentration under varying PS particle concentration as well.

5.7 E1 Sorption Kinetics of the PS Nanoparticles

The required time for the sorption equilibrium to be reached is an important parameter for the system design as this time will determine how long the particles will be kept in contact with the hormone solution. Determination of the sorption kinetics for PS particles is challenging as the separation method of the particles from the solution may take longer than the time for sorption equilibrium to be reached. Separation by the means of centrifugation takes four hours which is longer than the equilibrium time. Therefore, static filtration experiments using 3 kDa UF membranes were conducted to have some information on how much time is required to achieve sorption equilibrium. Prior to the experiments with PS nanoparticles, a blank kinetic experiment, where no nanoparticles are added, is conducted to check if there is any E1 sorption in the system. Afterwards, the sorption kinetic is studied at two different PS nanoparticle concentrations of 16 and 31 mg/L.
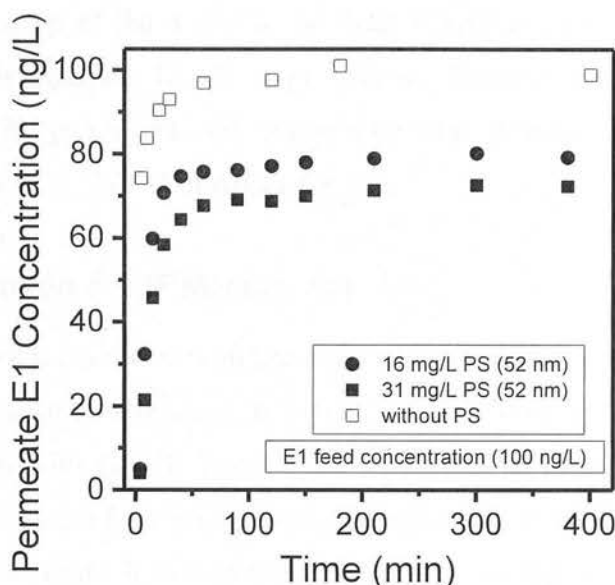
Figure 5-6 The kinetics of the E1 sorption on PS nanoparticles in stirred cell: static stirred cell experiment with 52 nm PS particles, 100 ng/L E1 with 1 mM NaHCO₃ and 20 mM NaCl background electrolyte, pH 7

Results presented in Figure 5-6 show that in the absence of the particles, the equilibrium E1 concentration is 9 % lower than the initial concentration indicating that membrane itself has a sorption affinity for E1. Similarly, less than 20 % of E1 and E2 removal is obtained with regenerated cellulose MF membranes due to the sorption [260]. Membrane sorption needs to be taken into account for the evaluation of the hormone sorption on PS nanoparticles in the hybrid system.

Results also show that sorption equilibrium in the system is reached within 50 minutes regardless of the fact that PS nanoparticles are present in the solution or not. It is likely that the sorption equilibrium takes longer time for the membranes than that for PS nanoparticles indicating that E1 sorption on PS nanoparticles reaches the equilibrium in less than 50 minutes. E1 equilibrium concentration depends on the PS concentration available in the cell and is 71 ng/L for 31 mg PS/L and 80 ng/L for 16 mg PS/L. However, the kinetics in a static filtration is different than continuous filtration in dead end system as both particle and E1 concentration change in time when a continuous filtration is performed. The kinetics and the variation in PS particle concentration in the cell during continous filtration experiments will be studied later in Section 5.10.1.

For the evaluation of the sorption, firstly it is required to know that the sorption equilibrium is reached in all experiments. Sorption equilibrium in filtration experiments is confirmed by monitoring the consecutive permeate sample concentrations as explained in Appendix A.5.

5.8   E1 Sorption on UF Membranes

Hydrophilic UF membranes with the expectation of minimum hormone sorption are selected in this study. However, in Figure 5-6, it is observed that 3 kDa membrane has sorption affinity for E1. Therefore, E1 sorption on all MWCO UF membranes needs to be known to have an accurate determination of the sorption capacity of the PS nanoparticles in the hybrid system. The data presented in Figure 5-7, are adapted from the work of Neale [267] and show that the E1 mass adsorbed is higher for smaller pore size membranes. Lower E1 sorption by higher MWCO membranes, during filtration experiments, is attributed to the shorter contact time between the solution and the membrane. It is also possible that smaller MWCO membranes are denser and provides a larger polymer area for the sorption.
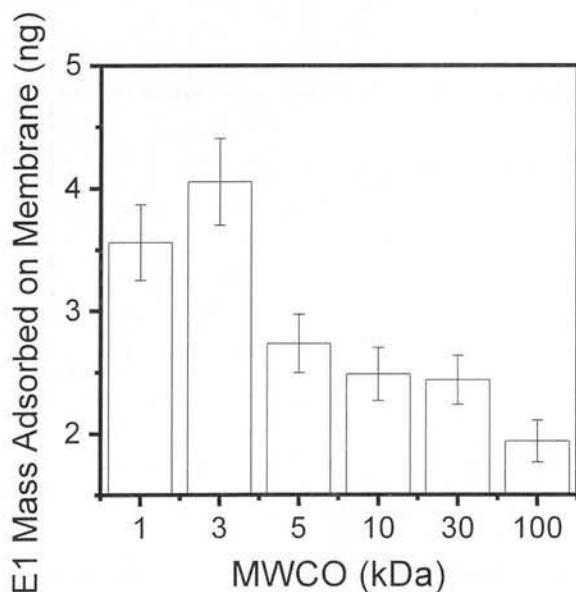
Figure 5-7 E1 sorption on UF membranes with different MWCO: filtration experiments with 100 ng/L E1 solution with 1 mM NaHCO₃ and 20 mM NaCl background electrolyte, pH 7 data adapted from [267]

5.9 The influence of PS Nanoparticle Size on E1 Sorption and UF Permeability

In this section, the influence of PS nanoparticle size on E1 sorption and UF permeability of the hybrid system is studied by varying the particle size and keeping the particle concentration constant at 17 mg/L with 30 and 100 kDa membranes. The experiments with 52, 81 and 465 nm particles are also conducted at 50 mg/L particle concentration with 3, 5 and 10 kDa. The results for E1 sorption and UF permeability are presented in Figure 5-8A and Figure 5-8B respectively.
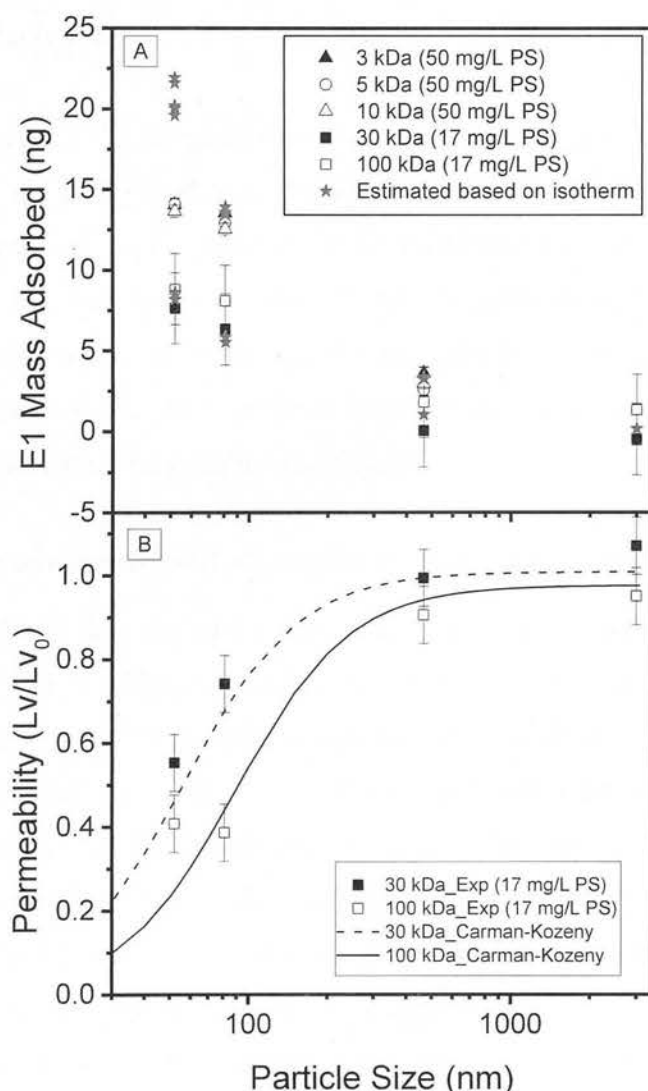
Figure 5-8 The influence of particle size on E1 adsorbed and permeability: filtration experiments with 52, 81, 465 and 3000 nm particles, 17 and 50 mg/L PS particle concentration, 100 ng/L E1 solution with 1 mM NaHCO$_3$ and 20 mM NaCl background electrolyte, pH 7.

Carman-Kozeny model with the assumption, deposit porosity is 0.4 (independent of particle size). Estimated: Based on the sorption isotherm obtained with the batch experiments and the experimental equilibrium E1 concentration

5.9.1 E1 Sorption with Changing PS Nanoparticle Size

Results presented in Figure 5-8A show that E1 mass adsorbed decreases with the decrease in particle size forming the deposit. At the same concentration, the smaller particle sizes provide larger amounts of active sites for the hormones to interact chemically and physically. When the particle size is decreased from 465 nm to 81 nm at 50 mg/L concentration, the E1 mass adsorbed is increased from 3 to 13 ng. For the particles larger than 465 nm, the surface area available becomes very small that E1 sorption is negligible.

The equilibrium E1 concentrations obtained in the filtration experiments are used to estimate E1 mass adsorbed using the linear isotherm obtained in Figure 5-5, on the left. The estimated results, given in Figure 5-8A, seems to agree with the most of the data except the ones obtained with 52 nm PS particles at 50 mg/L. Under these particular conditions, the available surface area is the largest and the E1 mass adsorbed based on the linear sorption isotherm seems to overestimate the E1 mass adsorbed obtained in the filtration experiment.

5.9.2 UF Permeability with Changing PS Nanoparticle Size

The permeability declines as the size of the particles forming the deposit decreases for both 30 and 100 kDa membranes as presented in Figure 5-8B. The pure water flux data show that PS deposition structure does not change when the hormone solution is introduced to the cell as there is no difference between the ultra-pure water flux after the PS particle deposition and flux during the hormone solution filtration (Figure 5-9). Permeability decline is higher for 100 kDa UF membrane than 30 kDa. Both PS particles and surface of the regenerated cellulose membranes are negatively charged. The membranes with larger negative zeta potential usually have more resistance against fouling due to the enhanced electrostatic repulsion between the negatively charged PS and membrane surface. The surface charge of 30 and 100 kDa membranes as displayed in Figure 5-2 are comparable to each other. Thus the

difference in permeability decline cannot be attributed to the surface characteristics of the membranes. Comparing the pure water flux of 30 and 100 kDa membranes, the average convective flux of 100 kDa (433 L/m^2.h) is higher than 30 kDa (326 L/m^2.h). Therefore, it is possible that more compact particle deposit is formed on 100 kDa due to the higher drag force and thus larger deposit resistance.

With the spherical particles, it is expected that more pores are constricted as the particle size decreases as the adjacent distance between the particles decreases [268]. Nevertheless, pore constriction is not expected to play a big role in this study as the smallest particle size is at least twice the size of the largest pore size.
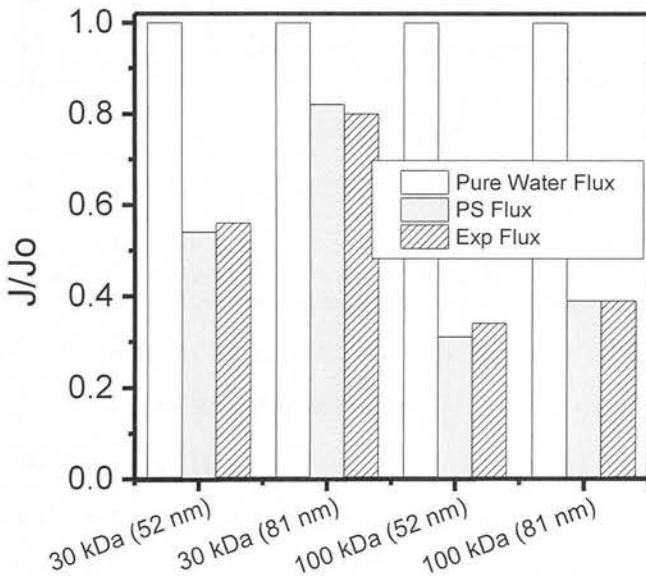
Figure 5-9 Comparison of pure water, PS flux and experimental flux for different particle size and MWCO membrane: PS flux: pure water flux of the membrans with PS nanoparticle deposit, Exp flux: experimental solution flux of the membrane with PS nanoparticle deposit, 100 ng/L E1 with 1 mM NaHCO$_3$ and 20 mM NaCl background electrolye, pH 7, 17 mg/L PS concentration

The decline in permeability as the particle size forming the deposit decreases can be explained by the increased deposit resistance. The calculated deposit resistance for different particle size is presented in Figure 5-10. The results show that the deposits formed on 30 and 100 kDa membrane exert similar resistances as the differences are within the error. The reason of the higher permeability decline with 100 kDa compared to 30 kDa can be attributed to the fact that the deposit resistance makes a bigger contribution to the overall resistance considering that the intrinsic membrane

resistance of 100 kDa membrane is an order of magnitude smaller than the 30 kDa membrane.
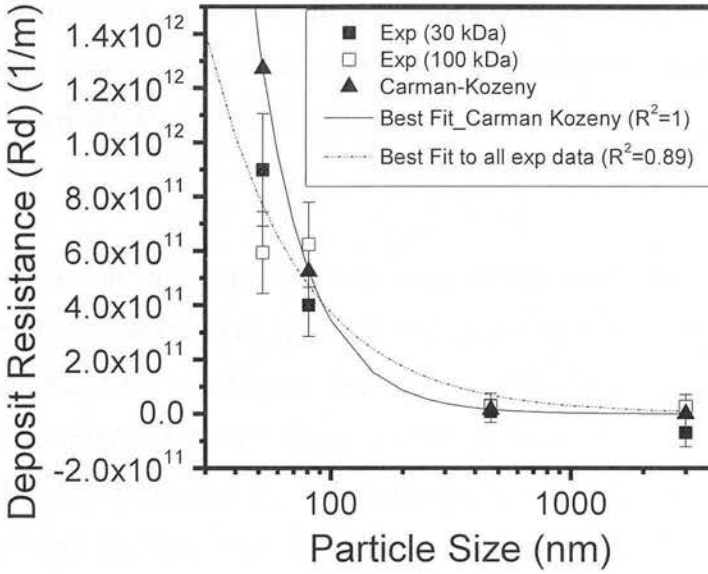
Figure 5-10 Deposit resistance with changing PS particle size: filtration experiments, 52, 81, 465 and 3000 nm particles, 17 mg/L PS concentration, 100 ng/L E1 solution 1 mM NaHCO$_3$ and 20 mM NaCl background electrolye, pH 7. Carman-Kozeny calculations assumptions, porosity is 0.4 (randomly packed deposit porosity), full particle mass retention (7.1 mg) and homogenous deposit thickness, porosity and thickness doesn't change with the particle size.

Using best fit line to the resistance data in Figure 5-10, a relationship is obtained between the particle size forming the deposit and the resistance applied by the deposit. The relationship is formulated into Equation 5-6, where R_d is deposit resistance (1/m), a and b are coefficients and d_p is the particle diameter (nm). Coefficients a and b are obtained from the best fit of the R_d data against the particle size and they are 2.0×10^{14} and 1.36 respectively.

$$R_d = \frac{a}{D_p^{\ b}}$$

5-6

Equation 5-6 is an empirical formula and is a simplified version of the Carman-Kozeny equation (Equation 5-4). Coefficient a can be expressed as in Equation 5-7, where ε is the deposit porosity (void fraction) and δ is the deposit thickness (1/m).

$$a = \frac{180(1-\varepsilon)^2}{\varepsilon^3}\delta$$

5-7

In the Carman-Kozeny equation, the deposit resistance is inversely proportional to the second power of particle size (D_p^2). The coefficient b which represents the power of particle size is 1.36 and it is less than 2.0 indicating that the experimental data do not agree with the Carman-Kozeny in that respect. Deposit resistance obtained by Carman-Kozeny equation seems to underestimate the deposit resistance for larger particles and overestimates for the smaller ones as already stated by Lee and Clark [142].

Carman-Kozeny results in Figure 5-10 are based on the assumptions that the flow is laminar, the particles are uniform, spherical and randomly packed (porosity: 0.4), full retention of the particles is achieved, the deposit thickness is homogenous and the porosity and the thickness do not change as the particle size changes. The uniform and spherical shape of the particles is confirmed by SEM images (Figure 5-3). In order to determine the turbulence in the stirred cell system, Reynolds number is calculated with Equation A 6-1 in Appendix A.5. Re is found to be 20100 which indicates a laminar flow in the cell considering that the flow is laminar for 8000<Re<32000 and is turbulent for 32000<Re [269].

The results show that for both membranes, the experimental resistance results for 52 nm are lower than the theoretical values. In order to understand this difference deposit thickness is analysed with electron microscopy for the deposit of 52 nm particles at 17 mg/L on 100 kDa membranes. Two of the FESEM images are given in Figure 5-11. Images show that the deposit is not homogenous and the deposit thickness varies over the membrane surface. Non homogenous deposit for PS nanoparticles is also reported by Wutzel and Samhaber [270]. Considering the fluid dynamics in the stirred cell, formation of non-homogenous deposit is not surprising. The shear stress in the stirred cell is calculated and presented in Figure A 6-1 in Appendix A.5. The shear stress increases along the radius from the centre outwards and there is a slow decline at the end of the circle indicating that the deposition of the particles varies on different locations of the membrane surface.
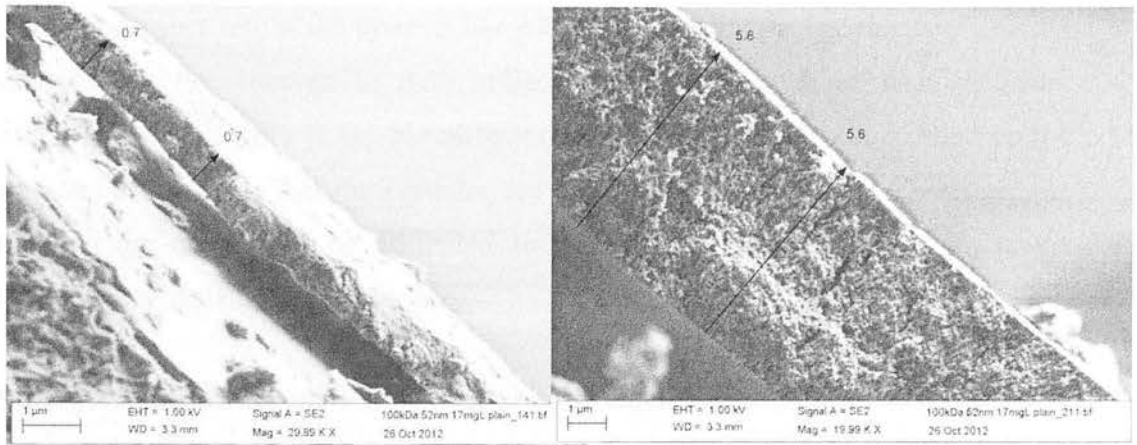
Figure 5-11 PS nanoparticle deposit of 52 nm at 17 mg/L concentration on 100 kDa membrane7

The average deposit thickness measured for 100 kDa is 3.5±1.6 μm. The porosity is calculated as 0.48 ± 0.06 which is higher than the porosity used for the Carman-Kozeny equation. Smaller particles, having smaller surface charge, are less stable compared to larger particles and tend to overcome the repulsion charges easier and aggregate more. Aggregated ones act like bigger particles, so the deposit resistance decreases as the particle size increases. As there is no difference in the deposit resistance deposited on 30 and 100 kDa membranes it is expected that the deposit characteristics such as deposit thickness and porosity will be the same. The deposit thickness is also calculated using Equation 5-5 where M_d is estimated with the mass balance equation (Equations 5-3) and the calculated value of 0.48 is used as deposit porosity. The calculated deposit thickness, 4.2 μm agrees with the average thickness value measured with microscopic images.

The velocities associated with different transport mechanisms depending on particle size are predicted for a size range from 10 to 3000 nm and shown in Table A 7-1 in Appendix A.7. The results show that the velocity associated with Brownian diffusion is larger than the convective flow velocity for the particles between 10 and 81 nm. Considering that the diffusional transport becomes more significant for the particles with the size less than 100 nm, it could have been expected that the flux decline would have been more severe with 81 nm particles compared to 52 nm as the diffusion velocity of 52 nm particles is higher than 81 nm particles. In this study the particles are filtered through the membrane until all the particles are deposited and

there is no water left in the system. For particles in such a packed deposit, extreme changes can be observed in their collective properties such as their diffusion coefficient and stability [132]. No diffusional force is expected to be exerted on the particles at the point that the particles are not in solution anymore. Therefore, the flux decline can solely be attributed to the increase in the deposit resistance following the resistance model theory.

5.10 The Influence of PS Nanoparticle Concentration on E1 sorption and UF Permeability

Expected trade-off between the E1 adsorption and UF permeability is studied for the hybrid system with varying concentration of 52 nm PS nanoparticles. The results for E1 mass adsorbed and UF permeability are given in Figure 5-12A and B respectively.
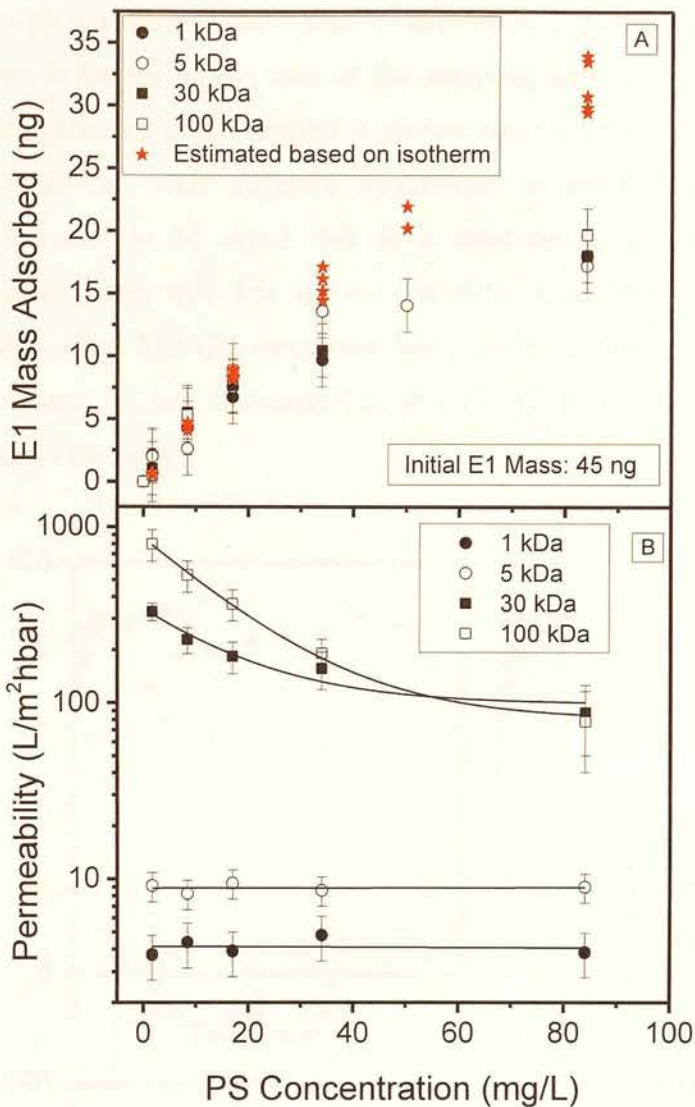
Figure 5-12 The effect of PS concentration on; A) E1 mass adsorbed and B) permeability of different MWCO UF membranes: filtration experiments, 1.7, 8.4, 17, 34 and 84 mg/L PS (52 nm) concentration, 100 ng/L E1 concentration with 1 mM NaHCO₃ and 20 mM NaCl background electrolyte, pH 7. Estimated: Based on the sorption isotherm obtained with the batch experiments and the experimental equilibrium E1 concentration

5.10.1 E1 Adsorption with Changing PS Nanoparticle Concentration

Results, presented in Figure 5-12A, show that E1 mass adsorbed is not dependent on the MWCO of the UF membrane used in the system indicating that the sorption equilibrium is reached in the system with all MWCO membranes. In order to understand the kinetics of the E1 sorption in the system better, the change in the permeate E1 concentration is studied for each MWCO membrane with different initial PS concentrations. The E1 equilibrium concentration for each MWCO

membrane with the same initial PS concentration is displayed against time and PS concentration in the cell at the time of the sampling and presented in Figure 5-13. When the E1 permeate concentration is plotted against time, it is observed that the sorption equilibrium with different membranes is reached at different times. However, it needs to be noted that in a dead-end filtration system, PS cell concentration increases with time and the rate of increase depends on the MWCO of the membrane. Each MWCO membrane has a different flow rate, thus the system reaches the same PS cell concentration at different times even if the initial PS concentration is the same.
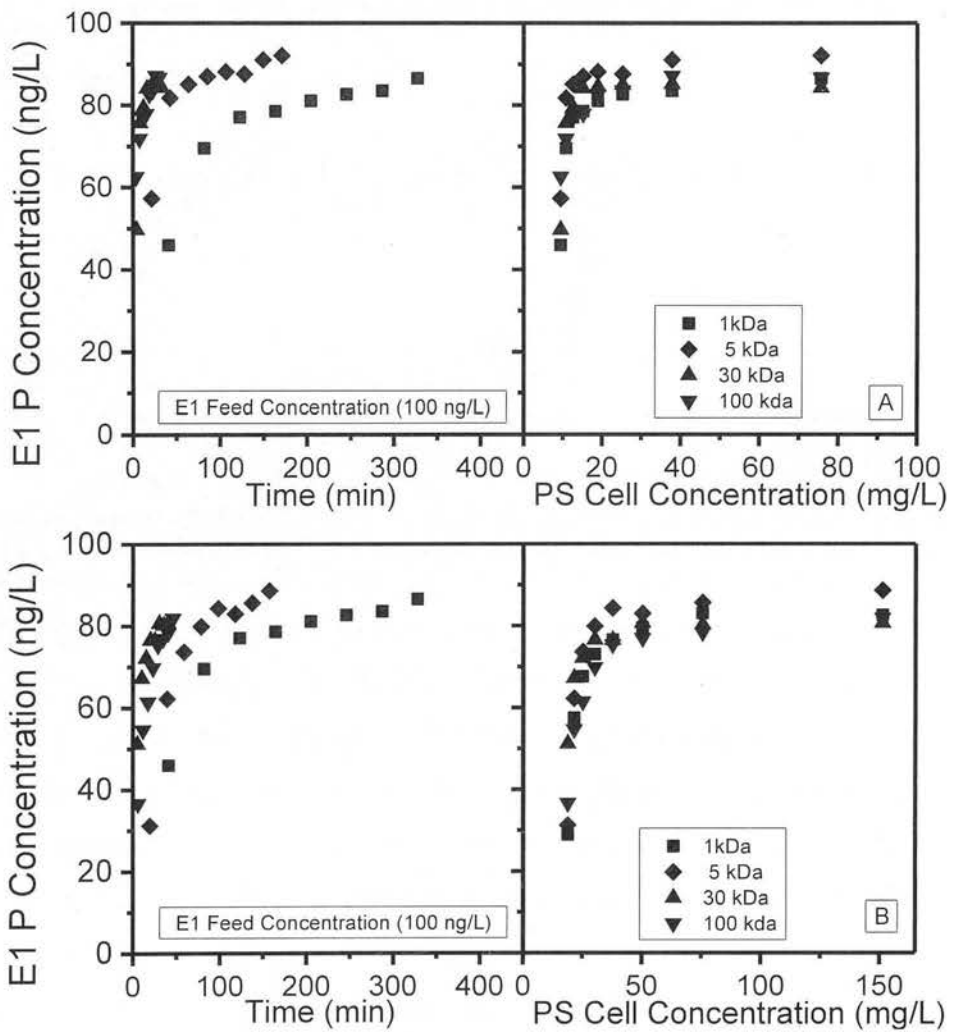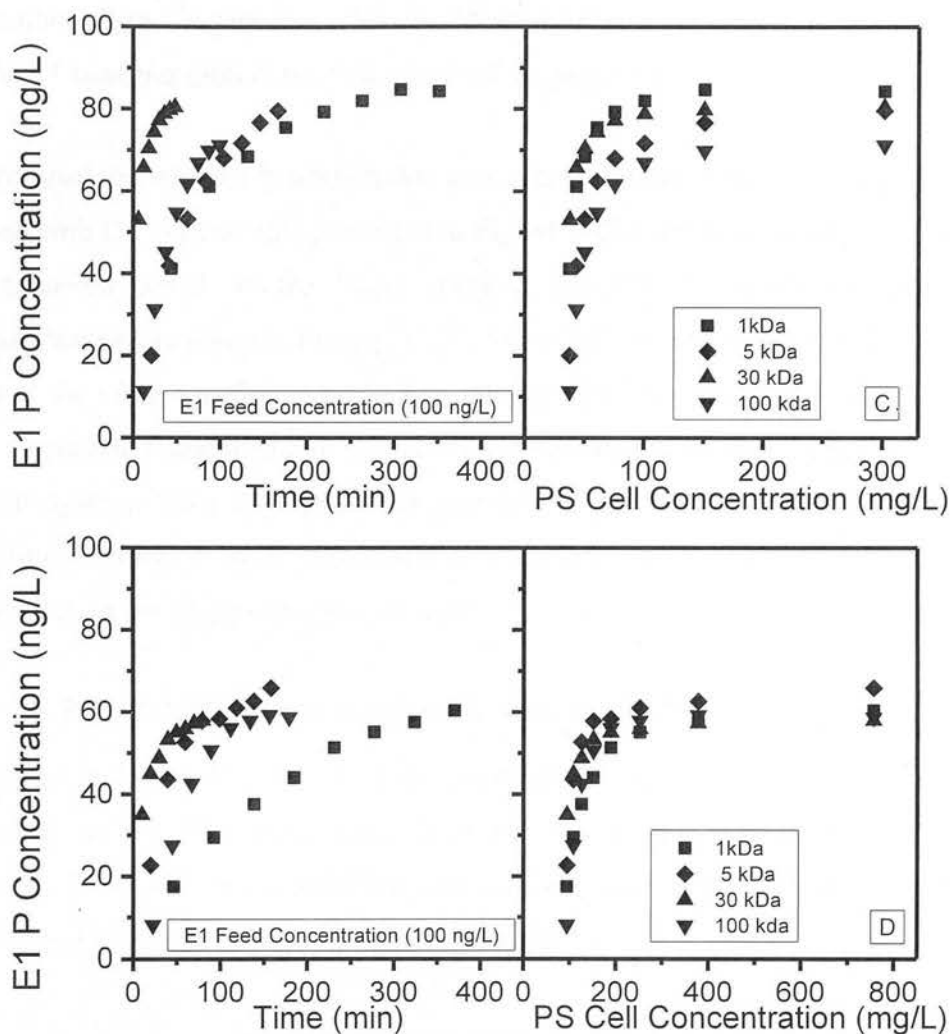
Figure 5-13 Permeate (P) E1 concentration change in time and PS (52 nm) concentration in the cell: 8.4 mg/L (A), 16.8 mg/L (B), 33.5 mg/L (C) and 84 mg/L (D): filtration experiments, 100 ng/L E1 concentration with 1 mM NaHCO₃ and 20 mM NaCl background electrolyte, pH 7

PS cell concentration is calculated for each sampling time and the E1 permeate concentration is re-plotted against this parameter. It is then observed for all membranes studied that sorption equilibrium is reached at the same PS cell concentration. It is also observed that the specific PS cell concentration at which sorption equilibrium is reached increases with the initial PS concentration. Variation in PS nanoparticle and E1 concentration in the cell, due to the nature of filtration, alters the adsorption and desorption equilibrium. It is observed after the initial decline, E1 permeate concentration starts increasing until it reaches the equilibrium. The increase in E1 permeate concentration can possibly be attributed to desorption of

the hormones from the particles when the E1 concentration in the cell becomes lower than the E1 concentration in the bulk phase of the particles.

For a comparison with the batch sorption experiments, equilibrium E1 concentrations obtained with the experiments presented in Figure 5-12A are used to estimate the E1 mass adsorbed based on the linear sorption isotherm (Equation 5-8) and the estimated values are given in Figure 5-12A. The filtration results agree well with the results of the batch sorption experiments only up to PS particle concentration of 17 mg/L, above which the isotherm seems to overestimate the E1 mass adsorbed in the filtration system. This overestimation is possibly due to the differences in the equilibrium dynamics of a batch and a filtration system and requires further investigation in the scope of further research.

5.10.2 UF Permeability with Changing PS Nanoparticle Concentration

Results, presented in Figure 5-12B the permeability declines for 30 and 100 kDa membranes as the PS concentration increases due to the increase in the deposit resistance. There is a linear relationship between the feed mass of the particles and the deposit resistance (Figure 5-14) confirming the cake filtration theory.
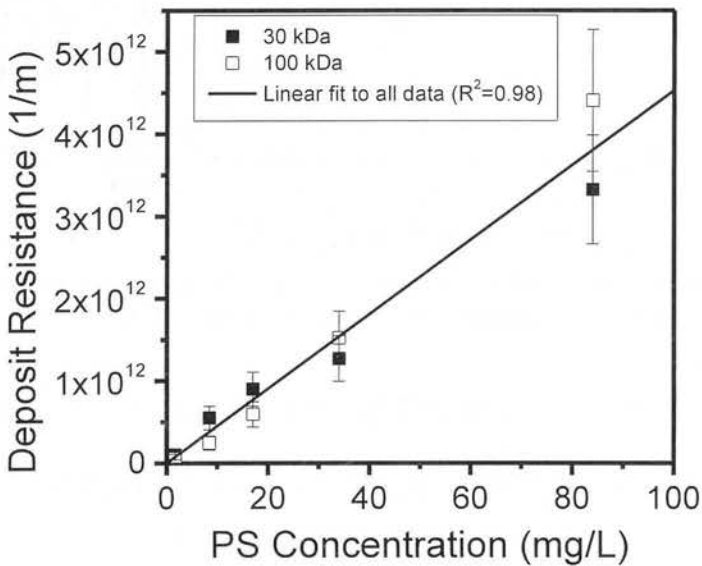
Figure 5-14 Deposit resistance with changing feed PS concentration: filtration experiments, 1.7, 8.4, 17, 34 and 84 mg/L PS (52 nm) concentration

In order to confirm this linear relationship, FE-SEM analysis is performed to determine the thickness of the deposit on 100 kDa membrane tested with three different initial PS concentrations. FE-SEM images are presented in Appendix A.7. The measured average thickness values are given in Figure 5-15. The linearity of the values confirms that the increase in the deposit resistance is due to the increased deposit thickness. Measured thickness values for each particle concentration are used to calculate the deposit porosity. The calculated porosities being 0.53 ± 0.08, 0.48 ± 0.06 and 0.46 ± 0.06 for 8.4, 17 and 34 mg/L of initial PS particle concentrations show that the deposit porosity does not depend on the initial particle concentration [142]. The deposit porosity is not expected to change unless the particle characteristics or the applied pressure in the system is varied [136] and both 30 and 100 kDa membranes were operated under 1 and 0.5 bar, respectively for all the initial PS concentrations.
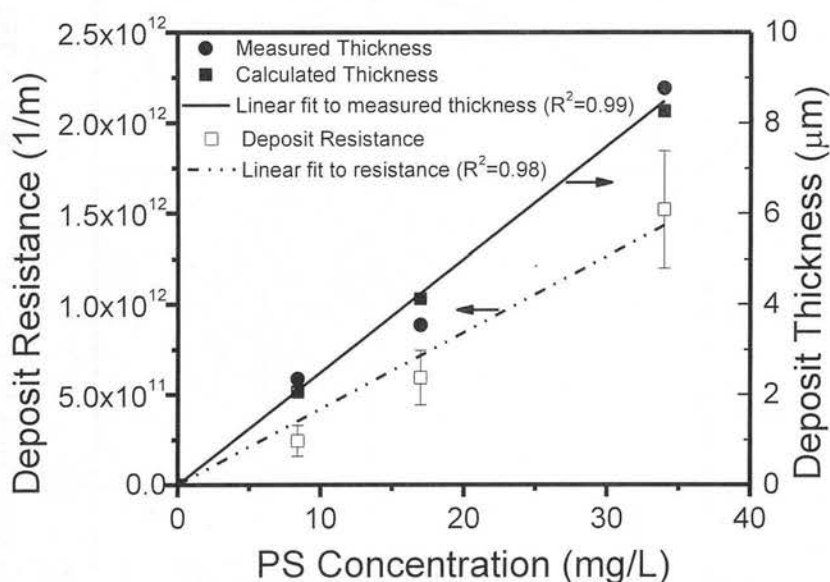
Figure 5-15 The change in deposit resistance and deposit thickness (measured) with feed PS concentration on 100 kDa membrane: filtration experiments, 8.4, 17 and 34 mg/L PS (52 nm) concentration

5.11 The Influence of Solution pH on E1 Sorption and UF Permeability

The influence of solution pH on E1 sorption and membrane permeability is presented in Figure 5-16A and B respectively. E1 adsorption is less on PS nanoparticles at pH above 10 due to electrostatic repulsion between the deprotonated E1 and negatively charged PS particles. As a consequence, E1 sorption on PS nanoparticle deposit

declines at pH above 10. The results agree well with the results of the batch sorption experiments conducted only with PS nanoparticles at varying pH (presented in Figure 5-5, on the left).

As it can be seen in Figure 5-16B, the deposit resistance does not change with changing pH indicating that there is no influence of pH on the deposit packing density.
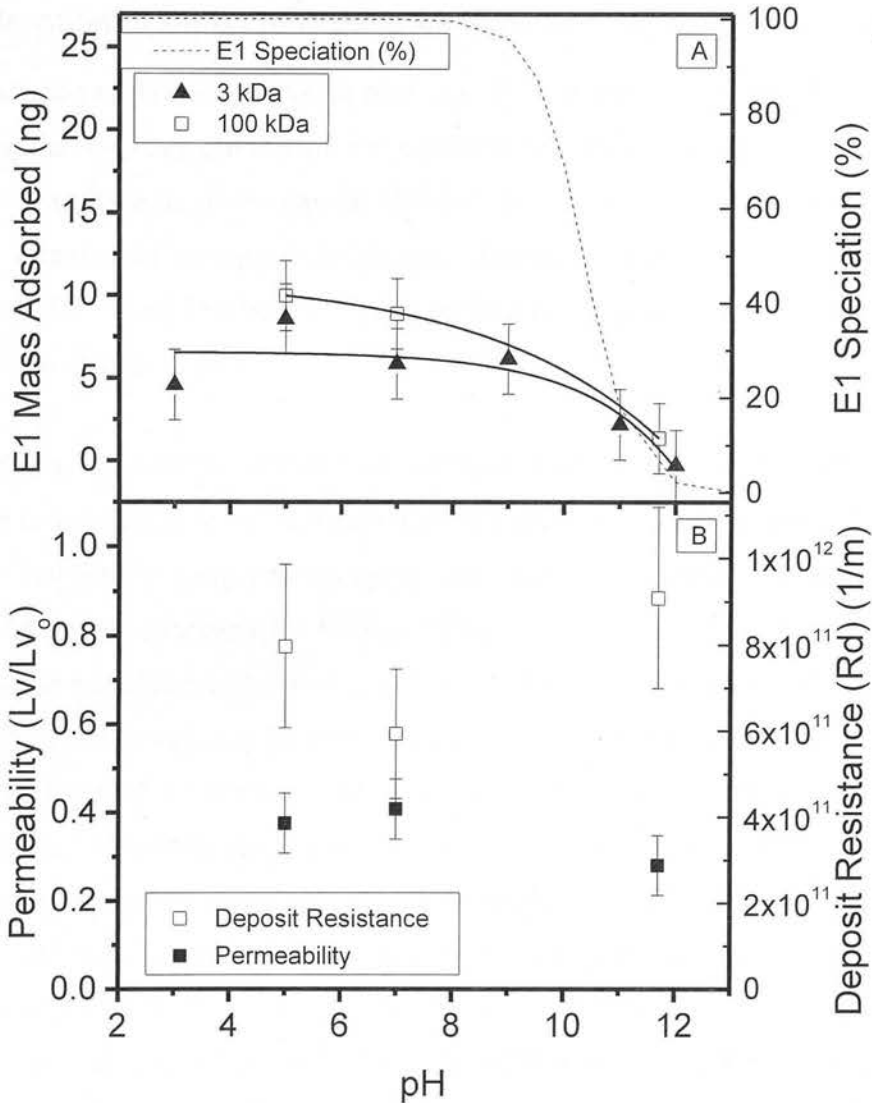
Figure 5-16 The influence of pH on: A) E1 mass adsorbed for 3 and 100 kDa B) Permeability and deposit resistance for 100 kDa. Filtration experiments: 17 mg/L PS (52 nm) concentration, 3 and 100 kDa, 100 ng/L E1 solution with 1 mM NaHCO$_3$ and 20 mM NaCl background electrolyte, pH 7

As the surface charge of the PS nanoparticles remains the same within the pH range, the interaction behaviour of the particles is not expected to change. The isoelectric

point of 100 kDa membrane is between pH 3 and 4. The surface charge of the membrane decreases from -12.5 to -20 mV as the pH increases from 5 to 10 respectively. The repulsion between the particles and the membrane might increase as the pH increases and fewer particles may accumulate in the deposit; however, this is not observed in this study. Therefore, it can be concluded that the pH only influences the E1 sorption in the system.

5.12 Sorption of Different Hormones in Hybrid PS Nanoparticle-UF

E1 is selected as the representative hormone to be studied in this chapter. However, studying the sorption affinity of PS nanoparticles for more than one hormone is mandatory to have an understanding whether the particles can be used as a sorbent for the removal of hormones in general. Therefore, the sorption of three other hormones, E2, P and T is studied in comparison to E1 with both batch and filtration experiments in this section.

For a direct comparison between the filtration and batch adsorption experiments, sorption is normalised by surface area (ng/cm^2) and compared in Figure 5-17. Results of batch and filtration experiments agree with each other. Figure 5-17 shows that the affinity of the PS nanoparticles for P is higher than the one for E2, T and P while a difference is not observed between E2, T and P. Preferential sorption of P on various polymers has been reported in other studies as well. Nghiem [271] showed that the sorption affinity of the hormones onto NF membrane with polyamide active layer is P>E1>T>E2. The work of Banasiak [272] on the sorption of steroids onto ion exchange membrane made of polystyrene divinlybenzene (PS-DVB) showed that the sorption affinity for each exchange membrane is as follows: for anionic exchange membrane (AEM) T<P<E2<E1 and for cationic exchange membrane (CEM) E2<T <E1<P. The sorption difference between the AEM and CEM is explained by the fact that each membrane has different hydrogen bonding capacity depending on the donor or acceptor groups they possess. Jansen *et al.* [273] stated that the P has a higher sorption affinity onto PS nanoparticles in the absence of surfactant compared to T since P is more hydrophobic than testosterone. The high affinity of PS particles for P

[274] is attributed to that fact that P has a finite degree of solubility in the polymer matrix [275].
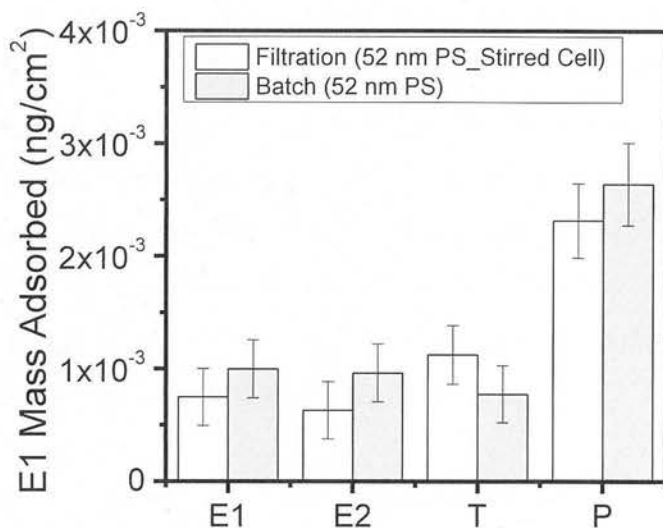
Figure 5-17. Hormone (E1: Estrone, E2: Estradiol, T: Testosterone, P: Progesterone) mass adsorbed per PS surface area: Filtration (3 kDa membrane) and batch experiments: 17 mg/L PS (52 nm) concentration, 100 ng/L E1 solution with with 1 mM NaHCO₃ and 20 mM NaCl background electrolyte, pH 7

Although hydrophobic interactions are expected to be the main responsible mechanism between the PS nanoparticles and hormones, a direct correlation between the hydrophobicity of the hormones and the sorption cannot be made. The chemical and physical characteristics of the four hormones are presented in Table 4-1. P and E1 are both hydrophobic compounds with relatively high and comparable K_{ow} values; however adsorption of P is significantly higher than E1. Similarly, charge interaction is not expected to play a role in preferential sorption of P as the dipole moment of P, T and E1 are very similar.

π-π stacking is another mechanism held responsible for the interaction of polystyrene based sorbents with sorbates [236-238, 276]. The difference between the π densities of the adsorbent and the corresponding sorbate determines the stability of the π-π interaction depending on whether the aromatic fragment is electron rich or deficient [236]. Although the benzene rings in E1 and E2 are electron rich, the aromatic ring in polystyrene is electron neutral. Therefore, π-π interaction is not expected to be a

major sorption mechanism for PS nanoparticles and estrogens especially for P since it does not have any benzene ring.

Although it is expected that PS nanoparticles are free of functional groups, due to the polymerization process some charged functional groups may be present on the surface [266] and these groups can undergo intermolecular interactions with the hormones such as H-bonding. The technical notes of the manufacturer state that sulfate functional groups are present on the particle surface [277] possibly to prevent the particles from aggregation. Considering that the pK_a value of sulfate is between 1 and 2 [266], H-bonding between P and sulfate is not expected as both P and sulfate groups are H acceptors [203] at the studied solution pH.

In conclusion, PS nanoparticles have similar sorption affinity for E1, E2, T and to a larger extent for P, indicating that various hormones can be removed with the hybrid PS nanoparticle-UF system.

5.13 Comparison of PS Nanoparticle Integration Method in terms of E1 Sorption

In this section, the PS nanoparticles are introduced to the system with two integration methods: pre-mixing and pre-deposition, for comparison. Figure 5-18 gives the E1 mass distribution in permeate, concentrate and adsorbed on PS in concentrate and adsorbed on membrane, for both methods. The mass distribution is calculated using the mass balance (Equation 5-3). Results show that, there is no obvious difference in overall E1 sorption between the two integration methods. For pre-mixed experiments, the results illustrates that the E1 mass in the concentrate and adsorbed on PS particles in concentrate is more than the double of the E1 mass on the deposited PS particles showing that the majority of the particles stay in the solution and do not deposit when the particles are premixed.
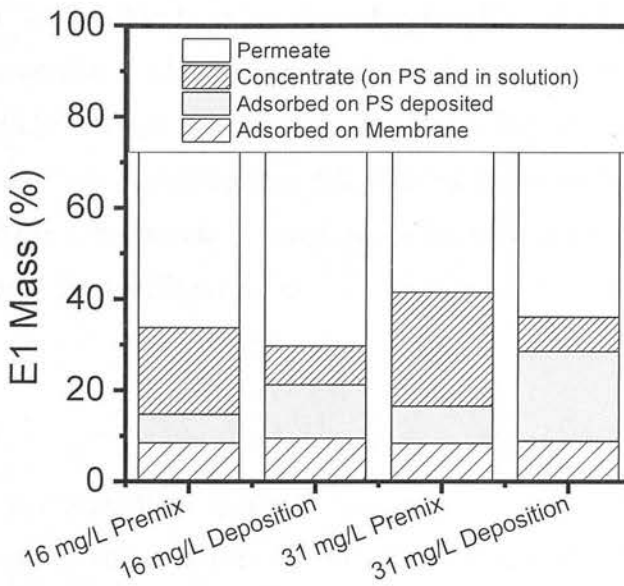
Figure 5-18 The E1 mass distribution in the system for premixing and deposition experiments: Premixed (for 3 hours) and deposition experiments, 3 kDa 100 ng/L E1 solution with with 1 mM NaHCO₃ and 20 mM NaCl background electrolyte, pH 7, E1 mass in the feed: 45 ng corresponding to 100 % mass

In pre-deposition experiments, the E1 mass adsorbed onto PS particles deposited is higher than the E1 mass in the concentrate and adsorbed on PS in concentrate showing that the PS particles are mostly deposited. This specific study is conducted only with 3 kDa membrane where no permeability decline is observed. Within the scope of future work, studying different integration methods with large MWCO membranes will enable having a better evaluation of the impact on membrane fouling.

5.14 Prediction of E1 sorption and Permeability for Changing PS Size and Concentration

The goal of this section is to predict the hormone adsorption (removal) and the UF permeability for the hybrid system with 100 kDa membrane designed with different size and concentration of PS particles. The results and the understanding obtained in the previous sections are used to do this prediction.

5.14.1 Prediction Methodology

R_d is calculated from the data obtained in the experiments of 17 mg/L nanoparticle concentration with 52, 81, 465 and 3000 nm particles filtrated through 100 kDa

membrane. A relationship between the calculated R_d and particle size at this specific particle concentration is obtained in Figure 5-10 and is described with Equation 5-6. For each particle size an S value is calculated using the R_d and M_p, the mass of particles applied (kg), with Equation 5-8 where ε is the porosity (void fraction), ρ_p is the density of the nanoparticle (kg/m^3), A_m is the membrane surface area (m^2) and D_p is the diameter of the particle (m).

$$S = \frac{[180(1-\varepsilon)]}{[D_p^2 \varepsilon^3]} \cdot \frac{1}{\rho_p A_m} = \frac{R_d}{M_p}$$

5-8

The S value represents the deposit characteristics including porosity specific to each particle size. M_p is calculated as for the experiment with 100 kDa membrane at 17 mg/L concentration of 52 nm particles assuming that all the particles will be deposited on the membrane surface. This assumption is made considering that the measured permeate particle concentration is negligible and the measured flux after the particle deposition and during the experiment is the same (Figure 5-9). The deposit mass will be the same for all particle size at the same concentration.

The validity of the cake filtration theory depends on the concentration of particles in the concentrate being much smaller than the concentration of the solids in the deposit [278]. In this experimental study, the particles are deposited on the membrane surface until no water was left in the system, therefore all the particles are in the deposit and M_p can be used as the mass of the particles in the deposit (M_d).

The change in R_d at different concentrations of 52 nm particles is calculated following the cake filtration theory where the particle mass is directly proportional to the deposit resistance [34]. The linear relationship between initial particle mass and the R_d is experimentally shown for 30 and 100 kDa membranes at particles concentrations of 1.7, 8.4, 17, 34 and 84 mg/L (Figure 5-14). The linear relationship cannot be considered if the deposit is compressible, however considering that the deposit compressibility is dependent on the changes in the applied pressure (ΔP) [279] and ΔP is not changing during the experiments, the theory can be applied. Even further, the linear increase in the deposit resistance due to the linear increase in deposit thickness

was confirmed previously with the average deposit thickness measurements presented in Figure 5-15.

R_d is predicted at different concentrations for each particle size by substituting S for each particle size and the M_p, corresponding to each concentration in Equation 5-9. S value is assumed to be constant when the feed particle concentration increases for each particle size since the porosity and thus the specific deposit resistance is not changing.

$$R_d = SM_p$$
<div align="right">5-9</div>

The E1 sorption and membrane permeability were predicted for each particle size of 52, 81, 100, 200, 300 and 465 nm at the concentrations of 1.7, 8.4, 17, 34, 50, 84, 100 and 150 mg/L. The permeability of a PS deposit of different size and feed concentrations is calculated using R_d values calculated as described above and dynamic viscosity of water at average operational temperature (21 °C) and the average membrane resistance using Equation 3-3 for 100 kDa membrane. Linear isotherm equation (Equation 5-8) is used to predict the equilibrium E1 concentration and E1 mass adsorbed on PS nanoparticles at various PS particle concentration.

5.14.2 Prediction Results and Validation

The results of the predicted E1 mass adsorbed and permeability of the system with 100 kDa membrane designed with different size and concentration of PS particles is given in Figure 5-19. In order to validate the predicted values, experiments with 465 nm PS particles were conducted at 17, 50, 79 and 100 mg/L initial particle concentrations with 100 ng/L E1 feed concentration. The data obtained in the previous sections with 52 nm PS particles at 1.7, 8.4, 17 and 84 mg/L initial particle concentrations is also presented. The prediction for the E1 mass adsorbed agrees with the most of the experimental data validating the Equation 5-8, which is determined based on linear sorption isotherm. However, when there is a large PS particle surface area available in the system such as 84 mg/L of 52 nm PS particles, the isotherm overestimates the E1 mass adsorbed in the filtration system as explained before.

Predicted permeability data does not agree with the experimental data as well as expected. Higher permeability data obtained experimentally may indicate that the predicted relationship between the R_d and the particle size (Figure 5-10) overestimates the R_d of the deposits formed of 52 or 465 nm particles.
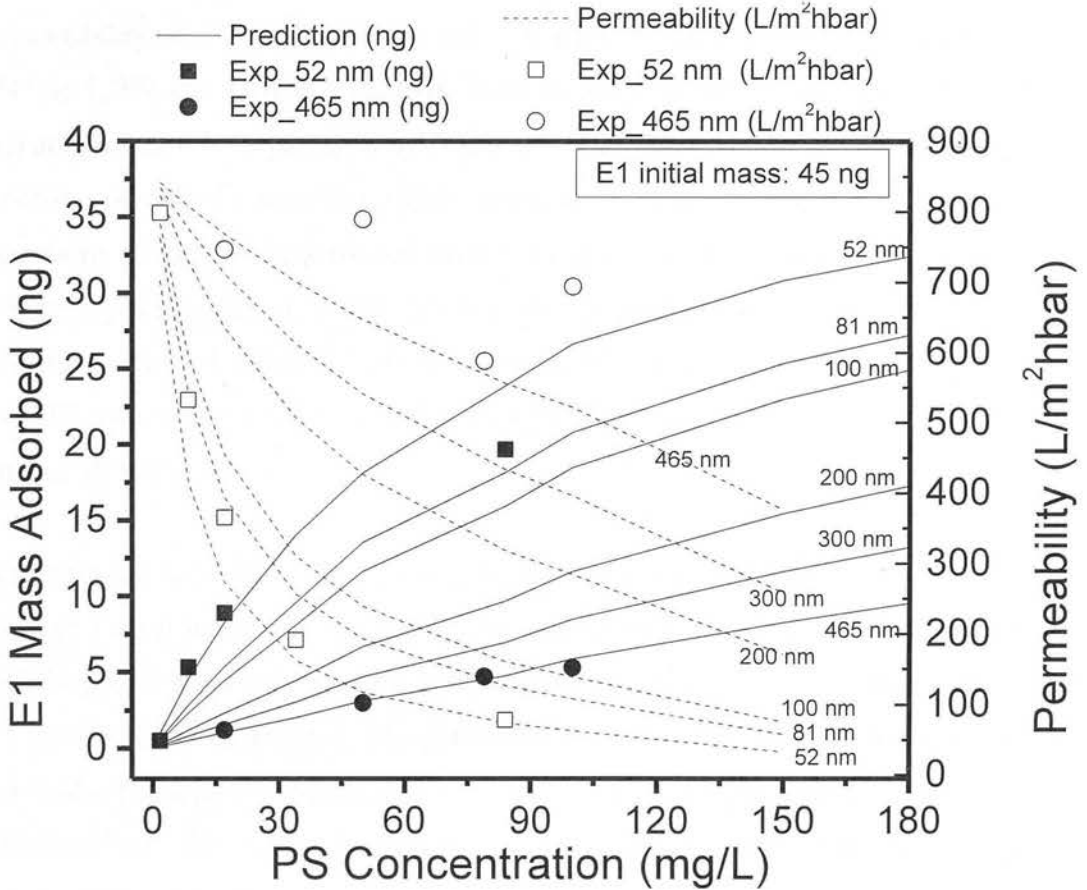
Figure 5-19 Predicted E1 mass adsorbed and permeability with changing PS size and concentration: filtration experiments, 100 kDa UF membrane, 100 ng/L E1 solution with 1 mM NaHCO₃ and 20 mM NaCl background electrolyte

In order to increase the hormone removal in the hybrid system, larger PS surface area is required. Larger surface area could either be obtained by using smaller size particles or increasing the particle concentration. Increased PS concentration results in lower UF permeability due to the increased deposit resistance. Less permeability decline was obtained with larger particles at the same particle loads. However, due to the smaller area provided by large particles, larger particle load was required for the system to obtain the same hormone removal as the smaller particles. A system with a

large sorbent load with large particles would result in similar permeability decline as the one with small concentration with small particles.

5.15 Evaluation of the System and Conclusions

The hybrid PS nanoparticle-UF system has a E1 removal capacity of 40% and a final permeability of 75 L/m²hbar when operated with 100 ng/L initial E1 concentration and 84 mg/L PS (52 nm) nanoparticle concentration. At such conditions, E1 sorption capacity of 52 nm PS particles is 476 ng/g (0.0004 ng/cm²) which is higher than the E2 sorption capacity of activated carbon which is 47 ng/g showing that PS nanoparticles are more efficient than activated carbon. Hormone removal and the permeability of NF/RO systems (presented in Table 2-2) are compared to the results obtained with the hybrid system. E1 removal of 40% is comparable to some but lower than most of the NF/RO systems but the permeability (75 L/m²hbar) is at least 5 times higher than most of the NF/RO systems.

The sorption capacity of the hybrid system is the same for E1, E2, T and P whereas it is higher for P indicating that the system is applicable for various hormones. Solution pH does not play a role on E1 sorption or UF permeability as long as it is below the pK_a values of the hormones. The permeability of the 100 kDa membrane with 52 nm particles deposit is not influenced by pH due to the stable particle surface characteristic. E1 mass adsorbed in the system is the same regardless if the PS nanoparticles are integrated into the system with a pre-mixing or pre-deposition method.

Considering that some NF and RO systems can remove E1 up to 99 %, a feasible hybrid system can only be achieved by employing nanoparticles with higher sorption affinity. Surface functionalized PS nanoparticles can provide the required high sorption affinity.

6 Hybrid Carboxylate Functionalized Polystyrene Nanoparticle-Ultrafiltration System for Hormone Removal

6.1 Introduction

The investigation in this chapter focuses on whether additional carboxylate groups on PS nanoparticles have an influence on the hybrid PS nanoparticle-ultrafiltration system performance in terms of E1 sorption and membrane permeability. The results obtained in the previous chapter concludes that the hybrid PS nanoparticle-UF system can compete with the existing NF/RO systems only if the sorption capacity of the PS particles for hormones is improved. One of the important reasons to choose PS nanoparticles as sorbent material for the system was that the particles are commercially available with various functional groups.

Ideally all the functional groups need to be studied for a better understanding of the underlying sorption mechanisms and a more reliable selection. However, in the scope of this study, one functional group is required to be selected for the experimental study. The carboxylate group is chosen as a suitable functional group of PS nanoparticles based on the expectation of enhanced hormone sorption due to the hydrogen bonding capacity of the carboxyl group and the fact that the particles are commercially available at the same size as the plain polystyrene particles allowing a fair comparison for their hormone sorption capacity.

Carboxlyate groups form when the solution pH increases above the dissociation constant (pK_a) of the carboxyl group. pK_a of the carboxyl group is between pH 4 and 5 [280, 281], indicating that variation in solution pH can result in important changes in particle functionality and stability. Therefore, carboxylated PS nanoparticles are required to be tested and compared to plain PS particles in terms of hormone sorption and membrane fouling under varying solution pH and particle concentration.

6.2 Selection of the Functional Group for PS Nanoparticle

Commercially available PS particles with specific functional groups are compiled and their bonding capacities with hormone molecules, mainly estrogens are explored. The commercially available functionalized PS nanoparticles and their chemical characteristics are given in Table 6-1. PS nanoparticles with two different functional groups or a group combined with an element are also available but are not included in the table. The functional groups for such PS nanoparticles include aldehyde/amidine, aldehyde/sulfate, carboxyl-bromo, chloromethly, sulfate/epoxy, sulfate-bromo and carboxyl functionalized DVB crosslinked. As these additional groups or elements increase the complexity of the adsorption process and make it more difficult to understand the underlying mechanisms, they are not considered for the selection process.

The chemical structure of the functional groups and DVB-cross linking unit is illustrated in Table 6-1. As no information could be obtained from the manufacturer on the chemical structure of the functionalized particles, the location where the functional groups are attached to the repeating units of the polymer is not known. Therefore, the chemical structure of PS with functionalized group cannot be provided. It is important to note that the solution chemistry, which can easily change by addition of surfactants, salts or other chemicals, during the manufacturing process, can influence the bonding between the functional groups and the main polymer to a great extent. Depending on where the functional groups attach to the polymer, the chemical properties of PS such as hydrophobicity and overall polarity may change. The technical note of the Bangs Laboratory, which is the manufacturer of many of the listed functionalized PS nanoparticles, state that sulfate groups as well as surfactants can be present on the particle surface for plain and functionalized particles [277].

The possible interaction mechanisms between the hormones and the functional groups are studied by looking at the chemical structure and characteristics of the functional groups (Table 6-1) and hormones (Table 4-1). While most of the

functional groups presented have hydrophilic properties, the polystyrene still possess hydrophobic properties. Although hydrophobic interactions might be hindered due to the attached hydrophilic groups, they can still play a role as an underlying mechanism on the sorption of the hormones on functionalized PS particles.

Many functional groups have the potential to undergo ionic bonding which happens between two oppositely charged molecules. If the hormone is negatively charged, like it is the case when pH is above the pK_a of the hormone, then it can be attracted to the positively charged functional groups. Similarly, positively charged hormones such as adrenaline [282] can be attracted to the negatively charged groups. When pH is less than the pK_a, estrogens are uncharged and ionic interactions are not expected to contribute to the sorption. As estrogens are the focus of this experimental study, ionic bonding potential of the groups are not considered for the selection.

Carboxylic acid is a weak base and neutral when pH is below the pK_a of the carboxylic acid. Once the solution pH is above the pK_a which is about 4-5 [280, 281], it deprotonates and carboxylate forms as it can be seen in Equation 6-1. The carboxylate group is polar and negatively charged.

$$\qquad\qquad 6\text{-}1$$

Carboxylic acid   Carboxylate anion
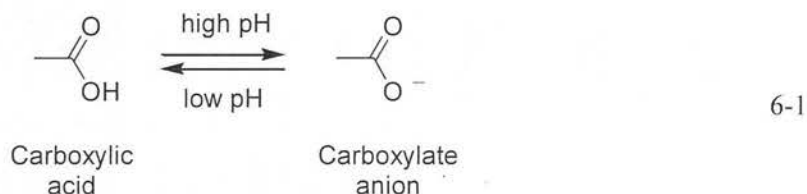
Neutral carboxylic acids are known to form strong intermolecular hydrogen bonds [283]. Both the carboxylic acid and the carboxylate group are therefore considered to have a high potential to adsorb hormones via hydrogen bonding in case of the carboxylic acid or ion-reinforced hydrogen bonding in case of the carboxylate.

Table 6-1 List of commercially available functional groups for PS nanoparticles and their chemical characteristics considered for the selection

Functional Group	Structure	Supplier	Size (nm)	Polarity	Charged[f]	Hydrophobicity	Possible intermolecular interactions	H-bonding ability[f]
Carboxylate	$-C(=O)O^-$	Polysciences Invitrogen Bangs Lab Spherotech	50 20&40 60 50-100	Polar[d]	Negatively	Hydrophilic[e,i]	Ionic, π-π and H-bonding[d]	2 H-acceptor
Primary amine	$H-N-H$	Polysciences Spherotech	100 200	Polar[a]	Neutral at high pH Positively at low pH	Hydrophilic[a]	Ionic and H-bonding[a]	2 H-donor 1 H-acceptor
Hydroxyl	$O-H$	Polysciences Spherotech	750 700-900	Polar[a]	Neutral	Hydrophilic[g]	H-bonding[a]	1 H-donor 1 H-acceptor
Sulfate	$-O-S(=O)(=O)-O^-$	Polysciences Invitrogen	200 20	Polar[f]	Negatively	Hydrophilic[c,i]	Ionic bonding	1 H-acceptor
Sulfonate	$-S(=O)(=O)-O^-$	Spherotech	700-900	Polar[j]	Negatively	Hydrophilic[h,i,j]	Ionic and H-bonding[k]	1 H-acceptor
Amidine	$H-N / N^+-H$	Invitrogen	20	Polar[m]	Positively	Hydrophilic[f]	Ionic and H-bonding[l]	2 H-acceptor 3 H donor
DVB-Crosslinked	(divinylbenzene)	Bangs Lab (36%DVB) Spherotech (non-uniform)	200 400-600	Nonpolar[o]	-	Hydrophobic[n,o]	Hydrophobic interactions[o]	None

[283], [b] based on its tetrahedral structure similarity to methanes [284], [c] based on the information on sulfate salts [285], [d] [286], [e] based on the carboxylate groups in soap [287], [f] based on the pK_a of the groups and their structure [g] [288], [h] based on the information on surfactant in soap [289], [i] [290], [j] [291], [k] [292], [l] [293], [m] [294], [n] [295], [o] [276]

Of all the functional groups in Table 6-1, the carboxylic acid is the only one which makes the benzene ring electron deficient and thus more likely to make π-π interactions with the electron rich benzene ring of the hormones like E1.

Hydrophilic primary amine groups are polar due to the difference in electronegativity between nitrogen and hydrogen atoms. The polarity and the free pair of electrons over the nitrogen atom make the group reactive. I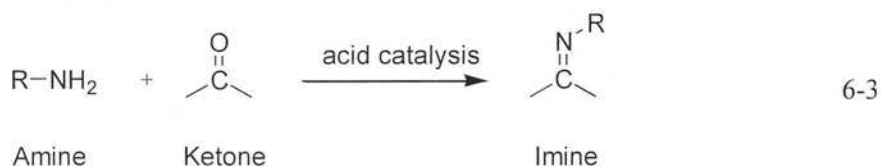n amine functional group, nitrogen with a free pair of electron can make hydrogen bonding as well as the two hydrogen atoms which can be shared with electronegative oxygen atoms in the hormone molecules. Therefore amines are both hydrogen donors and acceptors. When the amine group is attached to the aromatic ring, the availability of the lone pair on nitrogen atom is less as the electrons are delocalized around the ring. Aliphatic amine groups, which have no aromatic ring attached directly to the nitrogen atom, are more likely to form hydrogen bonds with other molecules since they are not directly attached to the benzene ring. Typical pK_a of an aliphatic amine is about 9-10, meaning at a pH< pK_a, the amine groups will be protonated and positively charged [296].

$$ -\overset{+}{N}H_3 \underset{\text{low pH}}{\overset{\text{high pH}}{\rightleftharpoons}} -\overset{..}{N}H_2 $$

Ammonium group   Amine

6-2
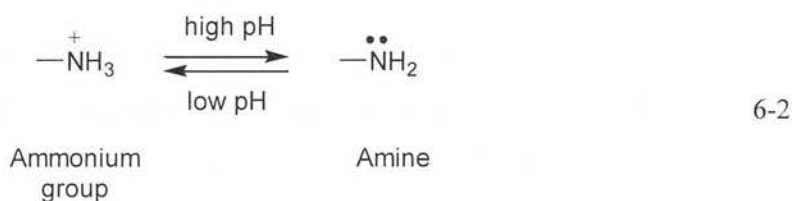
In addition, a PS with amine group can react with ketone groups of the hormone molecules as it is presented in chemical Equation 6-3 [296].

$$ R-NH_2 \;+\; \underset{\text{Ketone}}{\overset{O}{\underset{\|}{C}}} \xrightarrow{\text{acid catalysis}} \underset{\text{Imine}}{\overset{N\diagup^{R}}{\underset{\|}{C}}} $$

Amine   Ketone   Imine

6-3

Additionally it may provide a structure with PS retaining its hydrophobic properties as the hydrophilic group is not attached directly on the aromatic group and this can enhance the sorption of hormone on the particle.

Amidine groups have two nitrogen atoms and are positively charged up to the pK_a of the amidine which is 11 [297]. Like guanidine groups in the amino acid arginine, they form strong hydrogen bonds with carboxylate anions, acting both as hydrogen donor and acceptor as it can be seen in Equation 6-4 [191].

Amidine   Carboxylate

6-4

The overall polarity depends on the final structure and chemical stabilization of the group on PS particles as it is the case for the rest of the groups as well. Amidine functionalized PS particles are reported to be relatively more hydrophobic compared to carboxylated PS [285].

The polar hydroxyl group is capable of acting as a hydrogen bond donor (through its H) or hydrogen acceptor (through oxygen).

Although sulfate has a tetrahedral structure and it has an equal distribution of charge in all of its resonance structures, once the sulfate is attached to a polymer (usually by reacting a polymer with OH), it has only a single charge left and resembles more a sulfonate rather than the original sulfate as it can be seen in Equation 6-5.

Polymer with OH   Sulfate
functional group

6-5
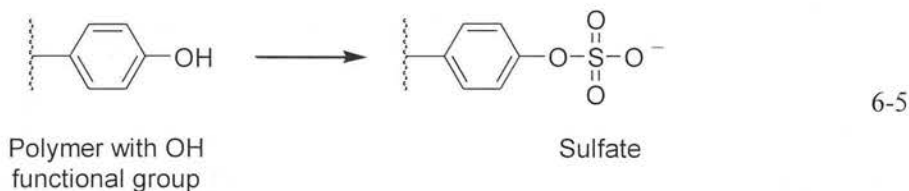
Sulfonate is a polar hydrophilic group. Although the structure suggests two double bonded oxygen atoms and a negatively charged oxygen atom, the negative charge is delocalised equally over all three oxygen atoms. The sulfonate group may have the capacity to act as a hydrogen bond acceptor [292]. Similar properties are expected for sulfate functional group. Although there are some statements that sulfate forms hydrogen bonds with water molecules [298] and fatty acids [299], the sulfate and sulfonate groups are not expected to react with neutral hormone molecules like estrogens, hence they are disregarded.

In general the presence of oxygen atoms in a functional group makes the bond more polar compared to nitrogen atoms as oxygen is more electronegative than nitrogen. It can be estimated by looking at the periodic table that N-H bond is less polar than C-O. The polarity of the bonds gives an indication on the strength of the hydrogen bond that the functional groups can make such as the more polar a molecule is, the stronger the hydrogen bonding. Therefore it is more likely that carboxyl groups will interact with the hormone molecules via hydrogen bonding more than the nitrogen containing functional groups such as amine or amidine.

PS-DVB, hyper-crosslinked polystyrene with divinyl-benzene, is a hydrophobic polymer. Depending on the degree of crosslinking, porosity and surface characteristics of the PS-DVB can change to a great extent. The water contact angle varies from 100-110° depending on the degree of the crosslinking [300]. Moreover the hydrophobicity of the internal and external surface area can be different as well [276]. It is likely that enhanced hydrophobicity and porosity due to the crosslinking of the PS particles can result in more hydrophobic interaction with the hormone molecules. Apart from the hydrophobic interactions the π-π interactions can also contribute to the adsorption to a certain extent [236].

Following the evaluation of the bonding capacity of all of the options, carboxylate, amine, amidine functionalized and DVB crosslinked PS particles seem to have more potential for interacting with hormone molecules. For the carboxylated PS particles it

is expected that hydrogen bonding will enhance the adsorption of the hormones. Besides, as it is mentioned before, among all the groups in Table 6-1, carboxylic acid is the only group which makes the benzene ring electron deficient and thus more likely to make π-π interactions with the electron rich benzene ring of the hormones like E1 [301]. DVB crosslinked PS particles may enhance adsorption due to the increased hydrophobic and possible π-π interactions. On the other hand amine and amidine groups show potential for hydrogen bonding with estrogens while maintaining hydrophobic characteristics of the PS nanoparticles. In order to make the final decision, the size and the manufacturing process were taken into account. Carboxyl/ate functionalized PS particles were selected as they are available from the same manufacturer at the same size (~50 nm) as the plain PS particles. The smallest available size for DVB-crosslinked and amine functionalized PS particles is 200 and 100 nm, respectively. Amidine functionalized PS particles can be purchased in custom size, however, they are more expensive compared to the other commercial particles. In order to study the influence of the functional group on the sorption any other variability in the system such as available surface area due to the particle size and the chemistry due to the differences in the manufacturing method are avoided with this selection.

6.3 Materials and Methods

Plain (52 nm) and carboxylated (48 nm) PS nanoparticles purchased from Polysciences were used in this chapter. The effective diameter and the zeta potential of the particles were measured as described in Section 3.3.1 and 3.3.2 respectively. Field Emission Scanning Electron Microscopy (FESEM) was used to image the nanoparticle deposit on membrane surface in order to analyse the homogeneity and thickness. The methodology is described in Section 3.3.4.

Radiolabelled [2, 4, 6, 7-3H] estrone (E1) was used to prepare the hormone solutions. The chemical and physical characteristics of E1 are given in Table 4-1. Hormone solutions were prepared in a background electrolyte solutions of 1 mM $NaHCO_3$, 20 mM NaCl. The solution was adjusted to pH 7 with 1 M HCl and 1 M NaOH unless

otherwise stated. Hormone concentration in the samples was analysed with a scintillation counter as described in Section 3.5.4.
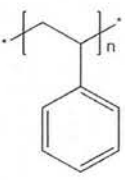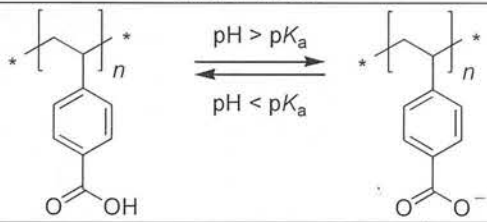
Batch adsorption experiments were conducted to test the E1 sorption on plain and carboxylated PS nanoparticles at different particle concentrations (8-79 mg/L). The pH experiments were performed only with carboxylated PS by varying pH between 3 and 12. For pH experiments, 29 mg/L of carboxylated PS particles were added into 100 mL of 100 ng/L E1 solutions. This concentration was chosen to have the same surface area as the area provided by 31 mg/L of 52 nm plain particles. This enabled a direct comparison of E1 sorption between the plain and carboxylated PS particles. The static adsorption protocol is explained in Section 3.6.2 in detail.

100 kDa PLHK membranes were used in this chapter, characteristics of which are given in Table 5-1. The information on the surface charge and morphology of the membrane is given in Section 5.4. The membrane filtration protocol used in this chapter is the same as the protocol described in Section 5.3.5 in order to have the same conditions to compare plain and carboxylated PS particles directly.

6.4   PS Nanoparticle Characteristics

The characteristics of the plain and the carboxylated PS nanoparticles are summarized in Table 6-2. Surface charge of the particles is studied by measuring the zeta potential. Figure 6-1 displays how zeta potential is changing within a pH range of 2-12. The results indicate that particles have a negative zeta potential value within the studied pH range while the variation is within the instrumental error. No difference in the zeta potential values is found between the plain and carboxylated PS particles. Obtained results for carboxylated particles contradict with the literature as carboxyl groups are expected to have a pK_a value at acidic pH. The neutral carboxyl group (COOH) is expected to deprotonate and become a negatively charged carboxylate (COO-) when the pH value increases above the pK_a as presented in Table 6-2.

Table 6-2 Physical and chemical characteristics of plain and carboxylated PS particles

Characteristics	Plain PS	Carboxyl/ated PS
Size [a] (nm)	52±8	48±7
Size measured [b] (nm)	48.5±0.2	47.5±0.4
Polydispersity	0.046±0.005	0.112±0.005
Chemical structure		
Hydrophobicity	Hydrophobic [c]	Hydrophilic functional group [d] Hydrophobic PS polymer
Possible intermolecular interactions	Hydrophobic π-π interactions (unlikely)	Hydrogen bonding Carboxyl (2 H acceptor& 1donor) π-π interactions (more likely than carboxylate) Carboxylate (2 H acceptor) π-π interactions (likely)

[a] **according to the manufacturer,** [b] **measured in background electrolyte of 20 mM NaCl and 1 mM NaHCO$_3$,** [c] **[302],** [d] **[280]**

The pK_a of the carboxyl groups on the carboxylated polystyrene nanoparticles is reported as 4.9 [281] and 4.64 [280]. The speciation of the carboxyl group is displayed in Figure 6-1 assuming that the pK_a is 5, considering the reported values. Absolute zeta potential and mobility of carboxylated particles is expected to increase as the pH increases above pK_a. However, this is not the case for the carboxylated particles studied. The negative zeta potential values can be attributed to the presence of these sulfate groups on the surface for both plain and carboxylated particles remaining from the synthesis, as the pK_a of the e.g. lauryl sulfate is around -1.5 to -2 [303]. The negatively charged sulfate groups could explain the invariable negative charge over the pH range studied for carboxylated particles. PS particles with carboxylate groups are hydrophilic [304] and relatively more hydrophilic compared to the particles with carboxyl groups. Both surface charge and the hydrophobicity of the particles play an important role for the hormone sorption.
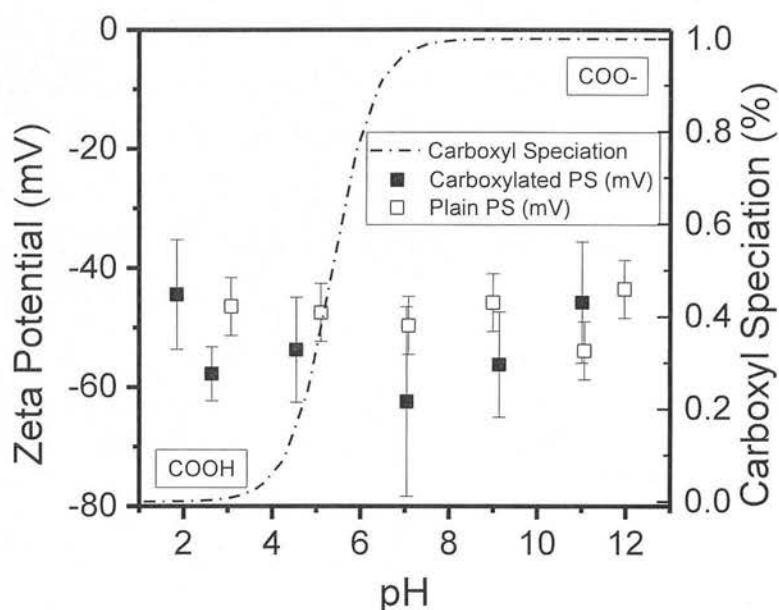
Figure 6-1 Zeta potential of carboxylated PS particles in 1 mM NaHCO₃ and 20 mM NaCl background electrolyte solution with changing pH and expected speciation of carboxyl groups (assumed pK_a: 5)

6.5 E1 Adsorption Capacity of Carboxylated PS Nanoparticles

The amount of E1 mass adsorbed on carboxylated PS particles, within a pH range of 3-11, is shown in Figure 6-2, on the left. E1 mass adsorbed does not change in the pH range of 3-10. Above pH 10, E1 mass adsorbed declines as E1 deprotonates and becomes negatively charged. Electrostatic repulsion between the negatively charged particle surface and deprotonated E1 is the reason of the decline in sorption.

The change in the E1 sorption capacity is plotted against E1 equilibrium concentration for the experiments where the available surface area for plain and carboxylated PS particles is increased by varying the initial particle concentration. The results given in Figure 6-2, on the right show that E1 sorption on carboxylated PS particles follow a linear isotherm like plain particles. Based on the linear fit of the experimental data presented in Figure 6-2, on the right, sorption constant (k) is determined as 7.13×10^{-6} which is an order of magnitude smaller than the k of plain PS particles (1.22×10^{-5}) indicating that the sorption capacity of the carboxylated PS particles is lower.

Hindered E1 mass adsorption may indicate that the adsorption is mainly due to nonpolar effects as the E1 is relatively nonpolar/lipophilic, as is the polystyrene (or most parts of the carboxyl functionalised PS). Considering that the carboxylated particles are negatively charged and relatively hydrophilic [252, 302] this may imply that the hydrophobicity of the PS particles play a bigger role in the E1 sorption than the capability of hydrogen bonding.
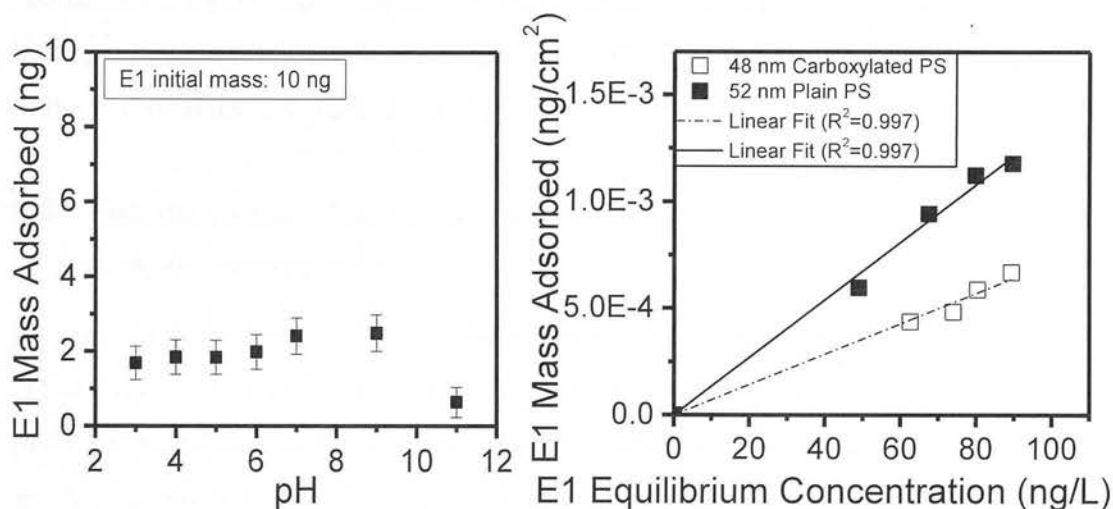

Figure 6-2 Left: E1 mass adsorbed with changing pH: batch experiments, 29 mg/L PS particles (48 nm), Right: Sorption isotherm determined by changing PS particle concentration: batch experiments, 100 ng/L E1 solution with 1 mM NaHCO$_3$ and 20 mM NaCl background electrolyte, 8-79 mg/L PS particles, pH 7

The interaction of the benzene rings in PS and hormone molecule via hydrogen or π-π bonding is unlikely as the ring in PS is electron neutral. Nevertheless, PS nanoparticles with carboxylate groups are expected to make π-π interactions with the electron rich benzene ring of E1 as these groups are expected to make the benzene ring of PS electron deficient. However, π-π interactions do not seem to contribute to the E1 sorption as the presence of carboxylate groups does not enhance the sorption.

Besides sulfate groups, mainly carboxylate functional groups are present on the carboxylated PS particles at neutral pH. The COO$^-$ and SO$_3^-$ functional groups are polar and therefore hydrophilic [123] whereas some of the benzene ring of the plain PS nanoparticles still carry hydrophobic properties as they do not possess additional

COO⁻ groups. Considering that the maximum amount of E1 adsorbed onto plain and carboxylated PS particles is the same, the hydrogen bonding may not be a contributing mechanism to the adsorption process in this case and hydrophobic interaction is possibly the dominant underlying mechanism. The addition of the carboxylated groups on PS surface seems to cause a lower sorption per surface area compared to the plain particles. It is likely that hydrophilic properties of the additional carboxylate groups prevent estrone molecules to approach the hydrophobic surface sites for the sorption to take place. Therefore, sorption capacity of the carboxylated PS particles is smaller than the plain particles.

6.6 The Influence of Carboxylate Functionality of PS on E1 Sorption and UF Permeability

Figure 6-3A and B present how E1 mass adsorbed and UF permeability, respectively, change with increasing concentration of carboxylated PS particles in comparison to plain PS particles. The trend in increase of E1 mass adsorbed is in parallel with the results obtained from the batch experiments. The E1 sorption capacity of carboxylated PS particles being smaller than the plain ones shows that a larger surface area is required for carboxylated PS to reach the same amount of sorption that can be achieved with the plain particles.

The permeability of the 100 kDa membrane is comparable for plain and carboxylated PS at different particle concentrations and the results are given in Figure 6-3B. The decline in the permeability with carboxylated particles follows the same trend of the plain particles. The permeability declines as the amount of carboxylated PS particles increases due the increased deposit thickness. This implies that the existence of the carboxyl groups on particle surface does not cause any changes in the particle-particle and particle-membrane interactions.
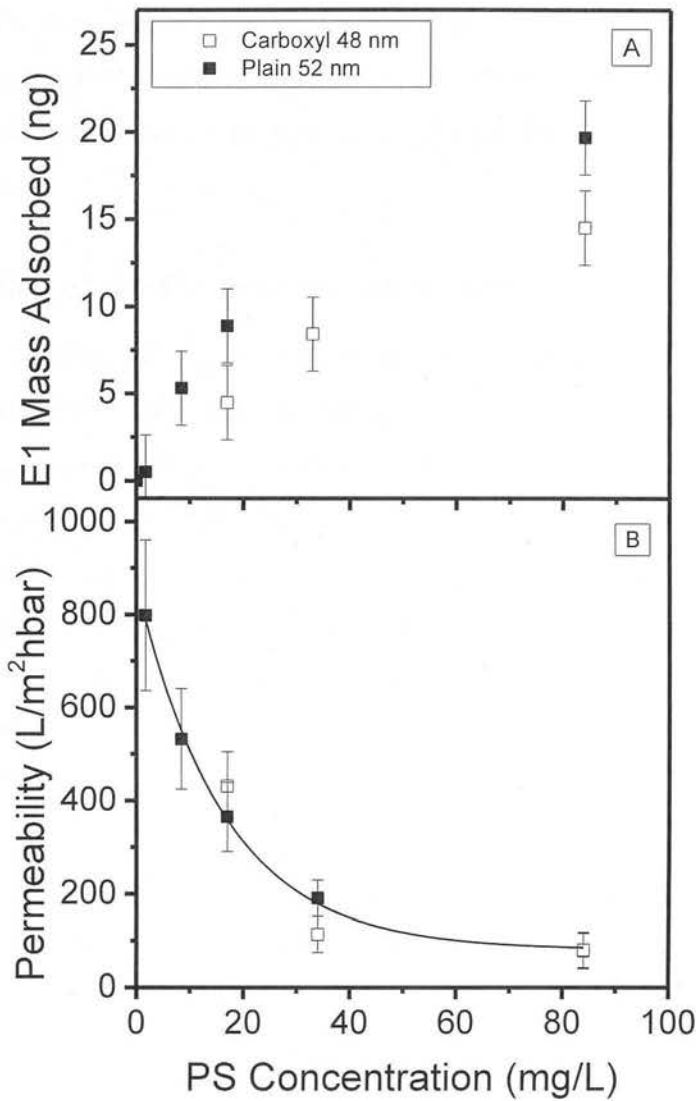
Figure 6-3 A) E1 mass adsorbed and B) permeability of 100 kDa with PS particle concentrations of 1.7, 8.4, 17, 34 and 84: filtration experiments, 100 ng/L E1 concentration with 1 mM NaHCO$_3$ and 20 mM NaCl background electrolyte, pH 7

In order to confirm this, the deposit resistance, thickness and porosity is compared for the experiment where the particles are deposited on 100 kDa membrane at 17 mg/L concentration (Table 6-3).

Table 6-3 Resistance, thickness and porosity for plain and carboxylated PS deposits on 100 kDa at 17 mg/L concentration

PS Type	Deposit Resistance (R_d) (1/m)	Deposit Thickness (μm)	Deposit Porosity
Plain_100 kDa	$5.94 \times 10^{11} \pm 1.53 \times 10^{11}$	3.54 ± 1.62	0.48 ± 0.06
Carboxylated_100 kDa	$4.56 \times 10^{11} \pm 1.25 \times 10^{11}$	3.76 ± 1.76	0.53 ± 0.09

The comparable thickness and porosity values indicate that there is no difference in the deposit characteristics between the plain and carboxylated PS particles. This is not surprising as both plain and carboxylated-PS particles have similar size and zeta potential values.

6.7   Evaluation of the System and Conclusions

Additional carboxylate groups on PS nanoparticles do not have any influence on the membrane permeability and do not enhance the E1 removal of the hybrid PS nanoparticle-UF system. Linear sorption model shows that a larger amount of carboxylated particles is required for the system to achieve the same E1 removal as the plain particles would do at certain concentration. At 84 mg/L nanoparticle concentration with 100 ng/L initial E1 concentration, E1 removal is 40 and 33 % and the permeability is 78 and 81 L/m^{2}hbar for plain and carboxylated PS particles, respectively.